DESIGN OF A BETA-GAMMA PERSONNEL BADGE USING THIN LiF THERMOLUMINESCENT DOSIMETERS

by

James Darren Gale

B.S., Kansas State University, 1983

A MASTER'S THESIS

Submitted in partial fulfillment of the
requirements for the degree

MASTER OF SCIENCE

Department of Nuclear Engineering
KANSAS STATE UNIVERSITY
Manhattan, Kansas

1984

Approved by:

Major Professor

TABLE OF CONTENTS

LIST OF FIGURES

APPENDICES FIGURES

LIST OF TABLES

APPENDICES TABLES

I. INTRODUCTION

Ever since the Three Mile Island nuclear power plant accident in 1977, the nuclear power industry has been attempting to improve their ability to accurately measure beta particle radiation. At that particular time, the thickness of most radiation sensitive elements in personnel badges, thermoluminescent dosimeters, was greater than the penetrating range of most beta particles. This meant that the active volume of the dosimeter would change with changing beta particle energy, and thus would introduce a drastic energy dependence into dose measurements. The ideal beta-gamma or shallow dose-deep dose dosimetry badge would be beta particle energy independent.

Dosimetry badges which are routinely used today vary as much as the locations of the facilities which require the monitoring. At the present time there are no industry-wide badge specifications. The only recommendations are that the dose be reported at a certain skin depth. This opens the door for many badge types and introduces a problem to the consumer of which type to use. The sophistication of a badge usually matches the number of radiation sensitive elements (anywhere from 2 to 8), but does not necessarily match its competence. A dosimetry badge must match the user's need, and also be easy to use and maintain.

Exposure to radiation has long been recognized as a source of biological damage, and many efforts have been made to develop procedures to measure personnel radiation and restrict it to safe levels. The current International Commission on Radiological Protection (ICRP) skin dose limit recommendation is 50 Rem/yr over the skin depth region of 5 to 10 mg/cm^2.[1] In the United States, a maximum permissible skin dose of

7½ Rem per calendar quarter is specified in the Code of Federal Regulations (10CFR20).[2]

The reason why the ICRP dose limitation is applied to skin from 5-10 mg/cm^2 is how the skin is layered. Skin is comprised of four layers which together make the epidermis.[3] The first two layers of skin are dead or dying cells. The third layer is made up of living but non-reproducing cells. The final layer, the stratum basale, is the layer of reproducing cells. It is generally considered that only the reproducing cells are capable of tumor formation after high radiation exposure. The mean density of skin has been found to be 1.145 g/μm^3, so the ICRP recommendations would apply to an average skin depth of 43.7 μm to 87.3 μm.[4]

Experimental and theoretical research was performed on the design of a personnel dosimetry badge and the characterization of thermoluminescent dosimeters (TLDs) to measure radiation doses to skin. The majority of work concentrated on exposure from beta particles. Beta dosimetry studies included an investigation of the Kansas State University thin graphite-backed lithium flouride TLDs and their capabilities for use in a personnel dosimetry badge. Theoretical research involved three methods for characterizing cover materials for a beta dosimeter. Two of the models studied, an electron range-energy relationship developed by Katz and Penfold, and an exponential model required the derivation of several equations. The other model required the use of a set of solutions to a multiple scattering model by Spencer and took advantage of work already performed by Berger.

The goal for this project was to develop a personnel dosimetry badge for beta-gamma dosimetry which would accurately measure the radiation dose to skin.

II. THEORY

A. Electron Range-Energy Distribution

It is essential when determining a badge design for measuring the absorbed dose that the radiation-sensitive materials and their covers be characterized so that the correct combinations of each can be found. In an effort to theoretically determine these characterizations with respect to their energy response, three models have been studied. The first of these is a simple approach of estimating the energy distribution of a beta spectrum arriving at the surface of a dosimeter by the use of an electron range-energy relationship.[5] The second model attempts to estimate the absorbed dose spectrum by use of a multiple scattering model. Finally, an exponential model was studied to characterize the energy absorption of beta particles.

In the proceding development which was selected to provide a means for estimating the energy distribution of beta particles as they penetrated absorbing media, the subscript i refers to particles incident upon the absorber surface and the subscript e refers to the particles emerging from the absorber which arrive at the TLD surface. Assuming that beta particles with kinetic energy E_i, flux density energy distribution $\phi_i(E_i)$, and range $R_i(E_i)$ are normally incident upon an absorber, particles emerging have kinetic energy E_e, flux density energy distribution $\phi_e(E_e)$, and range $R_e(E_e)$. The ranges of the incident and emergent beta particles are related by the total mass absorber thickness, r, which consists of the source window, the air between the source and dosimeter, and the cover material. These ranges are represented as:

$$R_i(E_i) = R_e(E_e) + r \ . \tag{2.1}$$

The emergent flux density spectrum is related to the incident spectrum by:[6]

$$\phi_e(E_e)\, dE_e = \phi_i(E_i)\, dE_i \ . \tag{2.2}$$

Since the particle energy can be expressed as a function of electron range, and the incident particle range can be expressed as a function of emergent particle range and absorber mass thickness, the following equation for the emergent energy spectrum distribution is obtained:

$$\phi_e(E_e) = \phi_i(E_i) \frac{dE_i}{dE_e} = \phi_i(E_i(R_e(E_e) + r)) \frac{dR_e(E_e)/dE_e}{dR_i(E_i)/dE_i} \ . \tag{2.3}$$

An electron range-energy relationship that Katz and Penfold[7] developed for aluminum was chosen for use in Eq. (2.3) to estimate the emergent beta particle spectrum:

$$R(E) = R_o E^n \ , \tag{2.4}$$

where $R(E)$ = range of beta particle in g cm^{-2},

$R_o = 0.412$,

E = beta particle kinetic energy in MeV,

and $n = 1.265 - 0.0954 \ln E$.

This relationship is valid for electron energies ranging from 10 keV to 2.5 MeV. Whereas R_o varies from one medium to another,[8] n remains nearly independent of the attenuating medium. Since the cover materials used in dosimetry work closely match aluminum in atomic number, and to simplify calculations involving Eq. (2.4), the value of R_o determined for aluminum was used for all attenuating media.

From a known energy distribution spectrum of incident beta particles, the energy of particles emerging from the absorbing medium can be evaluated by the following equation derived from Eq. (2.4):

$$E_e = \exp \{6.63 - 3.2376 [3.3067 - \ln R_e(E_e)]^{\frac{1}{2}}\} , \qquad (2.5)$$

where $R_e(E_e)$ was found from Eqs. (2.1) and (2.4) to be:

$$R_e(E_e) = 0.412 E_i^{ni} - r . \qquad (2.6)$$

By taking the derivative of Eq. (2.6) for incident and emergent particles, the ratio of derivatives in Eq. (2.3) is obtained:

$$\frac{dR_e(E_e)/dE_e}{dR_i(E_i)/dE_i} = \frac{E_e^{n_e-1} [n_e - 0.0954 \ln E_e]}{E_i^{n_i-1} \cdot [n_i - 0.0954 \ln E_i]} . \qquad (2.7)$$

The complete derivation of Eqs. (2.5) - (2.7) is presented in Appendix D.

The above model was applied to beta particle energy spectra data from Cross[9] for ^{147}Pm, ^{204}Tl, and ^{90}Y for several absorber thicknesses. Figs. 2.1 - 2.3 show the original spectra along with the resulting attenuated spectra. To help characterize these spectra, methods were developed to determine average and endpoint energies of these resulting spectra.

The two most commonly encountered values when characterizing beta spectra are average and endpoint or maximum energies. In this research, the average energies of the spectra were found by numerically integrating the area of the spectral-energy curve and then dividing by the integral of the spectrum. For a known spectrum this provides a fast method for determining average energy. The values for ^{147}Pm, ^{204}Tl, and

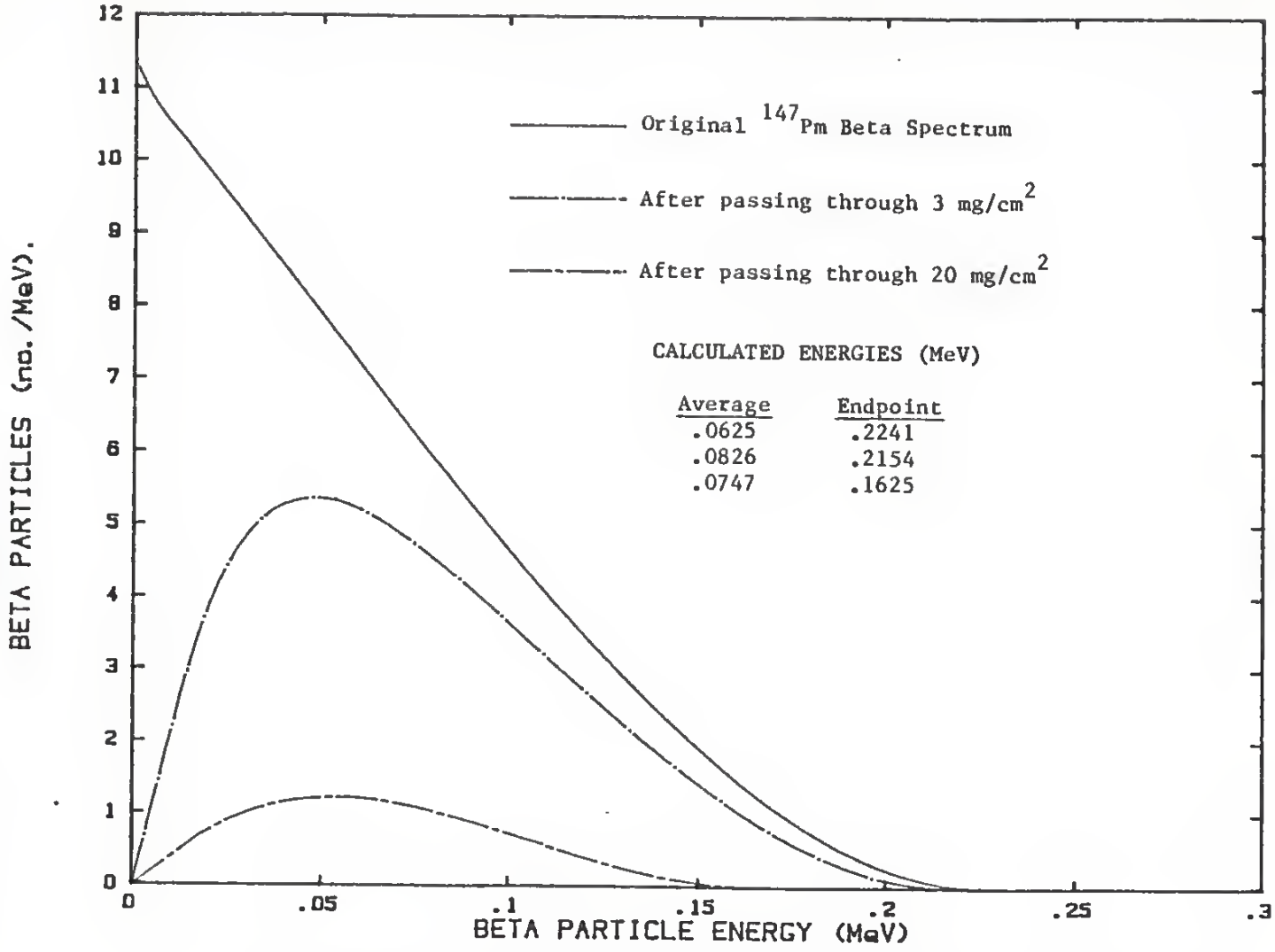

Fig. 2.1. Original and attenuated beta particle energy spectra for ^{147}Pm calculated using Katz and Penfold's electron range-energy relationship. Endpoint energies were found using Kurie plots.

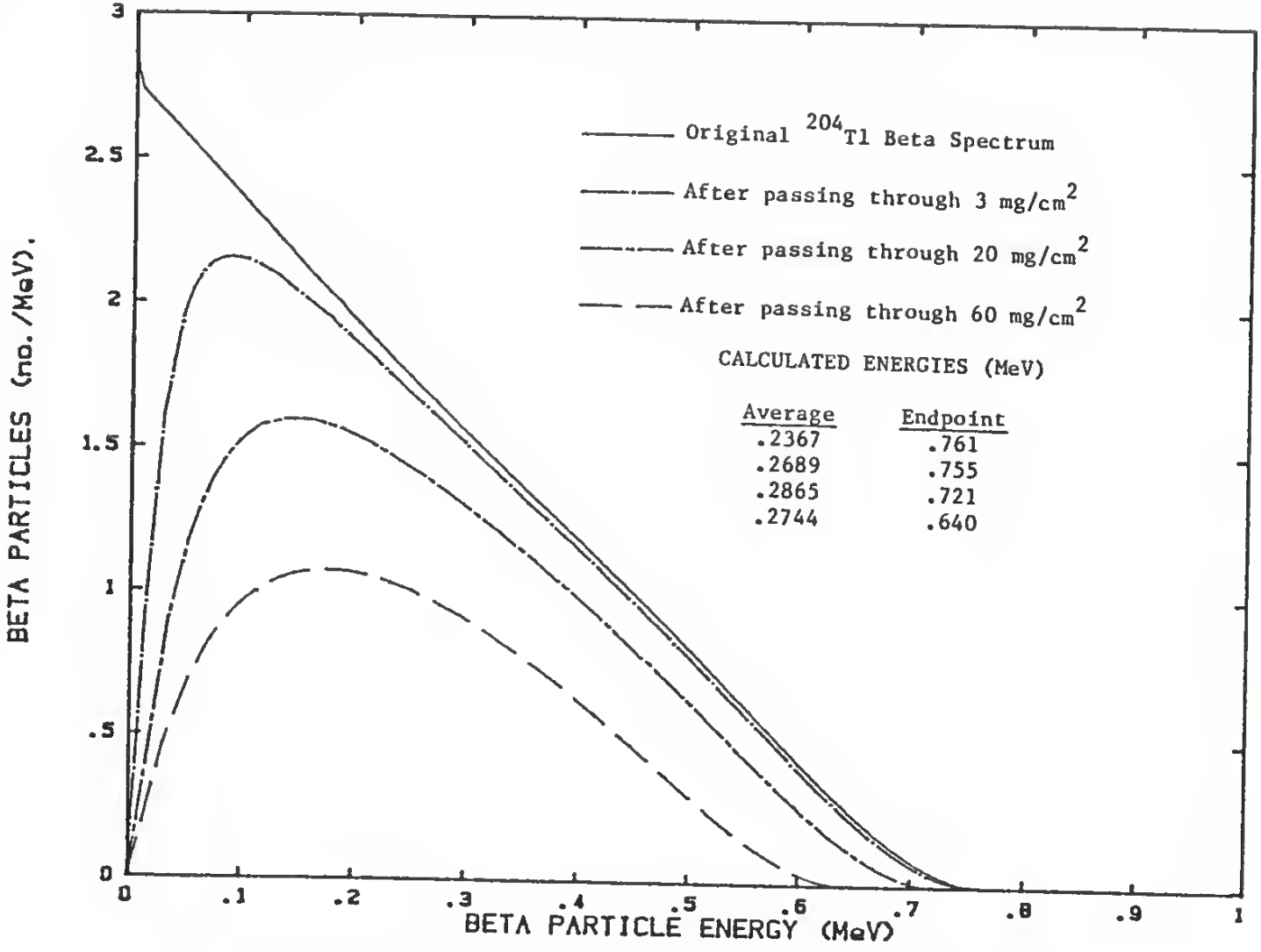

Fig. 2.2. Original and attenuated beta particle energy spectra for ^{204}Tl calculated using Katz and Penfold's electron range-energy relationship. Endpoint energies were found using Kurie plots.

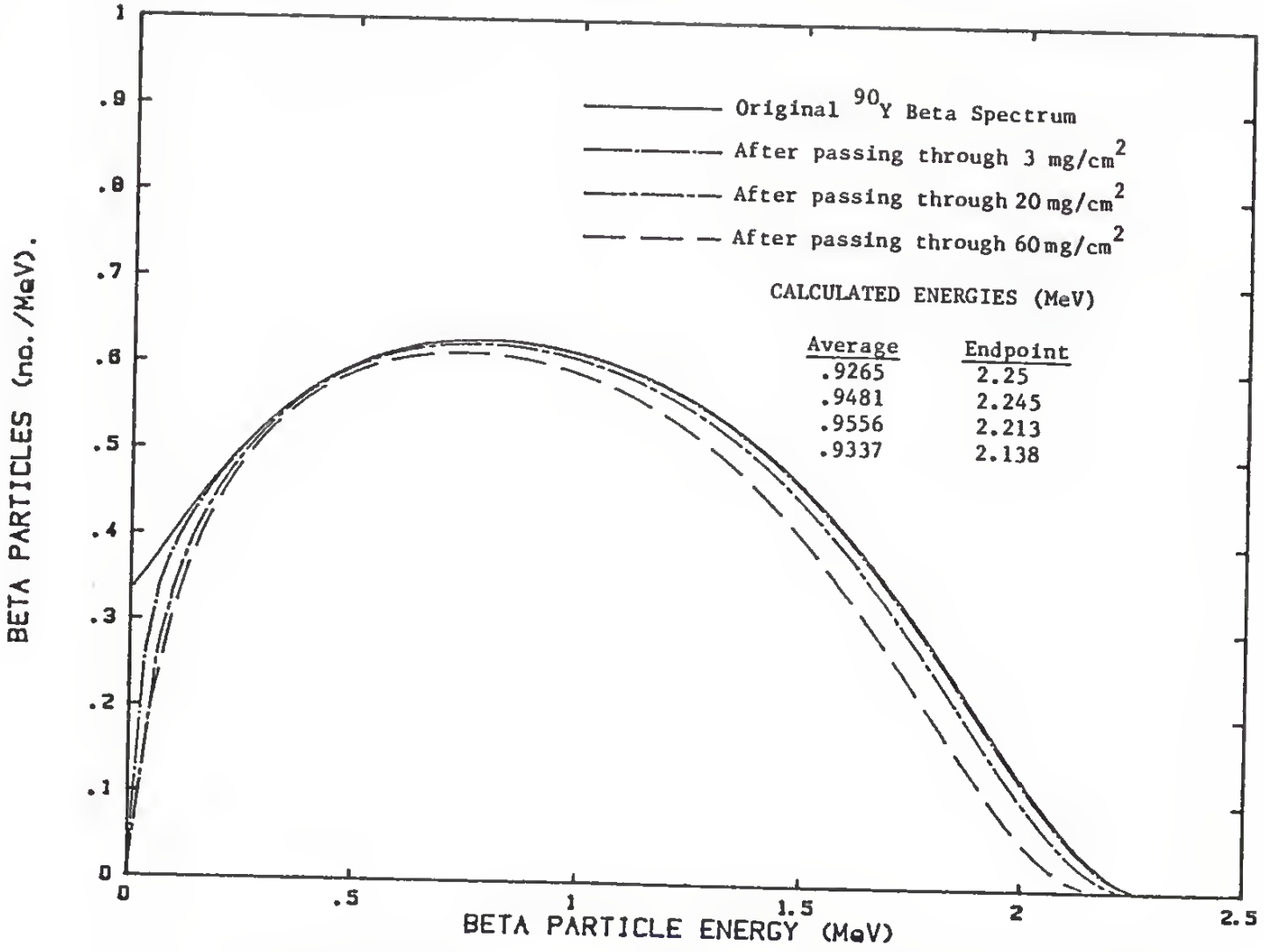

Fig. 2.3. Original and attenuated beta particle energy spectra for ^{90}Y calculated using Katz and Penfold's electron range-energy relationship. Endpoint energies were found using Kurie plots.

^{90}Y are shown in Table 2.1 for original spectra and for spectra after they have passed through a certain mass thickness. The average energies calculated for original spectra were compared to Numerical Data Table[10] values and were found to deviate 1.2%, 2.7%, and 0.6% from listed values for ^{90}Y, ^{204}Tl, and ^{147}Pm, respectively.

For determining maximum or endpoint energies of beta spectra a convenient approach comes from quantum mechanical theory of beta decay developed by Fermi.[11] The probability that a beta particle is emitted with total relativistic energy between W and W + dW is described as:[12]

$$N(W) = (g^2/2\pi^3)\, F(\pm Z,W)\, P\, W\, (W_o - W)^2\, S_n(W)dW, \text{ for } \pm e\ , \qquad (2.8)$$

where g^2 = a coupling constant,

$F(\pm z,W)$ = electron density or Fermi function.

$P = (w^2 - 1)^{\frac{1}{2}}$ = beta particle momentum,

$S_n(W)$ = shape factor,

$W = (E/m_e c^2) + 1$ = total relativistic energy of a beta particle with kinetic energy E, in units electron rest mass energy, $m_e c^2$, and

W_o = maximum relativistic energy with which the beta particle is emitted.

By rearranging Eq. (2.8) an expression which is linear with respect to W is obtained:

$$\left(\frac{N(W)}{\text{const. } F(Z,W)\ PW\ S_n(W)}\right)^{\frac{1}{2}} = W_o - W\ . \qquad (2.9)$$

A plot of the quantity calculated on the left side of Eq. (2.9) versus the relativistic total energy W for experimental data is known as a Kurie plot. The Kurie plot presents the beta spectrum as a straight line with a W-axis intercept at W_o. This intercept value is used to determine the endpoint energy of the spectrum.

Table 2.1. Average and endpoint (maximum) energies and the fraction of the number of particles remaining calculated for ^{90}Y, ^{204}Tl, and ^{147}Pm beta spectra as a function of absorber mass thickness (mg/cm^2).

	^{90}Y			^{204}Tl			^{147}Pm		
Attn. Thick.	E_{av} (MeV)	E_{max} (MeV)	Frac. Remain.	E_{av} (MeV)	E_{max} (MeV)	Frac. Remain.	E_{av} (MeV)	E_{max} (MeV)	Frac. Remain.
0	.926	2.250	1.000	.237	.761	1.000	.0625	.224	1.000
1	.943	2.248	.991	.260	.759	.930	.0774	.221	.748
2	.948	2.246	.986	.265	.757	.903	.0807	.218	.652
3	.948	2.245	.984	.269	.755	.880	.0826	.215	.580
4	.949	2.243	.982	.272	.753	.861	.0835	.212	.521
5	.952	2.241	.979	.274	.751	.843	.0840	.210	.471
6	.952	2.239	.977	.274	.749	.828	.0841	.207	.427
7	.952	2.237	.975	.276	.747	.814	.0841	.204	.388
8	.952	2.235	.973	.278	.745	.800	.0839	.201	.353
9	.954	2.233	.971	.279	.743	.787	.0838	.197	.322
10	.954	2.231	.969	.280	.741	.775	.0832	.194	.293
15	.955	2.222	.960	.284	.731	.720	.0796	.179	.182
20	.956	2.213	.951	.286	.721	.672	.0747	.162	.109
25	.953	2.203	.944	.286	.711	.631			
30	.951	2.194	.936	.286	.701	.594			
35	.950	2.185	.929	.285	.691	.559			
40	.948	2.175	.921	.283	.680	.527			
45	.945	2.166	.914	.282	.670	.497			
50	.943	2.156	.907	.279	.660	.469			
55	.940	2.147	.900	.277	.650	.442			
60	.937	2.138	.893	.274	.639	.417			
65	.935	2.128	.886						
70	.930	2.119	.880						
75	.928	2.110	.872						
80	.924	2.100	.866						
85	.921	2.091	.859						
90	.918	2.082	.852						
95	.914	2.072	.845						
100	.913	2.063	.838						
150	.877	1.969	.772						
200	.835	1.876	.708						
250	.797	1.783	.643						
300	.755	1.690	.580						

Evaluations of the Fermi function, F(Z,W), can be obtained from the solutions of the non-relativistic Schrödinger or relativistic Dirac equations for an electron in an electrostatic field. However, a simple approximation of the Fermi function was recently developed by Schenter and Vogel.[13] Their approach was based on the fact that the logarithm of F is a nearly linear function of Z, and the logarithm of a related function, G, is a nearly linear function of the square root of the electron kinetic energy, E. The expression for G is:

$$G = \frac{P}{W} F(Z,W) \ . \tag{2.10}$$

The resulting analytic approximation is given by:

$$F(Z,W) = \frac{W}{P} \exp \left\{ \alpha(Z) + \beta(Z) \left(\frac{W}{m_e c^2} - 1 \right)^{\frac{1}{2}} \right\} , \tag{2.11}$$

where $\alpha(Z)$ and $\beta(Z)$ are fitted parameters. The approximation is applicable for all atomic number Z and total electron energy W of practical interest.

The fitted parameters are based on electron screen corrected values of Behrens and Jänecke.[14] The ln G function changes its slope around $E = 1.2\ m_e c^2$; thus, the parameters are broken up into two regions:

$$\alpha(Z) = -0.811 + 4.46 \times 10^{-2}\ Z + 1.08 \times 10^{-4}\ Z^2, \tag{2.12}$$

and

$$\beta(Z) = 0.673 - 1.82 \times 10^{-2}\ Z + 6.38 \times 10^{-5}\ Z^2, \tag{2.13}$$

$$\text{for} \quad E < 1.2\ m_e c^2,$$

or

$$\alpha(Z) = -8.46 \times 10^{-2} + 2.48 \times 10^{-2}\ Z + 2.37 \times 10^{-4}\ Z^2, \tag{2.14}$$

and

$$\beta(Z) = 1.15 \times 10^{-2} + 3.58 \times 10^{-4}\, Z - 6.17 \times 10^{-5}\, Z^2, \qquad (2.15$$

$$\text{for } E \geq 1.2\, m_e c^2 .$$

The shape factor $S_n(W)$ describes differences in the probability function which are caused by beta particle transitions. For an allowed transition the shape factor $S_o(W) = 1$, which is the case for ^{147}Pm. For the ^{204}Tl and ^{90}Y spectra, a first forbidden unique shape factor was used, namely[15]

$$S_1(W) = P^2 + (W_o - W)^2 . \qquad (2.16)$$

By applying this method to the data from original and attenuated beta particle spectra, an endpoint energy can be approximated. When the shape factor in Eq. (2.16) was used, the known endpoint energy for the original spectrum was substituted for W_o to eliminate the need for an iteration process. The endpoint energies were found by extrapolating the Kurie plots to zero, and calculating the corresponding energy in MeV.

This model was used by evaluating the left side of Eq. (2.9) for each of the original and attenuated spectra mentioned before. Then, Kurie plots were made and the extrapolated W-axis intercept was determined. The endpoint energy was calculated from the W_o value. Table 2.1 lists these calculated values for the spectra already mentioned. Kurie plots used to determine the endpoints of selected attenuated spectra are shown in Appendix E.

Another characteristic of an attenuated beta spectrum is the fraction of original particles remaining after passing through an absorber. By numerical integration the area under the beta particle

spectral-curve was found for each of the original and attenuated spectra. Since the data from Cross[16] were tabulated aa the number of beta particles per MeV, the area under the spectral curve corresponded to the total number of particles present. For each attenuated spectrum, the area under the curve was ratioed to the area under the original spectrum and the fraction of particles remaining was found. Table 2.1 gives thia fraction for the apectra mentioned before as a function of mass absorber thickness.

By careful consideration of the values of average and endpoint energies, the fraction of particles remaining, and the calculated spectra as a function of maas thickness of absorber, a characterization can be formulated for a badge design. Whereas the preceding discussion dealt with electron range relationshipa, the following development uses the concept of multiple scattering in determining an absorbed dose distribution.

B. Multiple Scattering Theory

Another approach to estimate the effect of absorber materials on beta particle penetration is to conaider the absorbed dose distribution.[17] The required multiple scattering theory was developed by Spencer[18] who uaed hia theory for systematic tabulations of absorbed dose diatributions around point and plane sources in various media.[19] The absorbed dose distributions can be evaluated by uaing weighted sums of Spencer's distributions for several source energiea. The weighting factor is proportional to the beta particle spectrum in question.

The penetration and diffusion of the electrons is determined by two different events: (1) angular deflections from elastic Coulombic scattering of nuclei, and (2) energy loss from inelastic Coulombic

scattering from atomic electrons. The angular deflections are evaluated using the Mott scattering crosa section, and the energy losses are calculated by the Bethe stopping power theory.

A major proportion of spatial moments of the absorbed dose distribution are evaluated by numerical analysis of a group of coupled transport equations. By using the numerical values of the moments and assuming a functional form based on analytical considerations, the absorbed dose distribution is then realized. The limitation of this method is that it applies only to homogenous and unbound media. Hence, it can only be applied to individual absorbers and not to a series of media which might be between a beta source and radiation sensitive dosimeter element.

Whereas the absorbed dose distribution could be a very effective characterization parameter of an absorber material, the following discuasion reveals a method in which the absorbed dose data for a reference material such as water can be more easily utilized to predict useful data for several other materials. Let $\phi(x)$ define the absorbed dose fraction or the fraction of energy emitted which is absorbed in a sphere of radius x around a point source. For convenience, consider a fixed set of percentile distances, x_p, where[20]

$$\phi(x_p) = 4\pi\rho \int_0^{x_p} x^2 \phi(x)dx = \frac{P}{100} , \qquad (2.17)$$

where P = 5, 10, ... 95.

For instance, x_{90} is the radius of a sphere in which 90% of the emitted energy is absorbed. Percentile distance data for beta particles in water have been reported by Berger.[21]

The relationship between absorbed dose distributions in different media comes from the fact that a beta particle source placed in two separate media with slightly different atomic numbers has two particle distributions that are very similar in shape. A scaling procedure has been developed which uses this similarity in distributions. A scaling procedure by Cross[22] has been investigated systematically, and using indices 1 and 2 indicating the two media,

$$\phi^{(2)}(x) = (a_{21})^3 \left(\frac{\rho_2}{\rho_1}\right)^2 \phi^{(1)}(y) , \tag{2.18}$$

for a beta particle source where

$$y = a_{21} \frac{\rho_2}{\rho_1} x . \tag{2.19}$$

The relative attenuation factor, a_{21}, is a material constant independent of beta particle energy, provided that the atomic numbers of the two media are sufficiently close. If two media differ only in terms of their density, then a_{21} is unity and the scaling law is exact. An empirical formula which was obtained from Monte Carlo data for a_{21} values,[23] reveals how the relative attenuation factor increases linearly with respect to Z, namely[24]

$$a_{21} = (L^{(2)}/L^{(1)}) \, [1.0 + 0.0252 \, (Z - 6.60)], \tag{2.20}$$

in which $L^{(2)}/L^{(1)}$ is the ratio of mass stopping power in the medium to that in water (evaluated at 200 keV). Relative attenuation factors for various personnel badge cover, backing, and TLD materials were calculated and are shown in Table 2.2. It is from these values that data are obtained to compare absorbed dose fractions of several absorber media.

Table 2.2. Relative attenuation factors (a_{21}) for several personnel badge cover, backing, and TLD materials.

Material	$\bar{Z}^a$	$L^{(2)}$ (MeV cm^2 g^{-1})[b]	Density (g cm^{-3})	a_{21}
Water	6.60	2.844[c]	1.00[c]	1
Polyethylene	4.75	2.986	0.94[d]	1.01
Lucite	5.85	2.761	1.18	0.954
Carbon	6.00	2.493	1.6[e]	0.865
Air	7.36	2.466	1.23 (10^{-3})[g]	0.882
LiF	7.50	2.285[d]	2.63[d]	0.820
CaF_2	14.79	2.219	3.18	0.924
Teflon	8.25	2.32	2.20	0.846
Mylar	6.24	2.8	1.40[f]	0.977
Polystyrene	5.29	2.766	1.06[e]	0.944
Aluminum	13	2.188	2.70	0.880

[a] $\bar{Z} \equiv \sum_i \frac{n_i Z_i}{(\sum_i n_i Z_i)}$, where $Z_i \equiv$ atomic no., $n_i \equiv$ no. of atoms of element i.

[b] $L^{(2)} \equiv$ collision mass stopping power.

[c] Martin J. Berger, and Stephen M. Seltzer, National Bureau of Standards, "Tables of Energy Losses and Ranges of Electrons and Positrons," NASA SP-3012 (1964).

[d] G. G. Simons, "Gamma ray energy response of LiF and CaF_2: Mn TLD's," DOE Annual Report COO-5100-3 (Nov. 1979).

[e] Theodore Baumister and Lionel S. Marks, Standard Handbook for Mechanical Engineers, (McGraw-Hill Book Company, New York, NY, 1967).

[f] Melinex Films Technical Data, ICI Americas Inc., Plastics Division, Wilmington, Delaware.

[g] W.M. Kays and M.E. Crawford, Convective Heat and Mass Transfer, (McGraw-Hill, New York, NY, 1980).

Using the percentile distances of beta particles in water mentioned before, percentile distances, x_p's, were calculated for various personnel badge cover, backing, and TLD materials by the use of Eq. (2.19). These percentile distances can be used to estimate the decrease in an absorbed dose distribution as it passes through an absorber. Tables 2.3 - 2.9 list percentile distances for the materials mentioned above as a function of aversge beta particle energy. The corresponding graphs of percentile distances are presented in Appendix C.

Previously, the characterization of personnel badge materials has been developed by the use of two fairly unfamiliar techniques. The third and final model which will be developed has to do with a much more universal method.

C. Exponential Attenuation Model

If the beta particle energy absorption is assumed to occur exponentially, the fraction of energy absorbed F after traversing some distance x is given by

$$F = (1 - e^{-\beta\rho x}) \ , \tag{2.21}$$

where β is an effective sttenuation coefficient. Since specific attenuation coefficients for the TLD covers and phosphors are unavailable, a consistent method was chosen by assigning s 1% transmission to the range R (g/cm^2) where

$$\beta = \frac{-\ln (0.01)}{R} \ . \tag{2.22}$$

Values for R were calculated from Eq. (2.4). Since the expression for R applies to monoenergetic electrons, the maximum energy (endpoint) in the beta particle spectrum was chosen.

Table 2.3. Absorbed dose percentile distances (mg/cm^2) in water for beta particle spectra with given average energy.

E (MeV)	X_5[a]	X_{10}	X_{15}	X_{30}	X_{50}	X_{70}	X_{80}	X_{90}
.0621	.254	.546	.890	2.34	5.02	9.00	12.0	16.5
.1005	.582	1.26	2.07	5.34	11.0	19.3	25.2	34.1
.2433	2.50	5.52	9.21	23.2	43.9	72.8	92.5	121
.3444	4.50	9.82	15.5	34.7	68.0	128	200	317
.5063	8.18	17.6	27.7	60.8	115	192	251	343
.6670	12.6	26.8	41.5	88.2	160	247	303	380
.7378	16.3	31.9	47.4	94.2	160	240	291	362
.8266	18.0	36.2	54.5	110	189	283	343	427
.9367	20.5	42.5	64.2	131	228	344	418	517
1.0712	24.0	49.8	75.6	155	271	414	509	642
1.2317	30.0	59.5	88.4	175	295	436	525	647

[a] $\phi(X_p) = \frac{P}{100}$, P = 5, 10, ... 90.

Table 2.4. Absorbed dose percentile distances (mg/cm^2) in aluminum for beta particle spectra with given average energy.

E (MeV)	X_5[a]	X_{10}	X_{15}	X_{30}	X_{50}	X_{70}	X_{80}	X_{90}
.0621	.289	.620	1.01	2.66	5.70	10.2	13.6	18.8
.1005	.661	1.43	2.35	6.07	12.5	21.9	28.6	38.8
.2433	2.84	6.27	10.5	26.4	49.9	82.7	105	138
.3444	5.11	11.2	17.6	39.4	77.3	145	227	360
.5063	9.30	20.0	31.5	69.1	131	218	285	390
.6670	14.3	30.5	47.2	100	182	281	344	432
.7378	18.5	36.3	53.9	107	182	273	331	411
.8266	20.5	41.1	61.9	125	215	322	390	485
.9367	23.3	48.3	73.0	149	259	391	475	588
1.0712	27.3	56.6	85.9	176	308	470	578	730
1.2317	34.1	67.6	100	199	335	495	597	735

[a] $\phi(X_p) = \frac{P}{100}$, P = 5, 10, ... 90.

Table 2.5. Absorbed dose percentile distances (mg/cm^2) in muscle for beta particle spectra with given average energy.

E (MeV)	X_5[a]	X_{10}	X_{15}	X_{30}	X_{50}	X_{70}	X_{80}	X_{90}
.0621	.257	.552	.900	2.37	5.08	9.10	12.1	16.7
.1005	.588	1.27	2.09	5.40	11.1	19.5	25.5	34.5
.2433	2.53	5.58	9.31	23.5	44.4	73.6	93.5	122
.3444	4.55	9.93	15.7	35.1	68.8	129	202	321
.5063	8.27	17.8	28.0	61.5	116	194	254	347
.6670	12.7	27.1	42.0	89.2	162	250	306	384
.7378	16.5	32.3	47.9	95.2	162	243	294	366
.8266	18.2	36.6	55.1	111	191	286	347	432
.9367	20.7	43.0	64.9	132	231	348	423	523
1.0712	24.3	50.4	76.4	157	274	419	515	649
1.2317	30.3	60.2	89.4	177	298	441	531	654

[a] $\phi(X_p) = \frac{P}{100}$, P = 5, 10, ... 90.

Table 2.6. Absorbed dose percentile distances (mg/cm^2) in mylar for beta particle spectra with given average energy.

E (MeV)	X_5[a]	X_{10}	X_{15}	X_{30}	X_{50}	X_{70}	X_{80}	X_{90}
.0621	.260	.559	.911	2.40	5.14	9.21	12.3	16.9
.1005	.596	1.29	2.12	5.47	11.3	19.8	25.8	34.9
.2433	2.56	5.65	9.43	23.7	44.9	74.5	94.7	124
.3444	4.61	10.1	15.9	35.5	69.6	131	205	324
.5063	8.37	18.0	28.4	62.2	118	197	257	351
.6670	12.9	27.4	42.5	90.3	164	253	310	389
.7378	16.7	32.7	48.5	96.4	164	246	298	371
.8266	18.4	37.1	55.8	113	193	290	351	437
.9367	21.0	65.7	65.7	134	233	352	428	529
1.0712	24.6	77.4	77.4	159	277	424	521	657
1.2317	30.7	90.5	90.5	179	302	446	537	662

[a] $\phi(X_p) = \frac{P}{100}$, P = 5, 10, ... 90.

Table 2.7. Absorbed dose percentile distances (mg/cm^2) in lucite for beta particle spectra with given average energy.

E (MeV)	X_5[a]	X_{10}	X_{15}	X_{30}	X_{50}	X_{70}	X_{80}	X_{90}
.0621	.266	.572	.932	2.45	5.26	9.42	12.6	17.3
.1005	.609	1.32	2.17	5.59	11.5	20.2	26.4	35.7
.2433	2.62	5.78	9.64	24.3	46.0	76.2	96.9	127
.3444	4.71	10.3	16.2	36.3	71.2	134	209	332
.5063	8.57	18.4	29.0	63.7	120	201	263	359
.6670	13.2	28.1	43.5	92.4	168	259	317	398
.7378	17.1	33.4	49.6	98.6	168	251	305	379
.8266	10.8	37.9	57.1	115	198	296	359	447
.9367	21.5	44.5	67.2	137	239	360	438	541
1.0712	25.1	52.1	79.2	162	284	434	533	672
1.2317	31.4	62.3	92.6	183	309	457	550	677

[a] $\phi(X_p) = \frac{P}{100}$, P = 5, 10, ... 90.

Table 2.8. Absorbed dose percentile distances (mg/cm^2) in carbon for beta particle spectra with given average energy.

E (MeV)	X_5[a]	X_{10}	X_{15}	X_{30}	X_{50}	X_{70}	X_{80}	X_{90}
.0621	.293	.630	1.03	2.70	5.80	10.4	13.9	19.1
.1005	.672	1.45	2.39	6.17	12.7	22.3	29.1	39.4
.2433	2.89	6.37	10.6	26.8	50.7	84.1	107	140
.3444	5.20	11.3	17.9	40.1	78.5	148	231	366
.5063	9.45	20.3	32.0	70.2	133	222	290	396
.6670	14.5	30.9	47.9	102	185	285	350	439
.7378	18.8	36.8	54.7	109	185	277	336	418
.8266	10.8	41.8	62.9	127	218	327	396	493
.9367	23.7	49.1	74.1	151	263	397	483	597
1.0712	27.7	57.5	87.3	179	313	478	588	741
1.2317	34.6	68.7	102	202	341	503	606	747

[a] $\phi(X_p) = \frac{P}{100}$, P = 5, 10, ... 90.

Table 2.9. Absorbed dose percentile distances (mg/cm^2) in teflon for beta particle spectra with given average energy.

E (MeV)	X_5[a]	X_{10}	X_{15}	X_{30}	X_{50}	X_{70}	X_{80}	X_{90}
.0621	.300	.645	1.05	2.77	5.93	10.6	14.2	19.5
.1005	.688	1.49	2.45	6.31	13.0	22.8	29.8	40.3
.2433	2.96	6.52	10.9	27.4	51.9	86.1	109	143
.3444	5.32	11.6	18.3	41.0	80.4	151	236	375
.5063	9.67	20.8	32.7	71.9	136	227	297	405
.6670	14.9	31.7	49.1	104	189	292	358	449
.7378	19.3	37.7	56.0	111	189	284	344	428
.8266	21.3	42.8	64.4	130	223	335	405	505
.9367	24.2	50.2	75.9	155	270	407	494	611
1.0712	28.4	58.9	89.4	183	320	489	602	759
1.2317	35.5	70.3	104	207	349	515	621	765

[a] $\phi(X_p) = \frac{P}{100}$, P = 5, 10, ... 90.

Table 2.10. Absorbed dose percentile distances (mg/cm^2) in LiF for beta particle spectra with given average energy.

E (MeV)	X_5[a]	X_{10}	X_{15}	X_{30}	X_{50}	X_{70}	X_{80}	X_{90}
.0621	.310	.666	1.09	2.85	6.12	11.0	14.6	20.1
.1005	.710	1.54	2.52	6.51	13.4	23.5	30.7	41.6
.2433	3.05	6.73	11.2	28.3	53.5	88.8	113	148
.3444	5.49	12.0	18.9	42.3	82.9	156	244	387
.5063	9.98	21.5	33.8	74.1	140	234	306	418
.6670	15.4	32.7	50.6	108	195	301	370	463
.7378	19.9	38.9	57.8	115	195	293	355	441
.8266	22.0	44.1	66.5	134	230	345	418	521
.9367	25.0	51.8	78.3	160	278	420	510	630
1.0712	29.3	60.7	92.2	189	330	505	621	783
1.2317	36.6	72.6	108	213	360	532	640	789

[a] $\phi(X_p) = \frac{P}{100}$, P = 5, 10, ... 90.

Table 2.11. Absorbed dose percentile distances (mg/cm^2) in CaF_2 for beta particle spectra with given average energy.

E (MeV)	X_5[a]	X_{10}	X_{15}	X_{30}	X_{50}	X_{70}	X_{80}	X_{90}
.0621	.275	.591	.963	2.53	5.43	9.74	13.0	17.9
.1005	.630	1.36	2.24	5.78	11.9	20.9	27.3	36.9
.2433	2.71	5.97	9.97	25.1	47.5	78.8	100	131
.3444	4.87	10.6	16.8	37.6	73.6	139	216	343
.5063	8.85	19.0	30.0	65.8	124	308	272	371
.6670	13.6	29.0	44.9	95.5	173	267	328	411
.7378	17.6	34.5	51.3	102	273	260	315	392
.8266	19.5	39.2	59.0	119	205	306	371	462
.9367	22.2	46.0	69.5	142	247	372	452	560
1.0712	26.0	53.9	81.8	168	293	448	551	695
1.2317	32.5	64.4	95.7	189	319	472	568	700

[a] $\phi(X_p) = \frac{P}{100}$, P = 5, 10, ... 90.

If it is now assumed that the beta particle energy distribution remains unchanged aa the beta particles penetrate the medium, the general form of the doae equation for beta particles with endpoint energy E_o, becomes:

$$D(x) = \int_0^{E_o} dE\ \Phi(E)\ \exp[-\beta(E_o)\rho x]\ \frac{L(E_o)}{\rho}\ , \qquad (2.23)$$

where $\phi(E)$ = the beta particle fluence spectrum in electrons cm^{-2} MeV^{-1},

$L(E)$ = the material mass stopping power in MeV cm^2 g^{-1},

and x = the material thickness for an absorber with a density of ρ ($g\ cm^{-3}$).

Next, by taking the ratio of the dose at a depth X relative to the dose at the surface (x = 0), an expression is obtained

$$D(x)/D(0) = \frac{e^{-\beta(E_o)\rho x} \int_0^{E_o} dE\ \phi(E)\ L(E_o)/\rho}{\int_0^{E_o} dE\ \phi(E)\ L(E_o)/\rho}\ , \qquad (2.24)$$

which reduces to $D(x)/D(0) = e^{-\beta(E_o)\rho x}$. (2.25)

The advantage of expressing the doae at depth x as a ratio is obvious since the apectral dependence has been removed. The only remaining energy dependence is in the attenuation coefficient. By integration of Eq. (2.5) for both the cover and TLD element, we obtain an expression for the total dose absorbed in the TLD relative to the dose absorbed in a cover, namely:

$$\frac{D(TLD)}{D(C)} = \frac{\rho_c\ e^{-\beta(E_o)\rho_c x_c}\ (1-e^{-\beta(E_o)\rho_{TLD}\ x_{TLD}})}{\rho_{TLD}\ (1-e^{-\beta(E_o)\rho_c x_c})}\ . \qquad (2.26)$$

Figs. 2.4 - 2.8 show how the dose from a TLD compares to the dose between 5-10 mg/cm^2 by the use of Eq. (2.26). The figures show the ratio as a function of beta particle energy. The ideal situation is when the dose in the TLD is exactly equal to the dose at 5-10 mg/cm^2. This would mean a cover material 5 mg/cm^2 thick, and then a radiation sensitive layer of 5 mg/cm^2.

From careful consideration of Figs. 2.4 - 2.8, it is seen that the only good representation of beta dose at a depth of 5-10 mg/cm^2 comes from a radiation sensitive layer that is very similar in thickness. However, as will be discussed in a later section, abuses which the dosimeter must undergo while being used also play a vital role in design.

Whereas characterizing a radiation sensitive element for beta dosimetry has no clear cut path, gamma rays present an entirely different situation. Fig. 2.9 shows the attenuation of photons in two different mass absorber thicknesses as a function of energy. All photons encountered in dosimetry work are attenuated exponentially because their spectra do not change even at large depths.

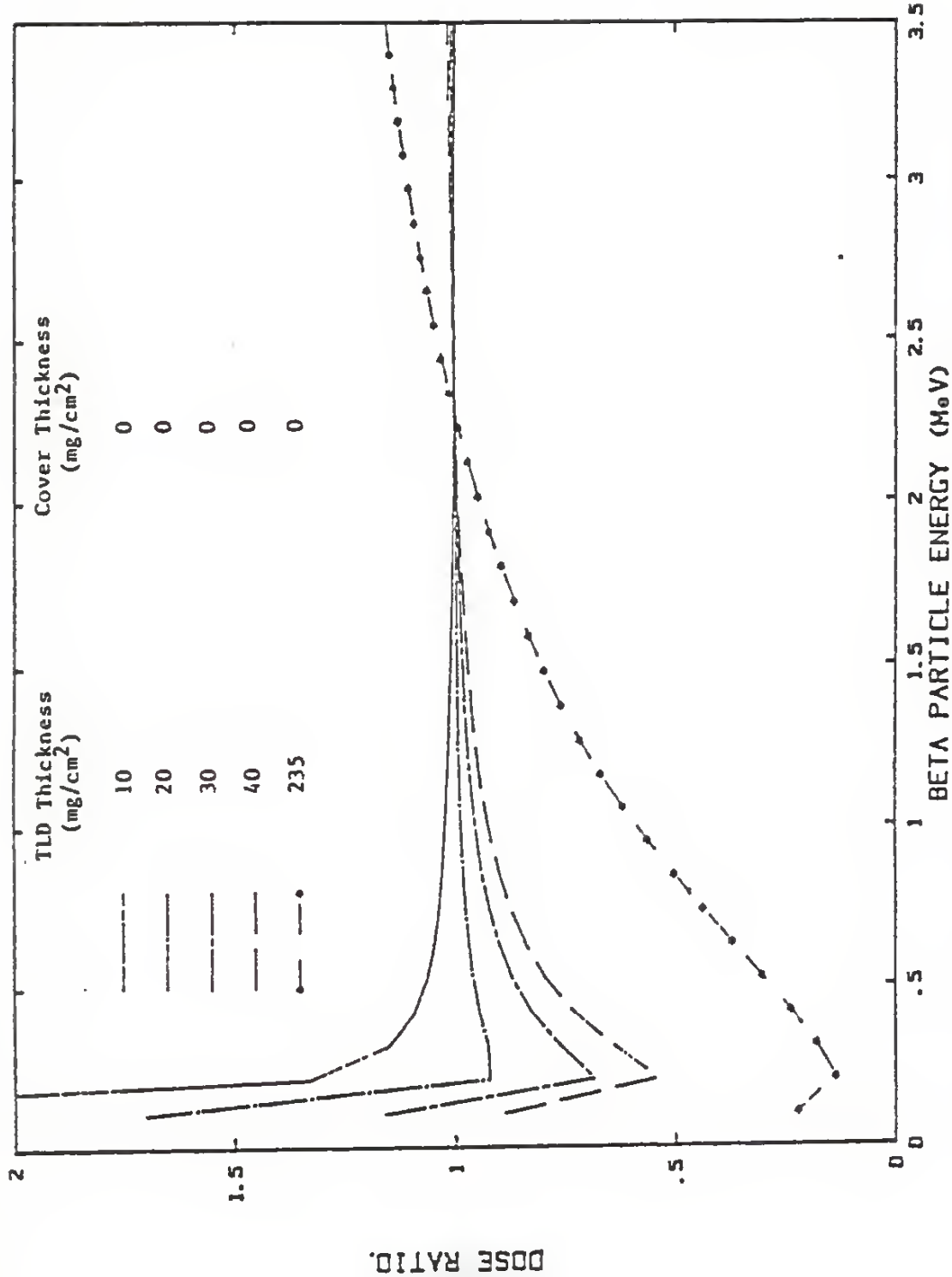

Fig. 2.4. Beta particle dose in a TLD relative to the dose between 5-10 mg/cm^2 for a bare TLD normalized to 2.27 MeV.

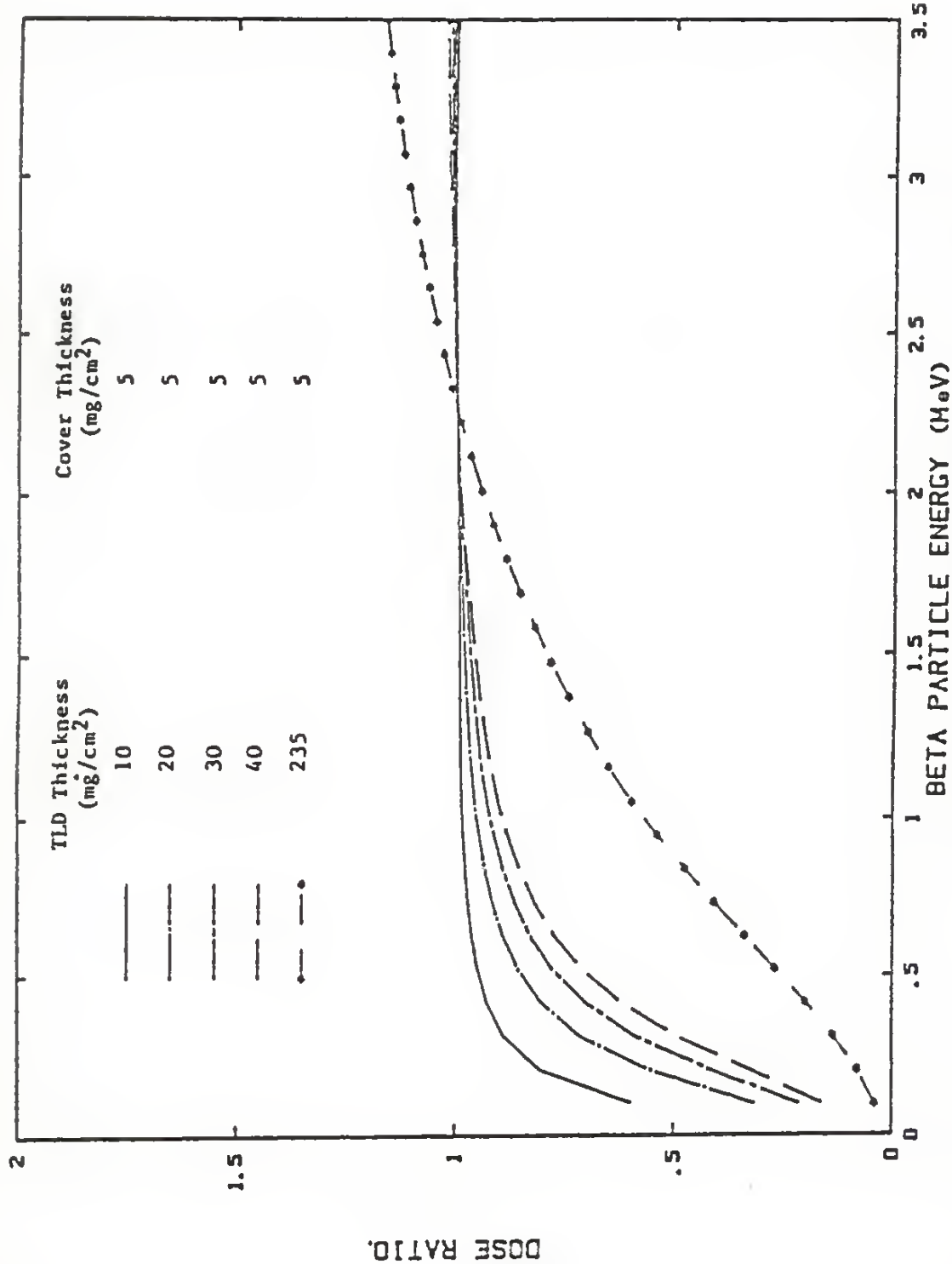

Fig. 2.5. Beta particle dose in a covered TLD relative to the dose between 5-10 mg/cm^2 normalized to 2.27 MeV.

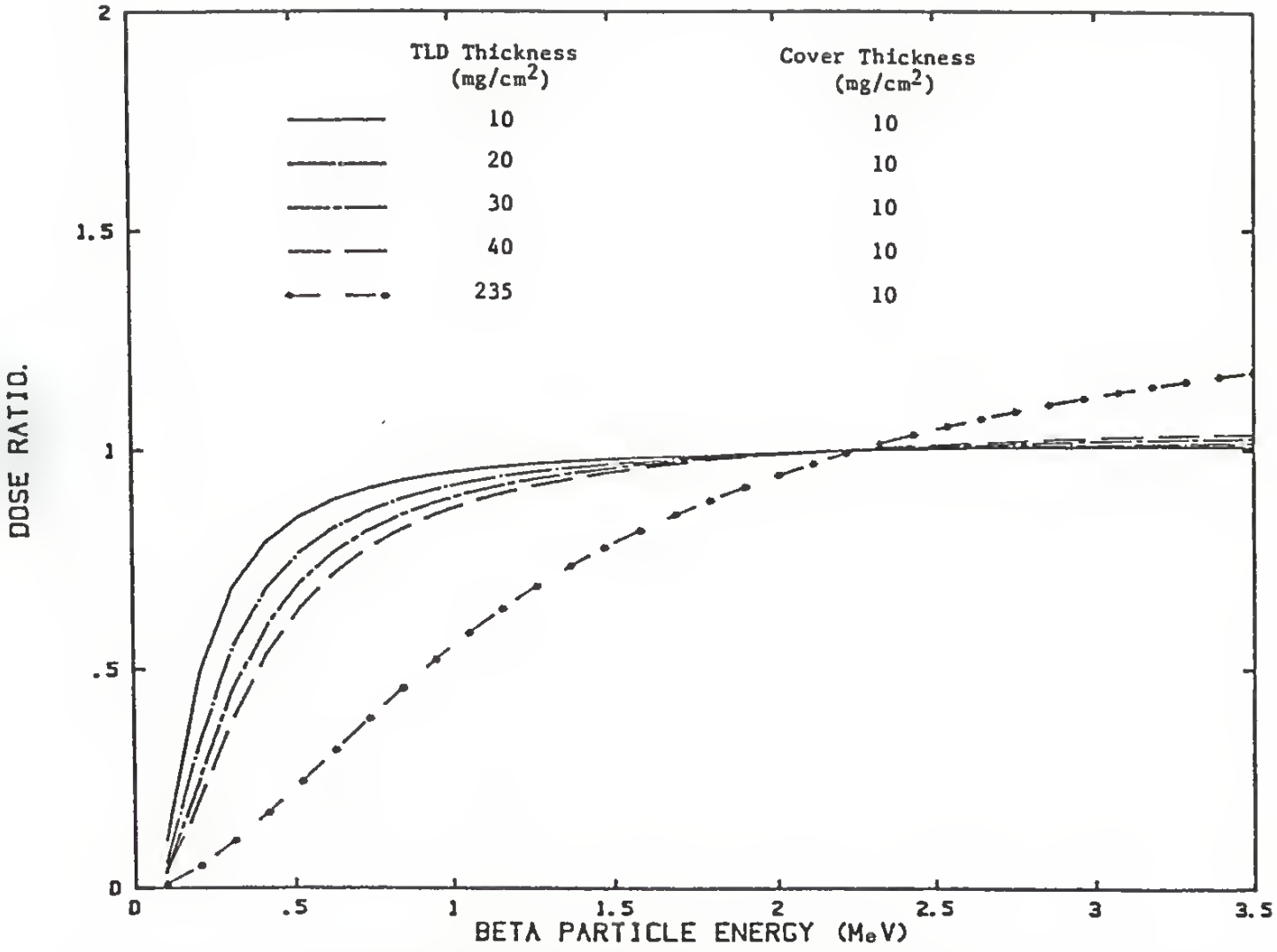

Fig. 2.6. Beta particle dose in a covered TLD relative to the dose between 5-10 mg/cm^2 normalized to 2.27 MeV.

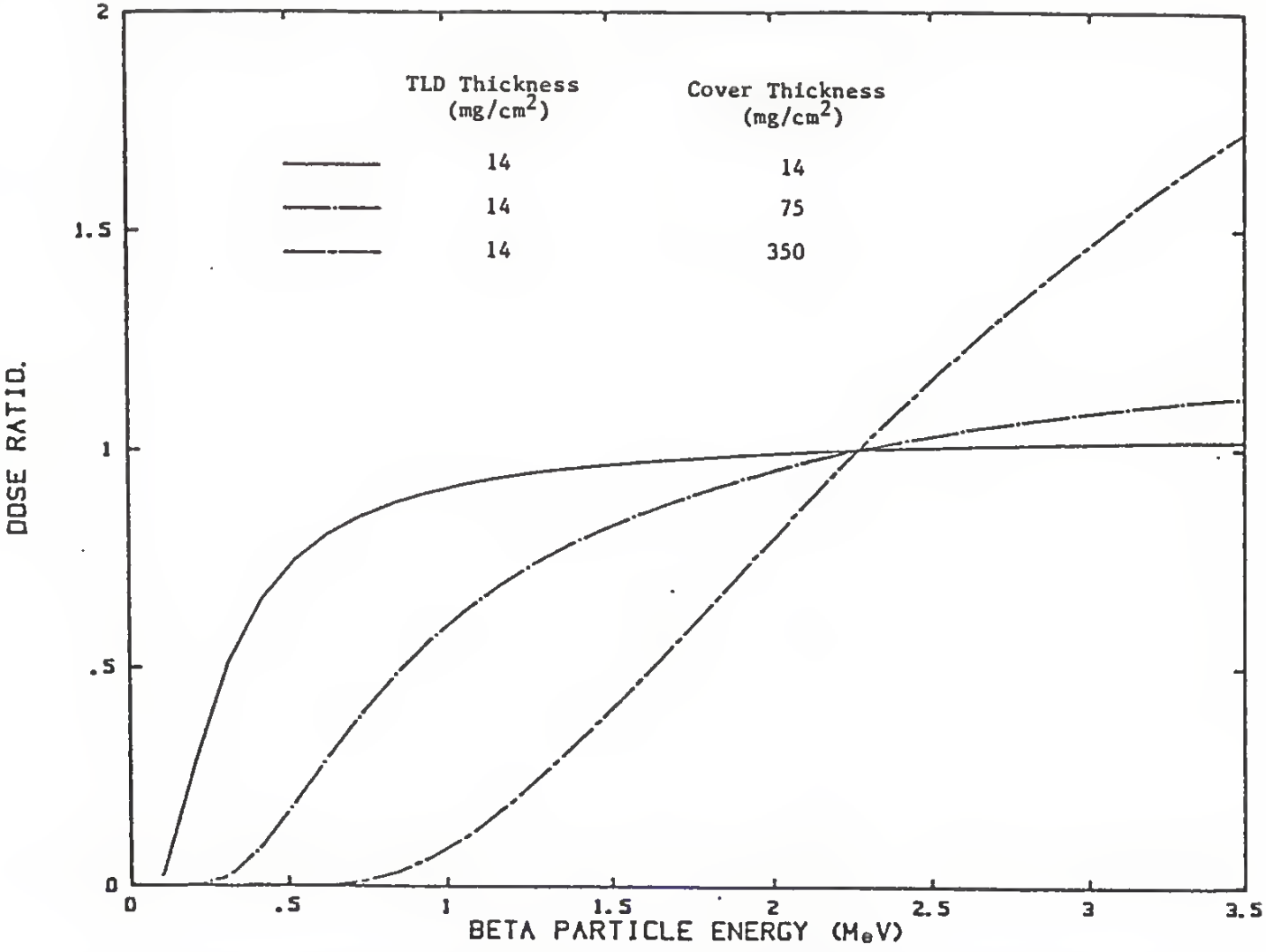

Fig. 2.7. Beta particle dose in a covered TLD relative to the dose between 5-10 mg/cm^2 normalized to 2.27 MeV.

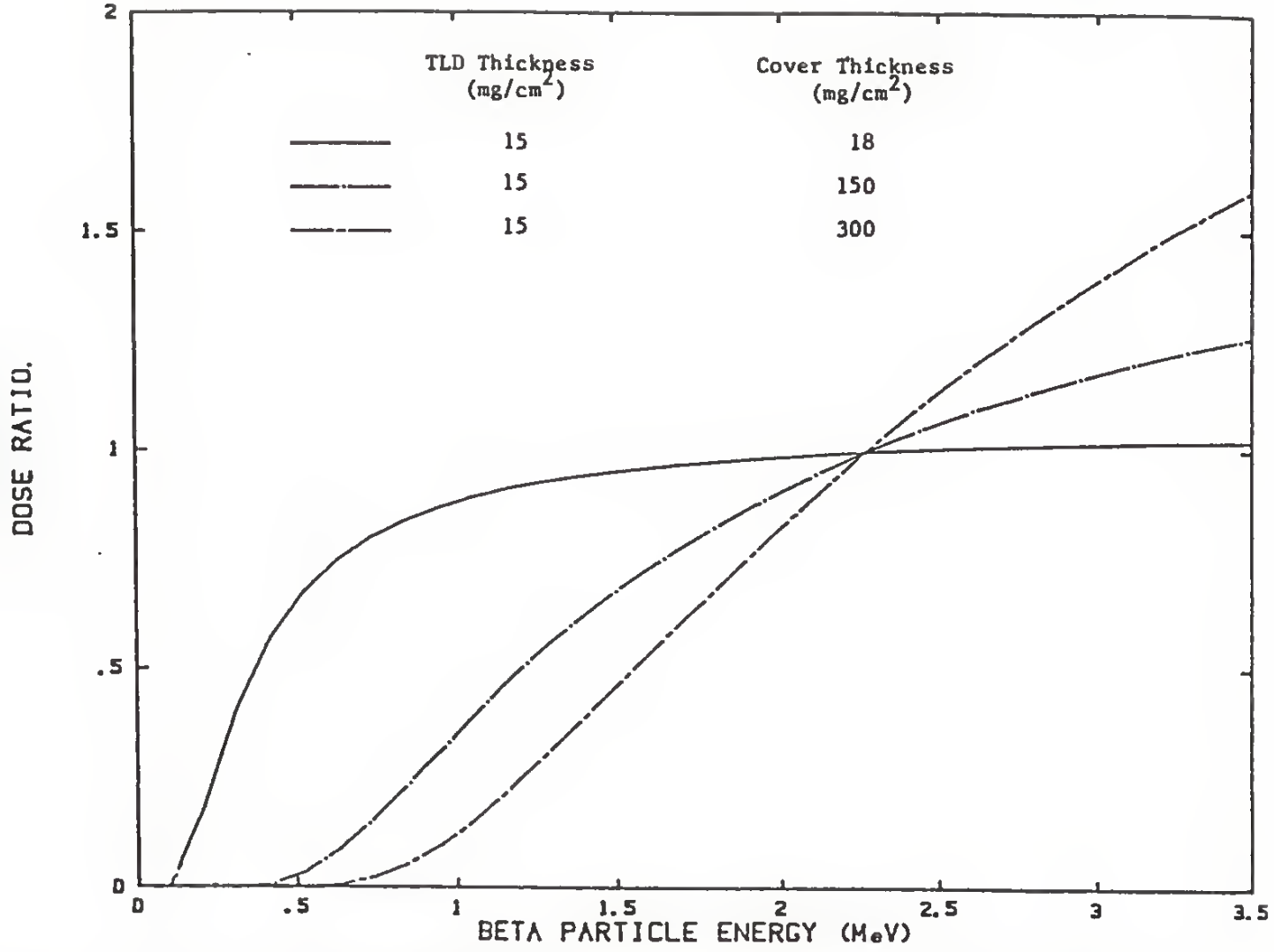

Fig. 2.8. Beta particle dose in a covered TLD relative to the dose between 5-10 mg/cm^2 normalized to 2.27 MeV.

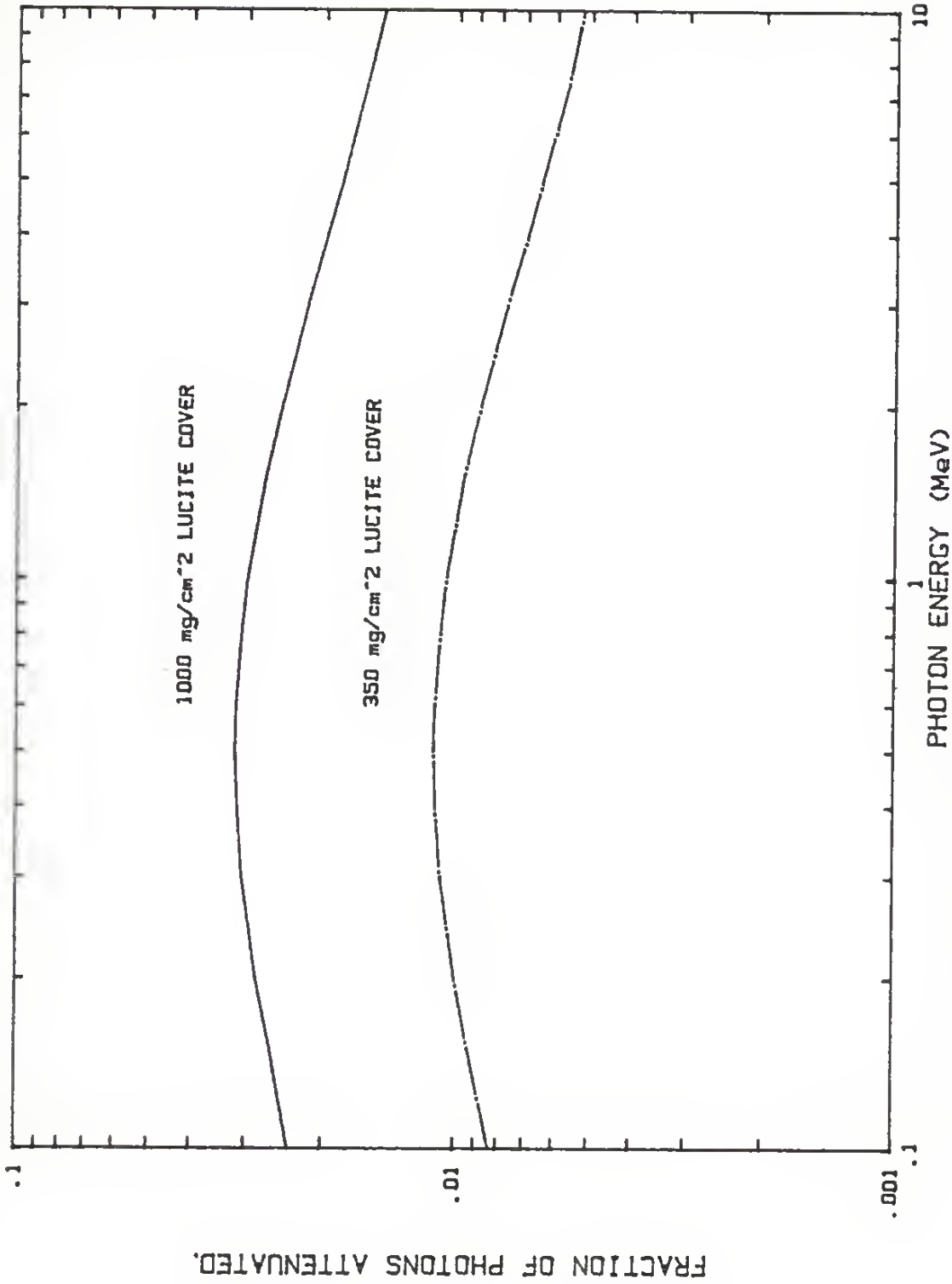

Fig. 2.9. Attenuation of photons in lucite as a function of photon energy for two absorber thicknesses.

III. BADGE DESIGN

A. Present State of Dosimetry Badge Design

The major reform in personnel dosimetry after the TMI accident came about when experimental investigations revealed that dosimeters were not responding in a manner consistent with established algorithms. At that time the standard personnel badge in use was a two-chip TL dosimeter consisting of a rugged plastic casing containing a TLD card. The TLDs were held in place in the aluminum card by two sheets of teflon. Both TLD elements were 235 mg/cm^2 thick (nominal 2.6 g/cm^3 density). The shallow dose element teflon cover was 35 mg/cm^2 thick, and the deep dose element was covered by 250 mg/cm^2 including the teflon and plastic casing.

The shortcomings of this badge were mainly due to the thicknesses of the cover materials and TLDs. Since many low energy beta particles cannot penetrate 35 mg/cm^2, the thin-covered element under-predicted the shallow dose. However, beta particles from other spectra (i.e. ^{90}Y, 2.27 MeV E_{max}) can penetrate up to 1100 mg/cm^2. This caused the thick-covered TLD to over-predict the expected value for the deep dose, which when subtracted from the thin-shielded element caused the shallow dose to be under-predicted even more.

Developments in badge design since then have produced dosimeters which can more accurately measure gamma ray exposures and beta particle doses. One such badge utilizes four TLD elements encapsulated in plastic with a plastic plate insert containing the TLDs. The elements are 15 mg/cm^2 thick and made by forming a mono-layer of phosphor granules on a substrate polyimide film. The beta particle dose element has a tissue equivalent teflon cover of approximately 14 mg/cm^2. The

shield thicknesses vary over the other elements from 320 to 1000 mg/cm^2 depending on the element's use. The large mass thickness is obtained using a .7 mm lead thickness so that the plastic badge case can be kept as small as possible. This allows for good angular response. However, it is not known what problems might be caused by radiation interactions in lead. This badge is commonly used today in reactor power plant facilities. It is sensitive to gamma-, X-ray, and beta particle radiation. A problem with the badge is that the teflon in the TLD element disallows high temperature annealing in the event that the badge is exposed to high levels of radiation.

Another badge used at the present time also uses a plastic badge cover, but has a metal insert. The major difference with this badge is that it involves eight radiation sensitive elements and detects beta particle, gamma-, X-ray, and thermal and fast neutrons. A sophisticated algorithm is required for such a thorough dosimeter.

This particular badge utilizes two elements for beta particle dose. The first element has a cover of 17 mg/cm^2 and is used to report the skin dose. The second element has a 64 mg/cm^2 shield and is used to predict the energy of the beta particles encountered. The TLD elements were made by spreading the phosphor out over a heat-resistant resin (10 mg/cm^2) and covering them with a transparent resin film (22 mg/cm^2). This badge is used in fuel reprocessing plants and fuel-grade plutonium production facilities as well as nuclear power plants.

Several other badges exist, but use many of the techniques already mentioned in one way or another. A major weakness of existing beta dosimeters is that the cover thickness over the beta dose element in the dosimeter is too thick. To give a true estimation of skin dose, the

element detecting beta particles must have a cover of approximately 5 mg/cm^2. Manufacturers argue that abuses which occur with use of the badges in industry require that at least 15-20 mg/cm^2 cover the elements to prevent contamination or actual damage. Another argument is that some TLD phosphors, such as lithium borate, are extremely susceptible to the environment and require strong covers to remain sensitive to radiation. Whatever the reason may be, badge design studies, in the area of beta dosimetry, remain active to find the solutions to these problems.

B. A New Badge Design for Beta Particle-Gamma Ray Dosimetry

A badge has been constructed at Kansas State University which utilizes nearly tissue-equivalent lucite and the KSU graphite-backed thin LiF TLD. Lucite has a density of approximately 1.18 g/cm^3 and average atomic number of approximately 6. These values compare favorably with 1.145 g/cm^3 and 7.3 for skin, respectively. By placing the radiation sensitive elements in a holder which closely approximates skin, a true representation of the skin dose may be achieved.

The new KSU badge is a two-element deep dose-shallow dose (gamma ray, beta particle) dosimeter. The shallow dose element is a KSU thin graphite-backed LiF TLD. Its mass thickness ranges from 20-30 mg/cm^2, but is of very rugged construction. The KSU thin TLD is constructed without the use of plastics, so high temperature anneals are allowed. The cover material chosen for the beta element was a 1 mil layer of aluminized mylar (3.15 mg/cm^2). This particular material was chosen for its strength and low Z number.

When the design for the deep dose element (gamma ray) cover was chosen, it was decided that a small loss in angular response of the beta

particles would be traded for the unknown effect of a dense, high Z material (lead) as a cover. A pyramid-shaped cover of lucite (1000 mg/cm^2) was added to the thin layer of lucite which is used as a top cover. As can be seen in Fig. 3.1, the pyramid-shaped cover allows for good angular response of gamma rays. However, the deep dose cover will shield beta particles coming in at less than approximately 34°.

The thickness of the bottom section of the badge was chosen so that it would provide a sufficient distance for backscatter saturation. The backscatter saturation thickness for high-energy beta particles is approximately 250 mg/cm^2. Thus, by making the bottom section approximately 850 mg/cm^2, backscatter saturation is achieved and photons will penetrate approximately the same mass thickness from the top or bottom of the dosimeter.

Two circular TLD wells were drilled in the bottom section of the badge approximately .1 cm deep and .95 cm dia. in order that a variety of TLDs may some day be tested in the badge. This size of hole will accommodate TLDs which are 235 mg/cm^2 thick and 6.35 mm x 6.35 mm in area (Harshaw's large TLD chips). However, for this research, the standard 3.175 mm x 3.175 mm chips were used. To connect the top of the badge to the bottom, a standard soldering iron was used to melt two edges together on one side of the badge. This allows for the top side to be raised and lowered as if connected by a hinge. The aluminized mylar thin element cover was secured to the bottom side of the top part of the badge to allow the user to remove the TLD's. Following irradiation, the TLD's from the KSU badge are removed in order that they may be processed in the KSU photon counting system to record the TL output.

The KSU two-element badge is a lightweight, solidly built dosimeter which closely approximates tissue. A way to attach the badge to the user has not been developed. However, one idea may be to attach a velcro piece to the badge. The user can then stick it to a velcro strip which has been attached to his clothing. The user can remove it easily, but should not lose it while it is being worn.

Admittedly, this badge does not contain all the developments which will solve the problems with beta particle dosimetry today. However, it is a design which attacks some of the major problems facing personnel dosimetry.

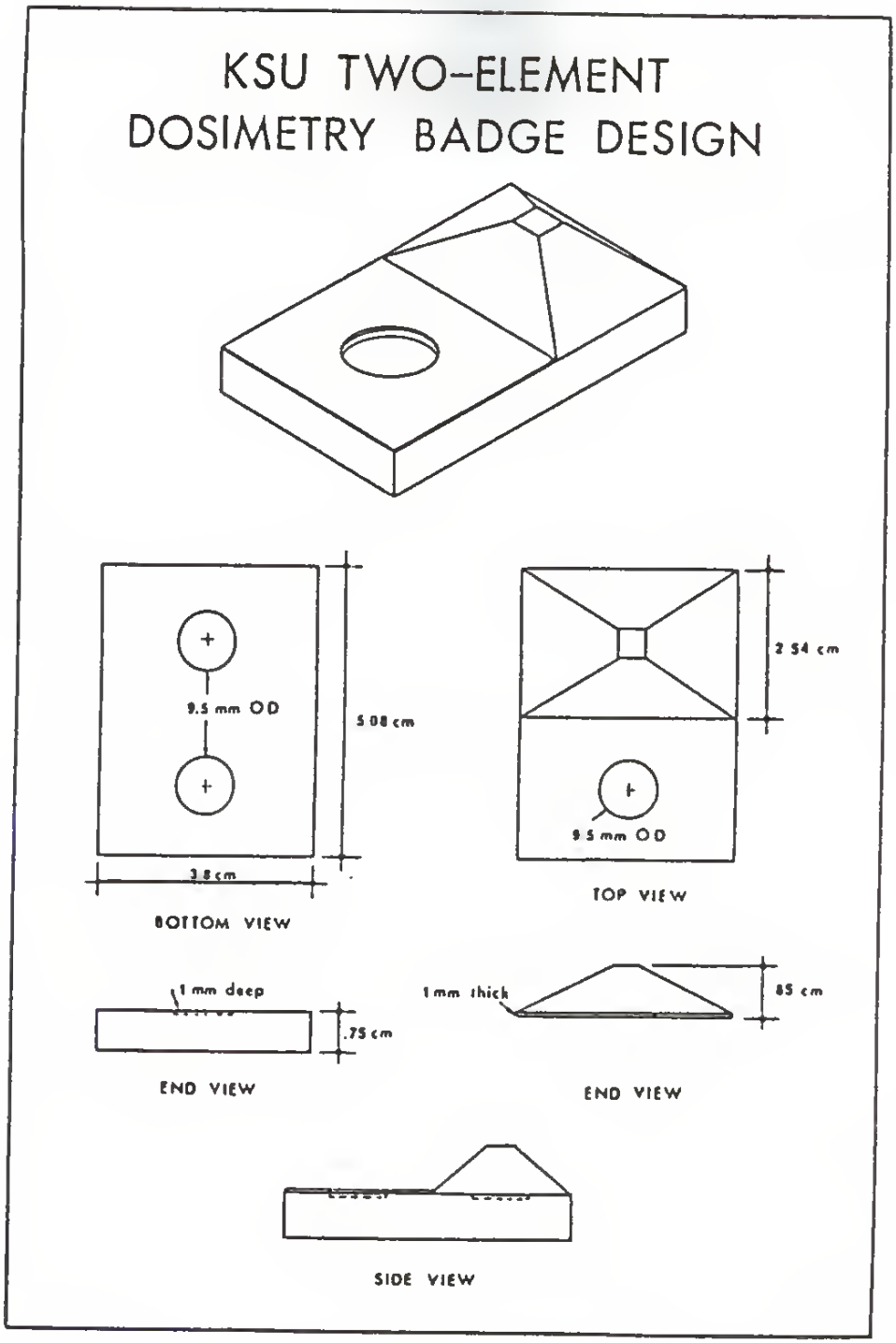

Fig. 3.1. Specifications of the KSU lucite two-element dosimetry badge design.

IV. MATERIALS, PROCEDURES AND INSTRUMENTS

A. Beta Dosimeters

One type of TLD material and two separate TLD configurations were evaluated with respect to their beta particle response. The first TLDs used, obtained commercially, were 3.175 mm x 3.175 mm x 0.89 mm-thick natural LiF (235 mg/cm^2). These solid chips provided dosimeters for use in determining the response of thick TLDs to beta radiation.

In addition to the standard commercial TLDs mentioned above, a locally assembled composite was constructed. This extensively studied composite consisted of adhering thin natural LiF (15-30 mg/cm^2) TLD wafers to a graphite backing.

The size of the graphite backing approximated the size of the commercial TLD mentioned above so that studies could be made by substituting this composite TLD for existing commercial chips. The graphite was approximately 4 mm x 4 mm x 0.89 mm-thick (151 mg/cm^2) and the TLD wafers were nominally 3.175 mm x 3.175 mm x 0.05 mm-thick. In this configuration the TLD wafers provided the skin dose information while the graphite backing was nearly tissue equivalent and provided support for the fragile wafer. These TLD composites could also be annealed at 400°C due to the use of a high temperature resistant polyimide adhesive. Characteristics of the adhesive material and a detailed description of the construction of the TLD composite are found in reference (25).

B. Beta Source

The beta particle source used throughout the course of this study was an 8.33 mCi $^{90}Sr/^{90}Y$ source. The source was encapsulated in

stainless steel and was packaged with a beryllium window of 23.5 mg/cm^2 mass thickness. During the course of this research, layers of mylar ($\sim$80 mg/cm^2) were added to shield the ^{90}Sr beta particles. The source capsule was mounted inside a polyethylene cylinder to minimize beta particle penetration through the sides and back and help reduce bremsstrahlung radiation. For this ^{90}Sr/^{90}Y source, the maximum bremsstrahlung production will be less than 2.1% of the total beta particle energy emitted.[26] For this reason.bremsstrahlung effects were ignored.

C. Beta Irradiations

Beta particle absorbed-dose irradiations were performed by arranging the TLDs in a circular configuration directly below the source. Two different source locations determined what materials were placed under the TLDs. For the first part of this research (the minimum detectable dose study, the annealing study, and an environmental effects study) each set of TLDs were placed on top of a 1.52 mm-thick styrene sheet which was supported by a 25.4 mm styrofoam block. The beta source was suspended from a string directly above the TLDs.

For the remainder of the study, a portable ^{90}Sr/^{90}Y source irradiator was assembled. The beta particle irradiator contained a tissue equivalent plastic phantom block approximately 400 mm x 400 mm x 160 mm-thick. The plastic phantom has a nominal density of 1 g/cm^3. TLDs were placed directly under a source housing (made of lucite, which completely encapsulates the ^{90}Sr/^{90}Y source holder) on top of the phantom block. All ^{90}Sr/^{90}Y irradiations were performed at a source-to-detector distance of either 50 or 60 cm.

D. Gamma Irradiations

Gamma irradiations were performed using two commercial irradiators containing ^{137}Cs and ^{60}Co sources. The ^{60}Co source was used for Kilorad-level doses, while the ^{137}Cs source was used for mrad doses. The TLDs were placed in a pyrex glass dish for ^{60}Co irradiations and placed in an equilibrium plexiglass holder for ^{137}Cs irradiations.

E. Annealing

Prior to each readout cycle, and immediately after each irradiation, TLDs were post-annealed for 10 minutes at 100°C in a covered pyrex dish. This procedure removed the low-temperature TL output which was not used to determine absorbed dose. The covered dishes were used to eliminate non-radiation induced TL which seems to occur when moisture condenses on a cooling TLD. A high temperature pre-irradiation annealing study was conducted and is reported in Section V.B.

F. Badge Construction

The machining of the KSU lucite badge was done by hand with the use of a band saw. The first step was to cut blocks of lucite which were approximately 2 inches square. The blocks were then cut in half, with each half being used as a top or bottom. The correct dimensions were etched into the lucite, and the band saw was then used to prepare the badges. The element wells in the bottom part and the hole through the top part of the badge were drilled using a simple milling machine. The final step was to melt two edges together to form a hinge and combine the two halves into a single element.

G. TL Analyzers

Two TLD reader systems were used to measure TL emissions. One system was a commercial TLD analyzer and the other was a KSU designed TLD photon counting system.

The commercial reader was a Harshaw analyzer which consisted of two major components: (1) a 2000-A thermoluminescence (TL) detector, and (2) a 2000-B automatic integrating picoammeter. During normal operation, the TL detector utilized a photomultiplier (PM) tube to measure the TL emissions. As the heat induced emissions were measured, the PM tube current was integrated by the 2000-B unit between the response integration temperatures of 130-200°C. This integrated charge was the desired quantity used to relate the instrument output to the radiation induced excitation within the dosimeters and was displayed on seven segment LEDs.

The KSU designed TLD photon system is controlled by a Motorola M6800 microprocessor. The microprocessor controls heating cycles, count times, replace temperatures, restart temperatures, and detects errors in readout procedures.[27]

V. RESULTS

A. Environmental Effects

A major advantage and one of the reasons LiF is a popular TLD material is its relative insensitivity to environmental effects. However, to confirm previous findings, LiF composite dosimeters were exposed to 100 mRad from a ^{137}Cs source and some of them were stored in the dark, while the remaining dosimeters were placed under a fluorescent light for either 19 h or 70 h prior to the measurement of the remaining TL. Light induced fading was not observed. Sunlight induced TL was investigated by placing the dosimeters in a north facing window for 2 h and 90 h. A small low temperature peak was observed when the TLDs were analyzed without a post anneal. When a post anneal of 100°C for 10 min was performed sunlight induced TL was not evident.

B. Pre-irradiation annealing

Annealing before TLDs are exposed to radiation refers to a temperature treatment which is selected to remove residual thermoluminescent (TL) emissions, modify the dosimeter's sensitivity to radiation, and remove unstable low temperature emissions. Many different annealing procedures have been reported. The two most often used procedures, for LiF, are 1 h at 400°C followed by 2 h at 100°C and 1 h at 400°C followed by 24 h at 80°C. Unfortunately, even though it is well known that the cooling rate drastically effects the TLD response, minimum attention is often given to the transition step between 400-100°C or between 400-80°C and then to room temperature. Maintaining a LiF TLD at an elevated temperature in a high humidity laboratory also greatly increases non-radiation induced TL. Due to the problems inherent in

annealing, many TLD users prefer to conduct all of their work without annealing. However, due to the presence of high temperature traps in LiF, low dose measurements following high dose irradiations requires pre-annealing to avoid residual signals from previous irradiations. One of the keys to performing accurate low dose measurements is to establish when and how to anneal a given type of TLD.

Optimum annealing must be TLD-type specific. For commercial chips and powders composed only of TLD material, the two annealing procedures mentioned above are well accepted. However, many widely used LiF-based dosimeter badges, LiF suspended in Teflon and composite dosimeters can't withstand temperatures as high as 400°C. If these dosimeters are purposely or accidently exposed to a high radiation dose and they can't be annealed to remove the high temperature traps, then they must not be used for future low dose monitoring. This is the unfortunate consequence of not having a selection of high temperature plastics or other tissue equivalent materials available for the fabrication of TLD badges suitable for personnel dosimetry.

An annealing experiment was conducted to evaluate the degree to which the residual high temperature TL could be removed from the thin graphite-backed LiF beta dosimeters. The limiting component is the adhesive-backed Kapton used to adhere the thin LiF chip to the graphite backing. It was found that annealing at 400°C for extended times caused discoloration of the Kapton and eventual weakening of the bond. Fortunately, as discussed below, extended annealing at 350°C didn't appear to damage these dosimeters and virtually complete removal of the high temperature traps was accomplished.

Two basic experiments were completed -- 1. a comparison between annealing for thick (35 mil) and thin (~2 mil) TLDs using a commercial mean level TLD analyzer and 2. the effect of annealing on thin TLDs using the K-State photon counting TLD analyzer. For each experiment, the TLDs were exposed to 1000 Rads of ^{60}Co, annealed at various temperatures for 10 min and in some cases simply readout twice and in other cases exposed to 100 mRad of ^{137}Cs and then read twice.

When the commercial TLD analyzer was used, 325°C for 10 min was found to remove the residual TL from the thin chips. However, this anneal was not adequate for the thick TLDs. For the thick TLDs, the second readout was 22% higher than their reading following 400°C for 1 h. Because the photon counting analyzer has a much higher sensitivity, detailed measurements were then performed with this instrument and thin TLDs.

Graphite-backed TLDs with a nominal thickness of 2.5 mils were irradiated at the 1000 Rad level and annealed in a covered pyrex dish. Annealing temperatures ranged from 275-350°C. The 10 min time period established using the commercial TLD analyzer was adopted for all of these measurements. Typical glow curve results are shown in Figs. 5.1-5.3 for the sequence of high dose - anneal - first read - second read. At 350°C for 10 min, the first and second readouts were identical (see Fig. 5.3). Moreover, these readouts matched the glow curves for unirradiated thin TLDs. Thus, the high temperature traps produced during the 1000 Rad irradiation were eliminated.

To verify that these thin TLDs could be used to measure low doses following a 1000 Rad irradiation and annealing, the TLDs were passed through the sequence of high dose - high temperature anneal - low dose -

100°C for 10 min post anneal - first read - second read. As shown in Figs. 5.4 and 5.5, the residual TL induced by the high dose irradiation decreased from a major component at 325°C for 10 min to an insignificant level when the TLDs were annealed at 350°C for 10 min. In addition, the small photon component, shown in Fig. 5.5, above the main TL glow peak is not recorded as TLD light emission by the photon counter since it is programmable and integrates only the peak region.

It was concluded from this study that the thin graphite-backed TLDs can be routinely annealed at 350°C for 10 min to remove the residual TL without damaging the dosimeter. It was also found, ss expected, that the high dose and high temperature treatments changed the sensitivity of the TLDs.

Based upon these results, it is interesting to note that 350°C for 10 min is adequate for thin TLDs and not for thick TLDs. Carlsson[28] reported that annealing at high temperatures should last only long enough to empty filled electron traps. For thin TLDs this is ∿10 min. In addition, it has been shown that recycling of LiF using the 400°C and 1 h anneal changes the sensitivity.[29] Hopefully, this effect would be decreased for the thin TLDs since both the temperature and anneal time are reduced.

C. Minimum Detectable Dose (MDD)

Application of dosimeters to personnel radiation monitoring requires establishment of the minimum dose level which can be detected for specific types of radiation. This, obviously, requires definition of minimum detectable dose (MDD). It has been recognized for some time that the background readings limit the MDD, however, recently MDD limits have not been based upon the magnitude of the background reading but on its

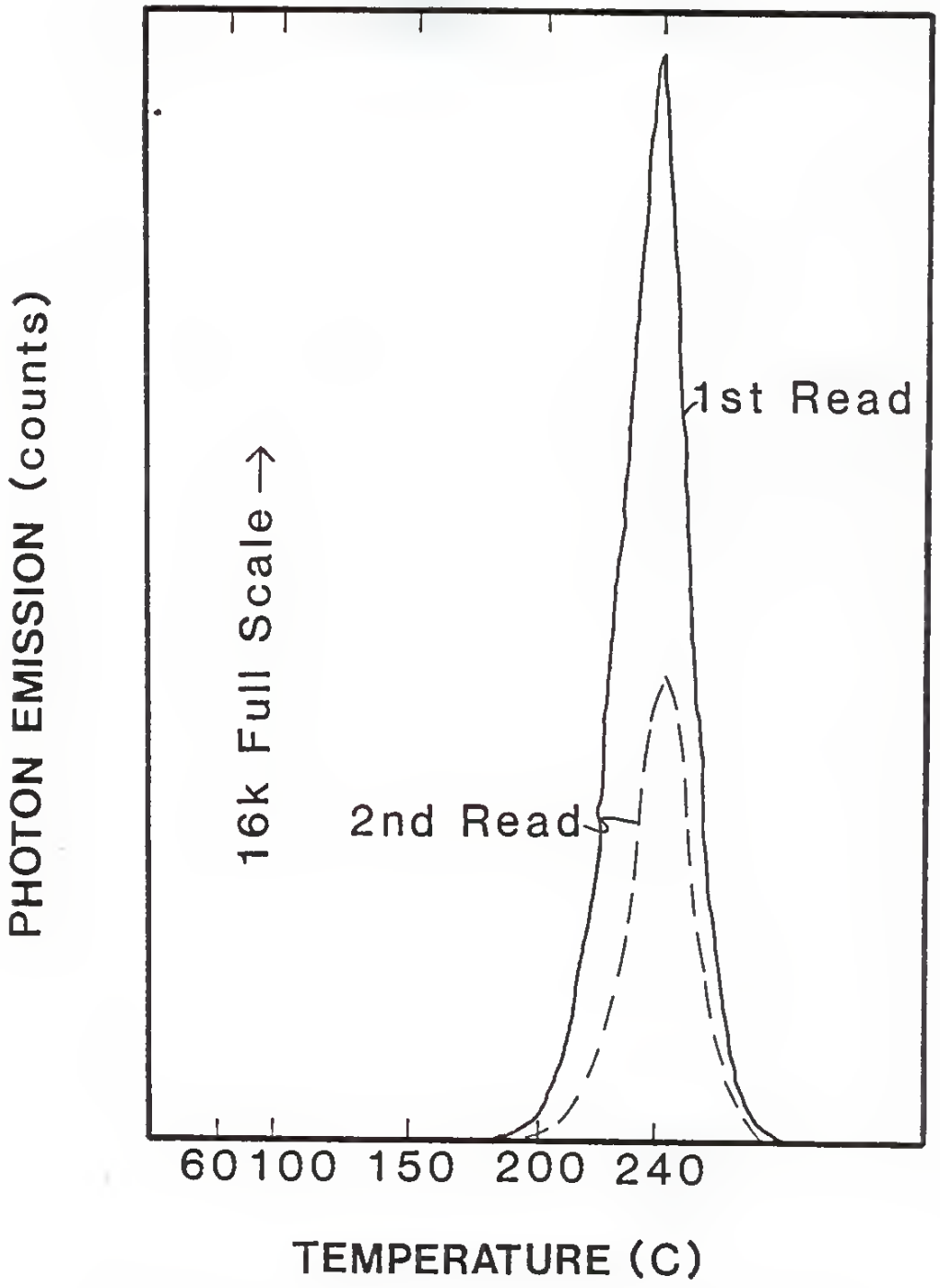

Fig. 5.1. Typical glow curves from a KSU graphite-backed thin LiF TLD after a 1000 R exposure to ^{60}Co gamma rays and a 300°C-10 min post-anneal.

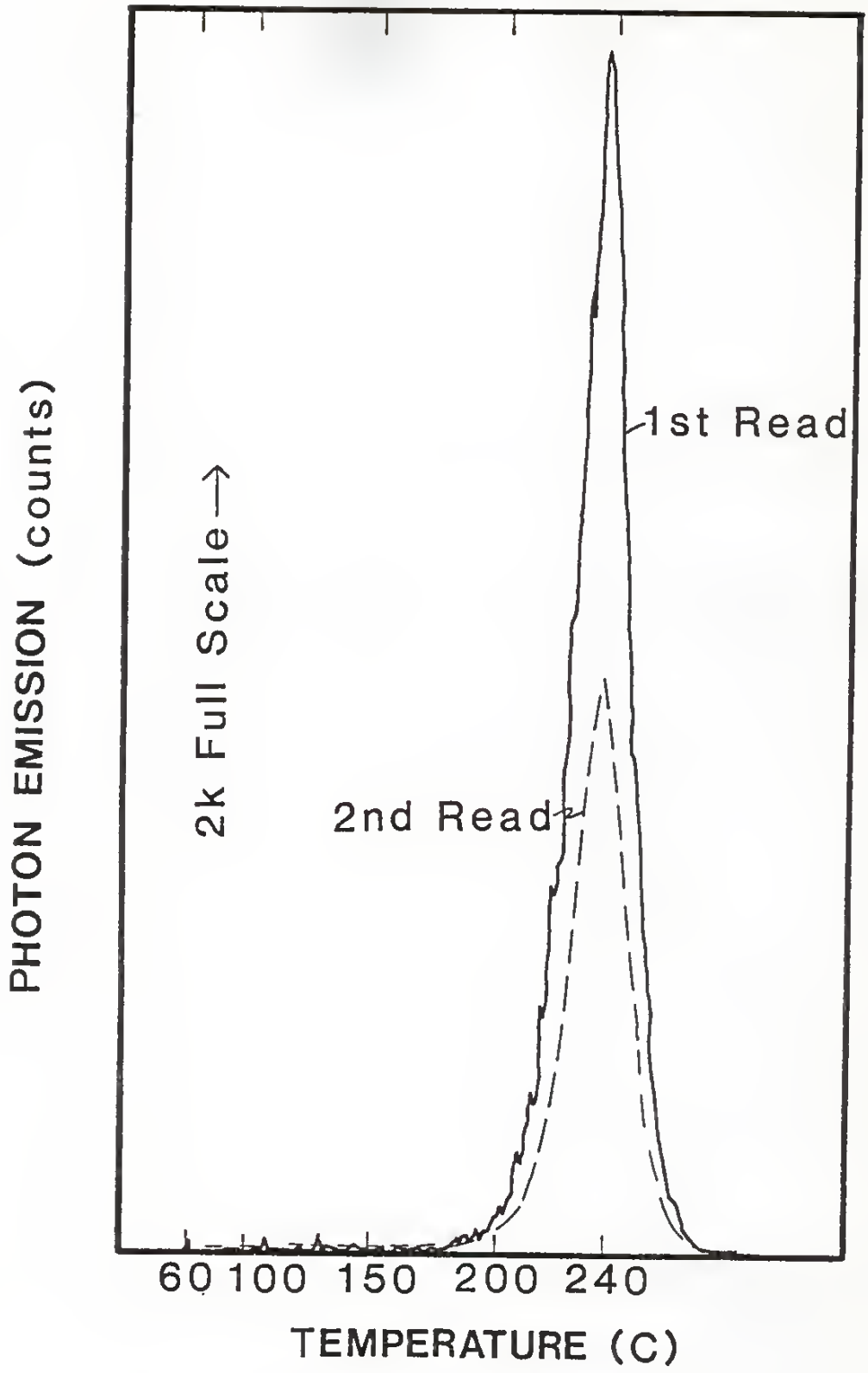

Fig. 5.2. Typical glow curves from a KSU graphite-backed LiF TLD after a 1000 R exposure to ^{60}Co gamma rays and a 325°C-10 min post-anneal.

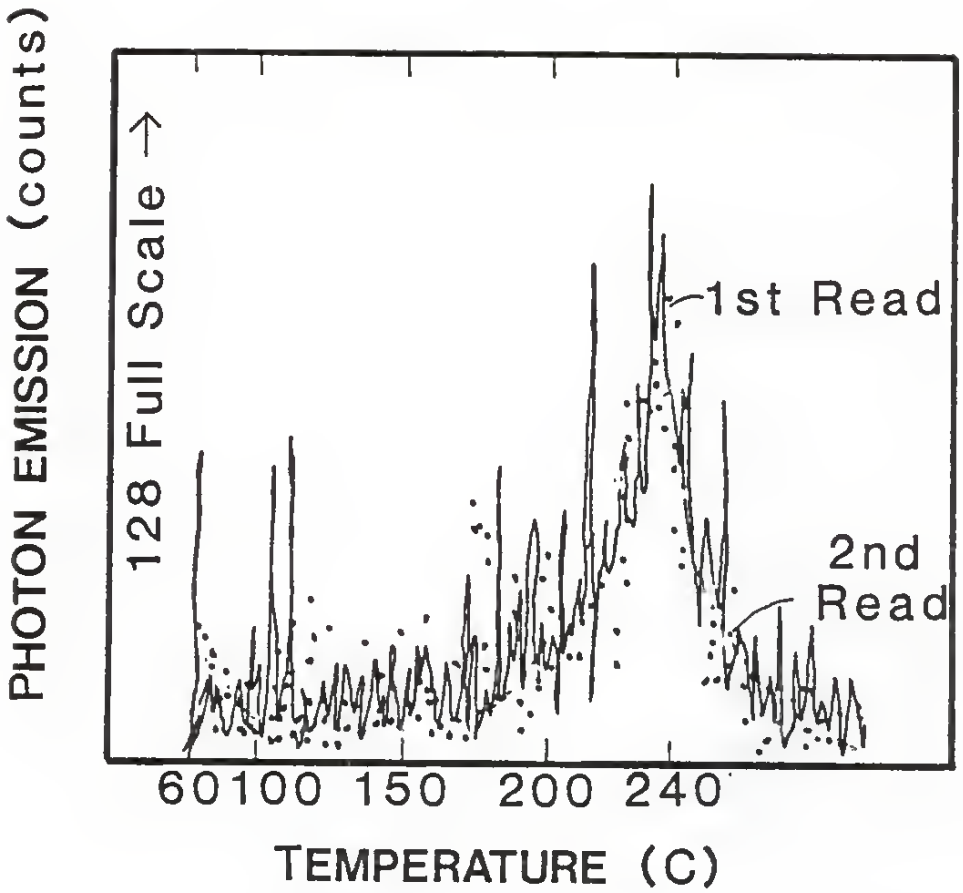

Fig. 5.3. Typical glow curves from a KSU graphite-backed thin LiF TLD after a 1000 R exposure to ^{60}Co gamma rays and a 350°C-10 min post-anneal.

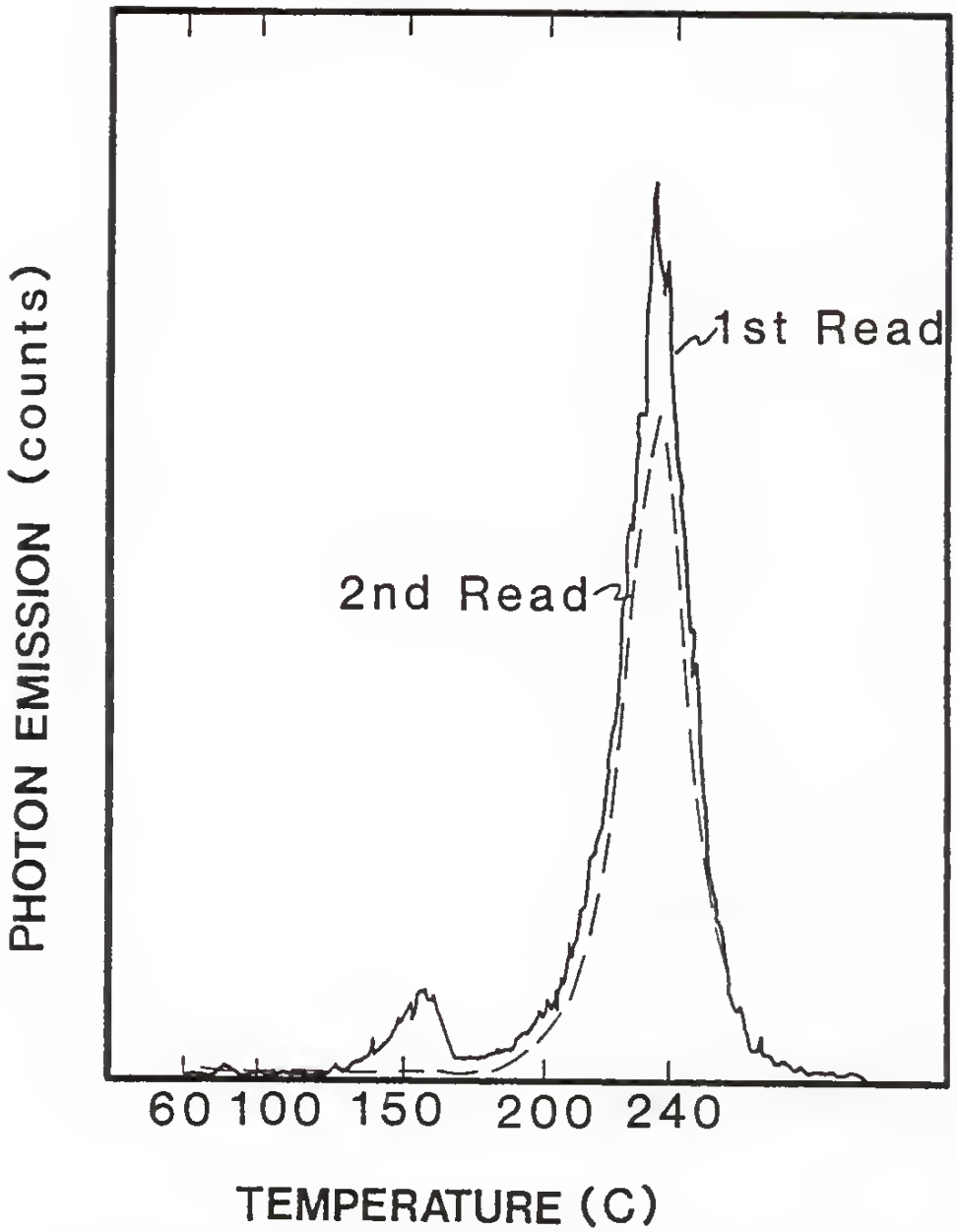

Fig. 5.4. Typical glow curves for KSU graphite-backed thin LiF TLDs after an exposure of 100 mR to ^{137}Cs gamma rays and 100°C-10 min post-anneal. Prior to this the TLD was exposed to 1000 R and post-annealed at 325°C for 10 min.

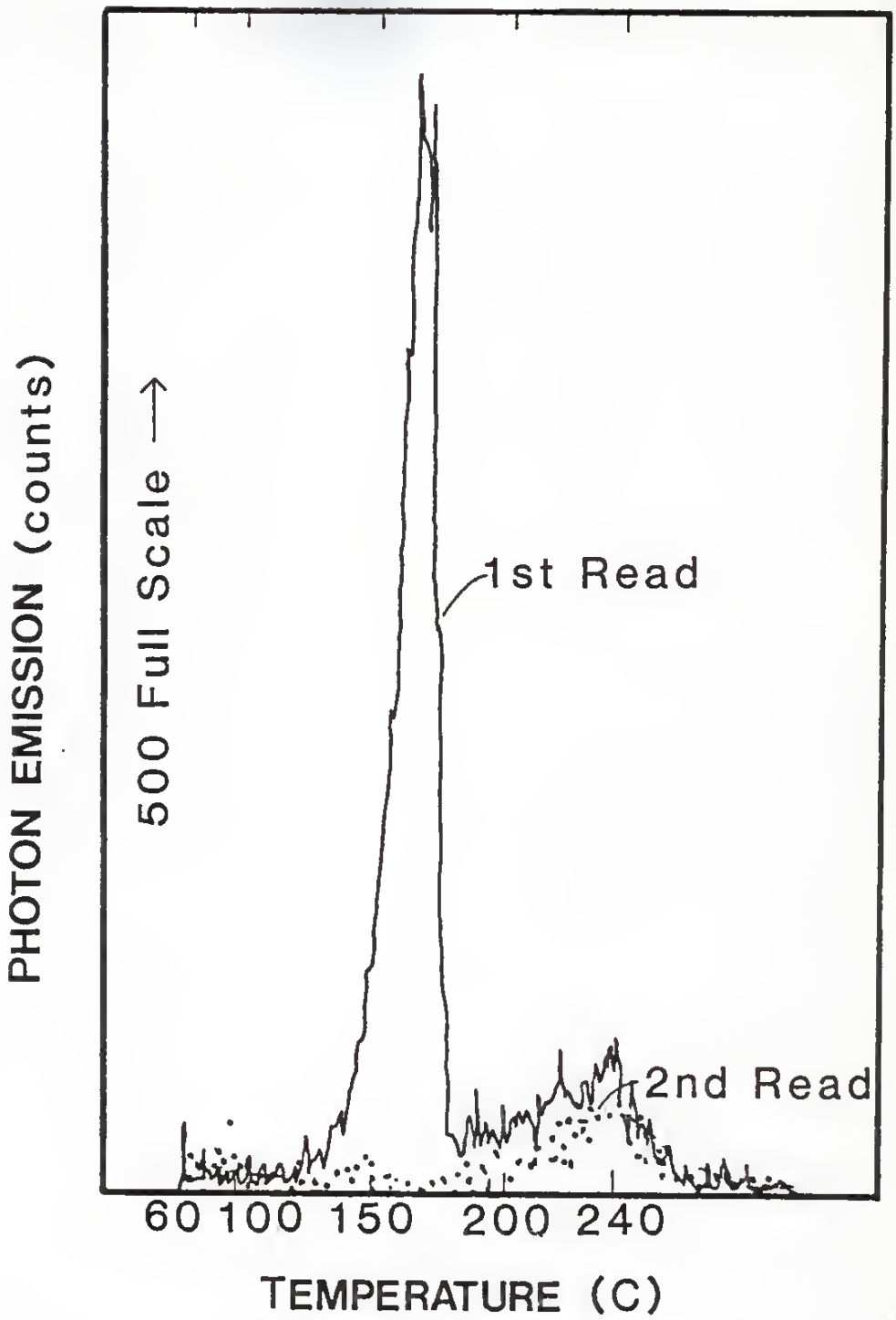

Fig. 5.5. Typical glow curves for a KSU graphite-backed thin LiF TLD after an exposure of 100 mR to ^{137}Cs gamma rays and 100°C-10 min post-anneal. Prior to this the TLD was exposed to 1000 R and annealed at 350°C for 10 min.

standard deviation. This is consistent with the general principles of radiation detection. Two commonly used definitions are that the MDD corresponds to 2 or 3 times the standard deviation of the instruments response to unirradiated TLDs. To be conservative, the definition adopted for this study of thin TLDs is -- the minimum detectable dose refers to the dose which is 3 times the standard deviation of the second readout of irradiated TLDs. For thin LiF TLDs processed on the K-State photon counting TLD analyzer, the standard deviation of the first or second readouts of an unirradiated TLD is essentially the same as the standard deviation of the second readout of an irradiated TLD.

Four factors which significantly contribute to the magnitude and standard deviation of an instruments background response are: 1. non-radiation induced TL from the TLD, 2. dark current from the photomultiplier tube (thermionic emission of electrons from the photocathode, ionization of gas molecules by energetic electrons, decay of radioisotopes in the PMT structure itself, and ohmic leakage for the current integration instruments), 3. thermal radiation from structural elements in the instrument during the heating cycle and 4. noise in the associated electronics. During the course of this study, the non-radiation induced TL was decreased to a minimum level. Thus, the standard deviations in the background or noise level was determined mainly by statistical fluctuations from photons stemming from items 2-4.

As defined, the MDD is dependent not only on the standard deviation of the background reading but also on the magnitude of the TLD signal. This signal strength is a function of the TLD efficiency (i.e., photons emitted/mRad), the light collection efficiency of the TLD analyzer, the PMT sensitivity, and the mode of recording the PMT output (either as

photons or current integration). Due to the small quantity of TL material present in thin dosimeters, a common concern is that the TLD efficiency will be too low for personnel radiation monitoring. Therefore, the MDD was measured for the K-State thin LiF TLDs.

To aid in understanding the meaning of the standard deviations calculated from the second reads of these thin TLDs, an analysis of approximately 450 second readouts, obtained with the photon counting analyzer, was completed. A Chi-squared goodness-of-fit test showed the fit was acceptable, within the 10% and 90% confidence levels, with a Chi-squared value of 15.89 and 10 degrees of freedom. The standard deviation of the no dose distribution was 42.1 counts, which is equal to approximately 1 mRad. It should be noted that the second reading of the thin, graphite-backed TLDs appeared to be totally random and did not display any relationship to the magnitude of the prior TLD dose (or first read). This fact was observed with doses up to several rads of gamma exposure. Due to this result, pre-annealing of these thin LiF TLDs is normally not required if the TL analyzer is set to integrate only the main glow peak.

A specific MDD experiment was performed by exposing thin LiF TLDs to low level radiation fields of both gamma rays and beta particles. Gamma ray measurements were made using a ^{137}Cs source positioned 60 cm from the dosimeters in a 2 mR/min field. Dosimeters with a nominal thickness of 20 mg/cm^2 were encased in a lucite electronic equilibrium shield, irradiated, post-annealed at 100°C for 10 min in a covered Pyrex dish, cooled for 5 min, and processed with both a current integrating analyzer and the photon counting analyzer. Three measurements were completed at each exposure level from 5 to 100 mR. The relative

sensitivity of each TLD was measured and sensitivity corrections were applied to correct for the differences in sensitivity due mainly to thickness variations. Figures 5.6 and 5.7 show the linear exposure response of these two TLD analyzers for gamma-ray irradiated thin TLDs. An example glow curve, measured with the photon counter, is shown in Fig. 5.8 for a 40 mR exposure. The standard deviation of the second readout was calculated averaging all values measured during this experiment, giving gamma-ray MDD values of 3.1 ± 0.5 mR for the photon counter and 13.2 ± 3mR for the current integrating analyzer.

These MDD's are consistent with the average readouts obtained from the low dose data. The mean of the net readout and its standard deviation for six TLDs at 5 mR was 229 ± 19 (8%) counts. Likewise, at 10 mR the current integrating analyzer result for six TLDs was 0.0773 ± 0.0178 (23%) nC. Corresponding results for single TLD measurements would be 229 ± 49 (21%) and 0.0773 ± 0.0436 (56%).

For the beta particle MDD study, bare LiF TLDs were positioned 60 cm from a point $^{90}Sr/^{90}Y$ source where the radiation field was 14.8 mRad/min. Beta particle instrument response data are shown in Figs. 5.9 and 5.10. An example glow curve, for a 60 mRad dose is presented in Fig. 5.11. The statistical MDD's for beta particles are 4.2 ± 0.3 mRads and 18.1 ± 1.3 mRad for the photon counter and current integrating analyzers, respectively.

Beta particle data were not measured at the low 4 mRad level. However, at 20 mRad the mean of the net readouts and their standard deviations for six TLDs was 730 ± 36 (5%) counts and 0.1407 ± 0.0257 (18%) nC. Single TLDs could be expected to give results of 730 ± 88 (12%) counts and 0.2407 ± 0.063 (45%) nC at the 20 mRad level. Original data from the MDD study are shown in Appendix A.

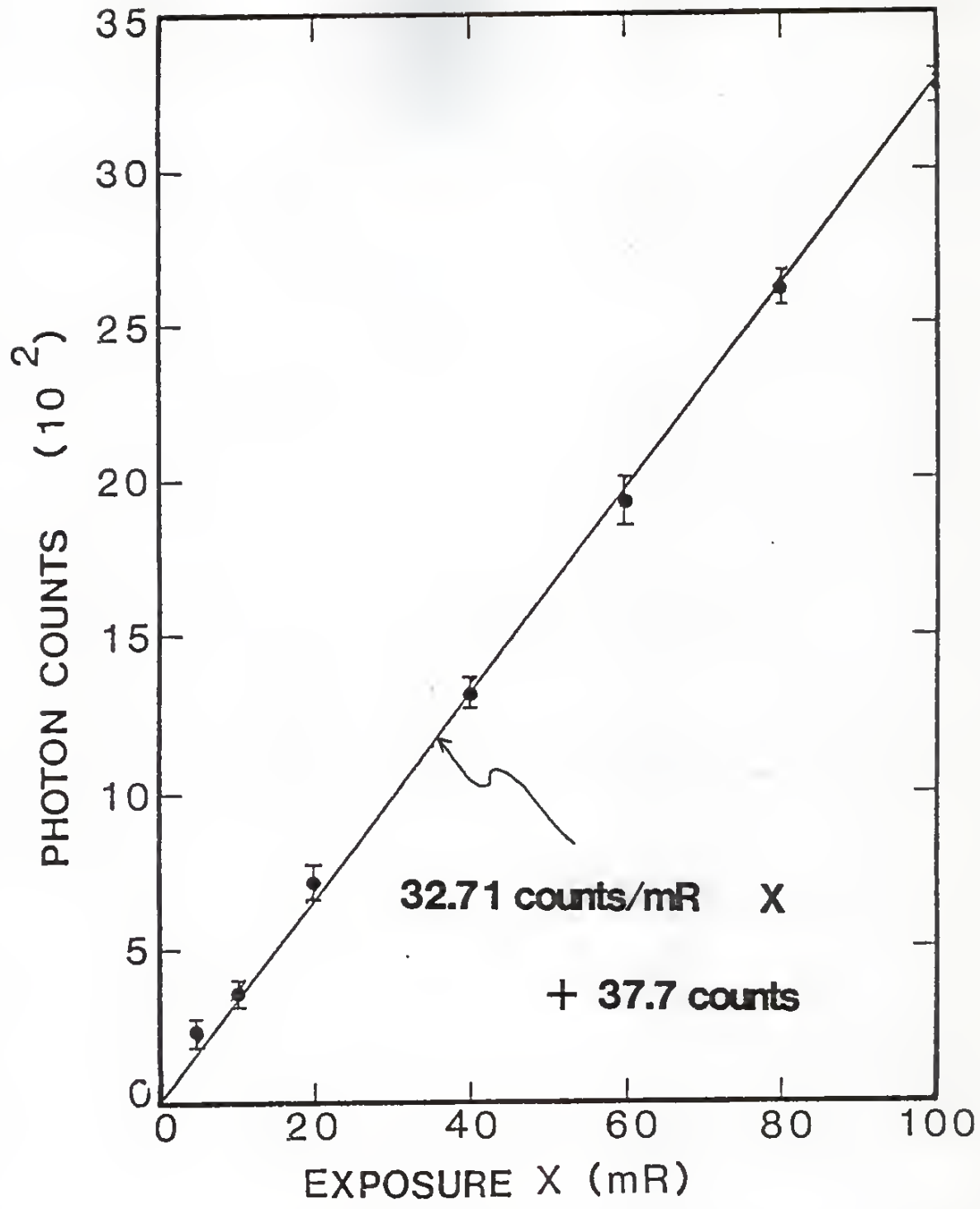

Fig. 5.6. Response of thin LiF TLDs to ^{137}Cs gamma rays measured with the KSU photon counting system.

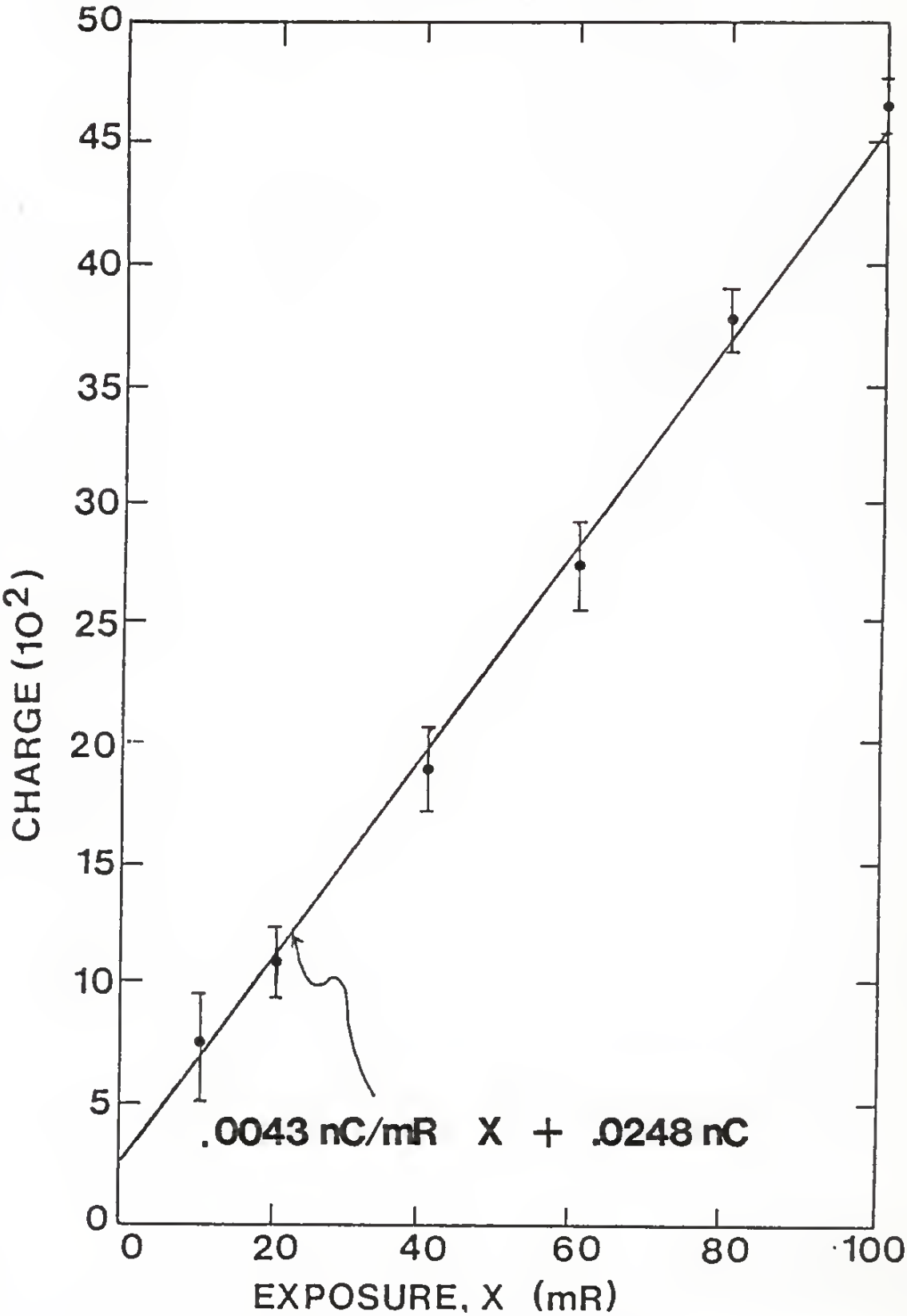

Fig. 5.7. Response of thin LiF TLDs to ^{137}Cs gamma rays measured with the KSU current integrating analyzer.

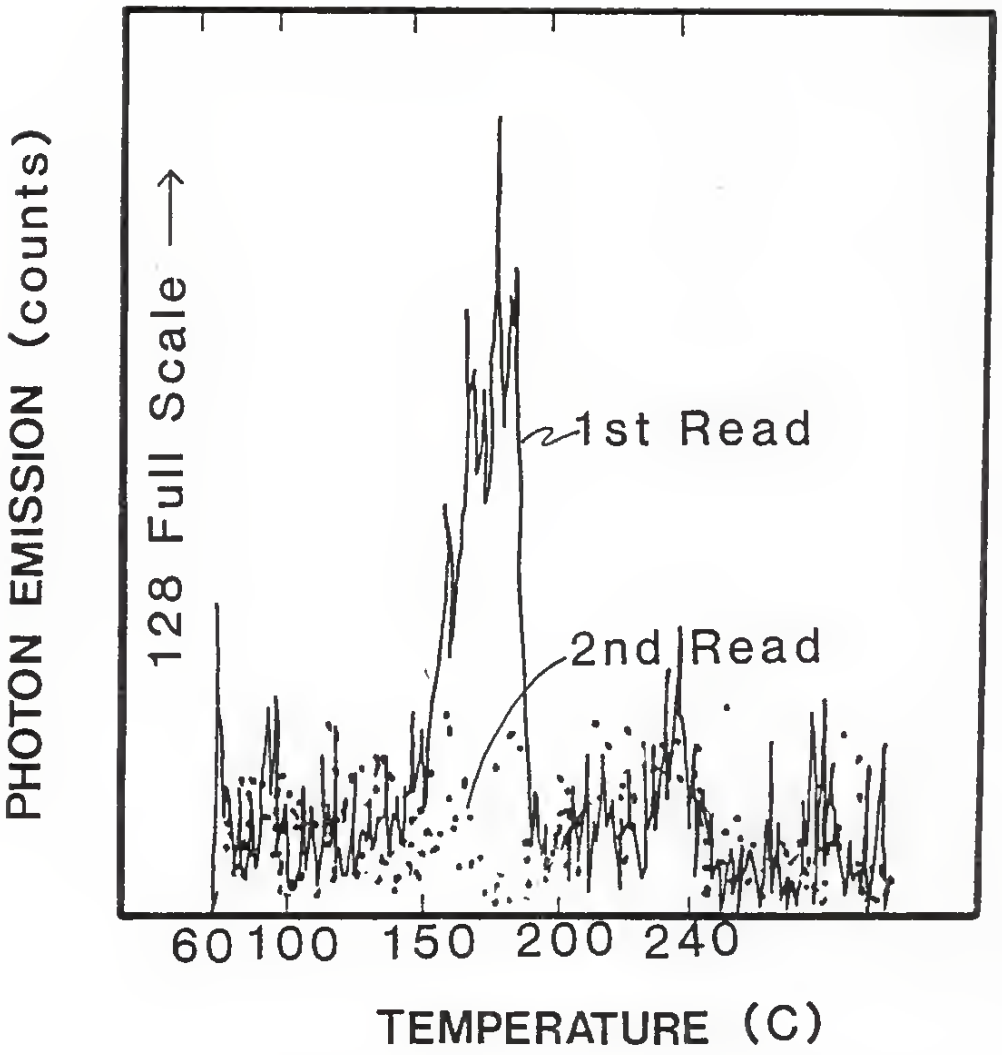

Fig. 5.8. Typical glow curves for a KSU graphite-backed thin LiF TLD after a 40 mR exposure to ^{137}Cs gamma rays and a 100°C-10 min post-anneal measured on the KSU photon counting system.

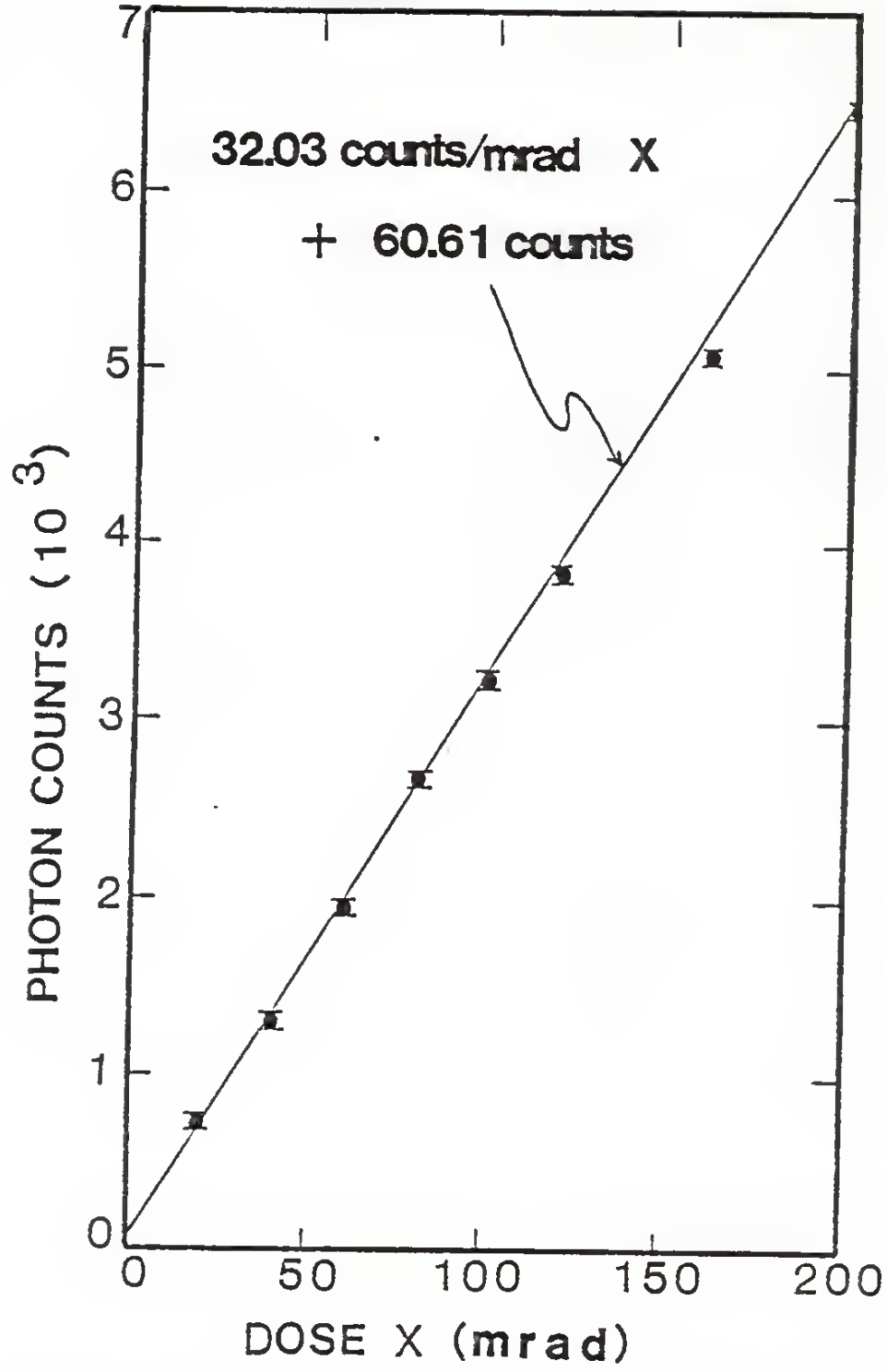

Fig. 5.9. Response of thin LiF TLDs to $^{90}Sr/^{90}Y$ beta particles measured with the KSU photon counting analyzer.

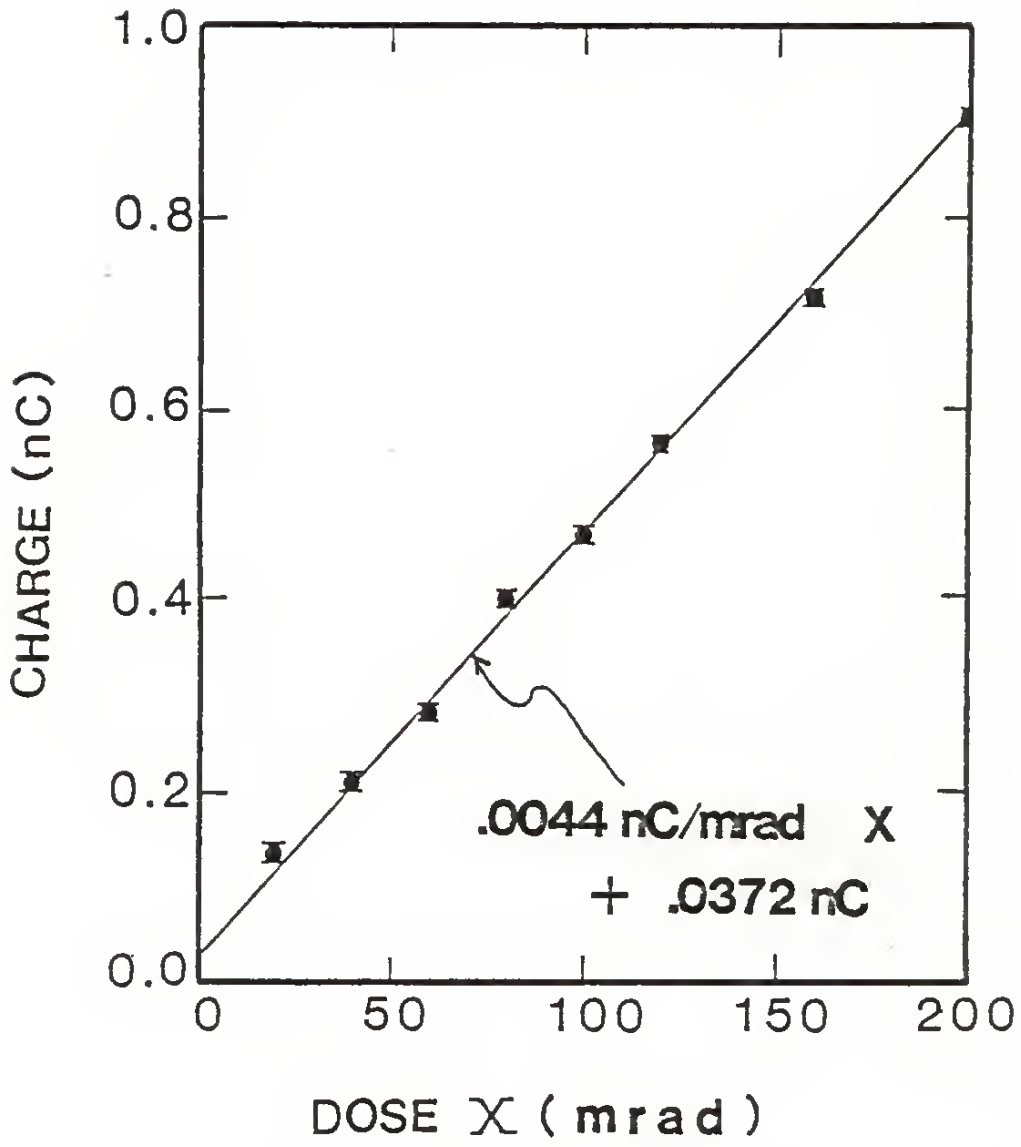

Fig. 5.10. Response of thin LiF TLDs to $^{90}Sr/^{90}Y$ beta particles measured with the KSU current integrating system.

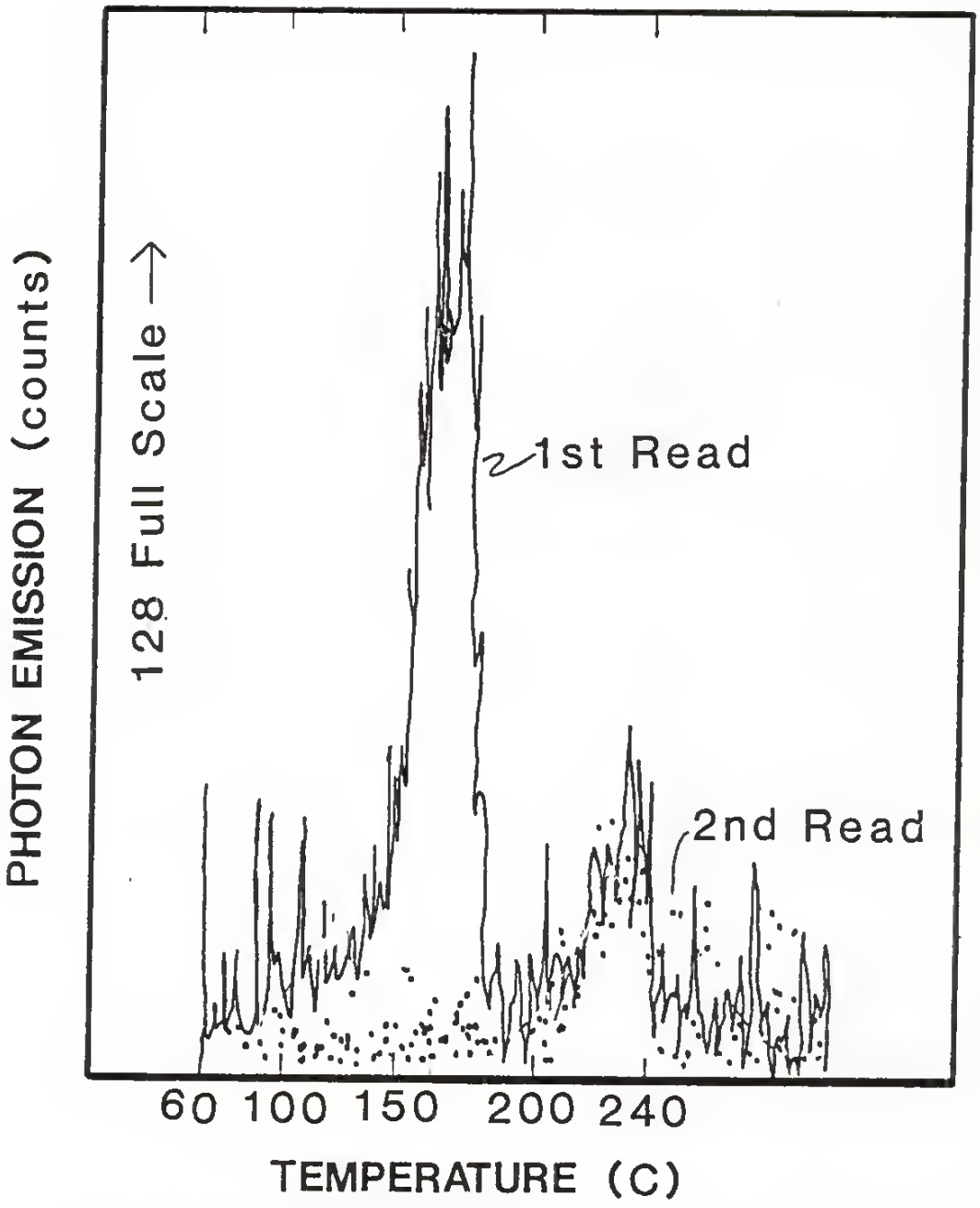

Fig. 5.11. Typical glow curves for a KSU graphite-backed thin LiF TLD after a 60 mrem exposure to $^{90}Sr/^{90}Y$ betas and 100°C-10 min post-anneal measured with the photon counting system.

D. Evaluation of the KSU Lucite Dosimetry Badge

Five lucite dosimeters were constructed according to the specifications shown in Fig. 3.1. In each badge, two thin KSU graphite-backed LiF TLDs were placed in the element wells. To evaluate the performance of the new design, several test runs were performed. Moreover, an algorithm was developed to allow calculation of the beta particle and gamma ray doses in an unknown field from the TL output recorded for each TLD element and corresponding calibration data.

1. An algorithm to calculate gamma ray and beta particle doses for a two-element badge

Since some of the beta particles from a ^{90}Y spectra can penetrate more than 1000 mg/cm^2, it was assumed that both TLD elements, 1 (3.15 mg/cm^2 cover), and 2 (1000 mg/cm^2), would have both a gamma ray and a beta particle response. Thus, to solve for two unknowns, the beta dose B and the gamma dose G, two equations were developed:

$$\beta_1 B + \Gamma_1 G = N_1 \quad , \tag{5.1}$$

and

$$\beta_2 B + \Gamma_2 G = N_2 \quad , \tag{5.2}$$

where β_1 = beta particle response of TLD under thin cover,

β_2 = beta particle response of TLD under thick shield,

Γ_1 = gamma ray response of TLD under thin cover,

Γ_2 = gamma ray response of TLD under thick cover,

N_1 = total thermoluminescent (TL) response of TLD under thin cover,

and N_2 = total TL response of TLD under thick cover.

Combining Eqs. (5.1) and (5.2) and solving for G, an expression is obtained to solve the gamma dose:

$$G = [(N_2/\beta_2) - (N_1/\beta_1)]/[(\Gamma_2/\beta_2) - (\Gamma_1/\beta_1)]. \quad (5.3)$$

Then, by substituting the value calculated for G in Eq. (5.3) into Eq. (5.1), the beta particle dose becomes:

$$B = [N_1 - (\Gamma_1 \times G)]/\beta_1. \quad (5.4)$$

2. Calibration of the KSU badge

To obtain the response values of the TLDs in the KSU badges, the badges were subjected to two separate irradiations. First the dosimeters were exposed to 100 mR of ^{137}Cs gamma rays; and, after a 100°C-10 min post-anneal to TL output from the photon counting system was recorded for each TLD. Then, the same procedure was done after a 108 mrad exposure to $^{90}Sr/^{90}Y$ beta particles. The response values (i.e. β_1) are found by taking the TL output and dividing by the corresponding exposure. For instance, β_1 is the beta particle response value for a thin cover. Hence, the TL output from the thin-covered TLD after an exposure to $^{90}Sr/^{90}Y$ divided by the exposure is the value for β_1, and so on for β_2, Γ_1, and Γ_2. Calibration data and response values are shown in Table 5.1 as sensitivity-corrected average values for the five badges.

A question which always arises during calibration is the relative sensitivity of TLDs to beta particles and gamma rays. Fig. 5.12 shows representative glow curves for thin LiF TLDs exposed to 103 mrad from a ^{137}Cs gamma ray source, and for thin TLDs exposed to 102 mrad from a ^{90}Y beta particle source. By careful observation of Fig. 5.12 and from the fact that the slopes of the beta particle and gamma ray sensitivity curves are approximately the same (Figs. 5.6 and 5.9, or Figs. 5.7 and 5.10), the beta factor for an uncovered TLD is approximately 1.

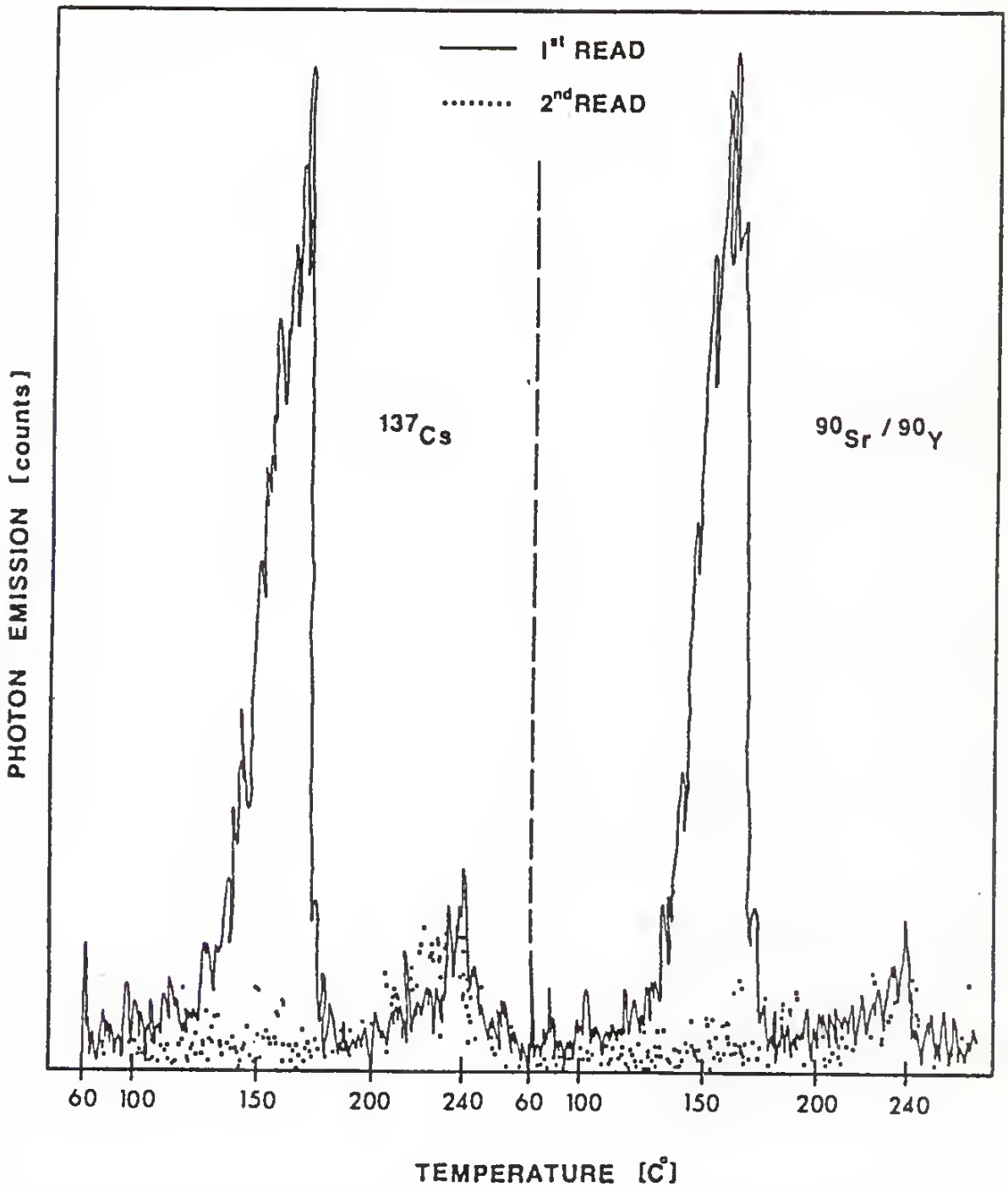

Fig. 5.12. Representative glow curves for thin LiF TLDs exposed to 103 mrad from a ^{137}Cs gamma ray source and thin TLDs exposed to 102 mrad from a ^{90}Y beta particle source.

However, the TLDs in the KSU badge are covered. Thua, beta particles which are created by gamma rays are shielded. This results in a lower gamma sensitivity for both elements, but particularly element 2. From the results tabulated in Table 5.1, the KSU badge beta factor (β_1/Γ_1) is 1.08. However, the relative gamma ray sensitivity for element 1 to element 2 (Γ_1/Γ_2) is 1.37 which shows the dramatic effect of the thick shield on beta particles created by gamma rays.

3. Mixed beta particle, gamma ray field test resulta

The final step of the evaluation was to expoaure the badges to mixed gamma ray, beta particle radiation fields and test the badges' performance. Dosimeter responae evaluations were tested at several dose ratios. This was done to insure that the badges would reapond in either high gamma or high beta dose regions, or a mixture of the two.

The tests were performed at dose ratios of nominally 1 to 1, 5 to 1, and 10 to 1. For the 1 to 1 test, the gamma dose was measured 9.6% high and the beta dose was 10.4% low for 50 mR and 50 mrad expoaures, respectively. For a gamma dose of 250 mR and beta dose of 54 mrad, the measured values were 2.4% and 5.2% high, respectively. For the other 5 to 1 test, the beta and gamma doses were both low, 3.1% and 13.2%, respectively. For the first 10 to 1 test, the gamma exposure (large dose rate) was measured 3.6% high, and the beta exposure (low dose rate) was 1.2% high. For the final test, the beta dose measured was 5.0% below the 325 mrad level, and the gamma dose was 29.7% below the 30 mR level. See Table 5.2 for the tabulated final results of the badges' mixed-field tests and Appendix G for the invididual TLD readings.

Table 5.1 Calibration results of 5 KSU lucite badges using thin graphite-backed TLDs and reported as sensitivity-corrected averages. The gamma ray dose was 101 mR and the beta particle dose was 109 mrad.

ELEMENT SHIELD	ELEMENT RESPONSE Gamma Dose TL (counts)[a]	Beta Dose TL (counts)	RESPONSE PARAMETERS (counts/mR or mrad)
Thin Cover	3724.6	4306.8	$\Gamma_1 = 36.88$ $\beta_1 = 39.88$
Thick Cover	2712.4	202	$\Gamma_2 = 26.86$ $\beta_2 = 1.87$

[a]Counts correspond to number of TL emissions recorded by the photon counting system.

Table 5.2. Final test results for the KSU two-element lucite badge. The badges were exposed to mixed fields of beta particles and gamma rays at ratios of nominally 1 to 1, 5 to 1, and 10 to 1.

Gamma Ray Exposure Given (mR)	Beta Particle Dose Given (mrad)	Measured Gamma Gamma Ray Dose[a] (mR)	Measured Beta Particle Dose[a] (mrad)
50	54	54.8 ± 2.1	48.4 ± 2.7
250	54	256.1 ± 3.8	56.8 1 3.4
50	272	43.4 ± 1.4	263.5 ± 6.4
300	33	310.8 ± 6.5	33.4 ± 1.0
30	325	21.1 ± 2.0	308.9 ± 6.2

[a]Average of 5 TLD elements.

VI. CONCLUSIONS

Several studies were performed with KSU thin graphite-backed TLDs and thick commercial TLDs by performing irradiation experiments with beta and gamma sources. Several beta dosimetry concepts have been clarified from the results of those studies.

A good indication of why only 3.15 mg/cm^2 is a sufficient shield for the beta dose element is LiF's relative insensitivity to the environment. By using a composite LiF TLD of rugged construction, a 1 mil aluminized mylar layer is ample thickness to prevent the contamination of the element in a radiation field.

The minimum detectable dose that a dosimeter can detect is a function of both the radiation sensitive element and the analyzing system. Whereas the TL phosphor must have enough material present to be fairly sensitive to radiation, the noise levels in the analyzing system must remain constant. If the standard deviation of the second readout of a TLD is large compared with the radiation induced light emission from the TLD, then a different analyzing system (or TLD) must be investigated. The KSU photon counting system was shown to be ideal for measuring photon emission from the less sensitive thin graphite-backed LiF TLDs.

By using a thin graphite-backed LiF TLD in the KSU personnel badge, these badges may accidentally be exposed to high dose fields (1 KR range) of radiation and still be used. Teflon-matrix thin TLDs have the disadvantage of melting at high temperatures. KSU thin TLDs can be annealed at high temperatures to remove the high temperature traps which occur at high exposures. However, since a sensitivity change will accompany this process, a new sensitivity factor would have to be found.

It was also shown that the KSU two-element badge can be used in a mixed beta-gamma field to measure the desired beta and gamma components. However, a need for increased gamma dose sensitivity is evident. The results showed that in a high beta dose field, the gamma dose was under-predicted each time, which points to the need for higher sensitivity from element 2 (1000 mg/cm^2 cover).

VII. SUGGESTIONS FOR FURTHER STUDY

The ultimate design for a personnel dosimeter badge is one which accounts for neutrons and X-rays as well as gamma rays and beta particles. The two-element KSU badge concept should be extended to three- and possibly four-elements to broaden its use. Also, several other radiation sensitive materials such as CaF_2 and $Li_2B_4O_7$ should be tested for possible inclusion into the badge design because of their higher sensitivity.

Continued research should also be performed on the two-element design to optimize the low gamma dose response. Investigations should be made by substituting a thick TLD element (i.e., the Harshaw 3.175 mm x 3.175 mm x .89 mm standard LiF chip) for the thin element which was used for the deep dose. The thick chip has a much higher sensitivity, and would be able to detect much lower gamma doses. Also, an angular response investigation for both beta particles and gamma rays should be performed.

The effects of a high Z, dense cover material such as lead should also be investigated. If the response of such materials to radiation could be characterized, their use as a shield material would improve the angular response of dosimeters to beta particles.

An additional study should be performed on the backscatter effect introduced by the graphite backing on the thin KSU TLD. Experiments should show the effect on the response of the TLD as a function of varying graphite thickness.

Finally, it is suggested that future annealing studies for both thin and thick TLDs be based upon the concept of UV light induced phototransfer.[30] Jain showed that phototransfer occurred from the

~400°C region to the lower peaks, 150 and 200°C. Thus, it would be possible to anneal at 330°C. This would be an ideal procedure for the thin graphite-backed TLDs. Whereas short duration anneals at 400°C are possible, extended exposures to 400°C darken the polyimide adhesive material and weaken its bond.

VIII. ACKNOWLEDGEMENTS

I would like to take this opportunity to express my deepest gratitude to Dr. G. G. Simons for his help and guidance during this research project and during the preparation of this thesis. I am also thankful to Tim DeBey for his insight at the beginning of my work on this project.

I would also like to express my appreciation to the Battelle Pacific Northwest Laboratories for sponsoring this research and providing the necessary financial support.

Finally, I would like to thank my wife, Marsha, for her tireless support.

IX. REFERENCES

1. International Commission on Radiological Protection, "Recommendations of the International Commission on Radiological Protection," ICRP Publication 26, (Pergamon Press, Oxford, 1977).

2. Division of Rules and Records - United State Regulatory Commission, "Standards for Protection Against Radiation," Title 10, Chapter 1, Part 20, Code of Federal Regulations, (U.S. Government Printing Office, Washington, D.C., 1978).

3. M.S.H. DiFiore, Atlas of Human Histology, 4th edition, Lea and Febigen, Philadelphia (1974), pp. 100-101.

4. W.S. Snyder, Chairman, "Report of the Task Group on Reference Man," ICRP Publication 23, (Pergamon Press, Oxford, 1975).

5. K.D. Stansbury, "Evaluation of a $^{90}Sr/^{90}Y$ Beta Beam Flattening Filter," Master's Thesis, Kansas State University (1984).

6. A.B. Chilton, J.K. Shultis, and R.E. Faw, Principles of Radiation Shielding (Prentice-Hall, Englewood Cliffs, New Jersey, 1984), pp. 67-74.

7. L. Katz and A.S. Penfold, Rev. of Mod. Phys. 24, 28 (1952).

8. D.C. Rogers and G.E. Gordon, Nucl. Inst. and Meth., 37, 262 (1965).

9. W.G. Cross (private communication).

10. M.J. Martin and P.H. Blichert-Taft, Nucl. Data Tables, 8:1-198, (1970).

11. R.E. Lapp and H.C. Andrews, Nuclear Radiation Physics, 4th ed. (Prentice-Hall, Englewood Cliffs, New Jersey, 1972), pp. 218.

12. A.C.G. Mitchell, in Beta- and Gamma-Ray Spectroscopy, edited by K. Siebahn (North Holland, Amsterdam, 1955), pp. 240-245.

13. G.K. Schenter and P. Vogel, Nucl. Sci. and Engg., 83, 393, (1983).

14. H. Behrens and J. Jänecke, Numerical Tables for Beta Decay and Electron Capture, Springer Valeg, Berlin (1969).

15. C.S. Wu and S.A. Moszkowsky, Beta Decay, (Interscience Publishers, New York, NY, 1966), pp. 58-106.

16. W. G. Cross (private communication).

17. M.J. Berger, "Distribution of Absorbed Dose Around Point Sources of Electrons and Beta Particles in Water and Other Media," NM/MIRD Pamphlet No. 7, (1971).

18. L.V. Spencer, Phys. Rev., 9, 1597, (1955).

19. L.V. Spencer, "Energy Dissipation by Fast Electrons," National Bureau of Standards Monograph No. 1., (1959).

20. Berger, p. 9.

21. Berger, p. 16.

22. W.G. Cross, Phys. Med. Biol., 13, 611, (1968).

23. Berger, p. 13.

24. Berger, p. 15.

25. T.M. DeBey, "Skin Dosimetry Using Thermoluminescent Dosimeters," Master's Thesis, Kansas State University (1983).

26. DeBey, p. 35.

27. DeBey, p. 36.

28. C.A. Carlsson, "Thermoluminescence of LiF: Dependence of Thermal History," Phys. Med. Biol., 14, No. 1, 107 (1969).

29. J. Wald, L.A. DeWerd, and T.G. Stoebe, "Long Term Recycling Characteristics of LiF (TLD-100) Dosimeter Material," Health Physics, 33, 303 (Sept. 1977).

30. V.K. Jain, "Phototransfer, Sensitization and Re-estimation of Dose in Lithium Flouride TLD," Health Physics, 41, 363 (1981).

APPENDIX A: MINIMUM DETECTABLE DOSE STUDY

Gamma ray and beta particle response experimental data.

Table A.1. Gamma ray response data for thin LiF TLDs.

TLD ID	THICKNESS (mg/cm²)	100 mR Exposure						80 mR Exposure					
		1st[a]	2nd[b]	1st	2nd	1st	2nd	1st	2nd	1st	2nd	1st	2nd
A	16.7	4494[c]	385	4500	307	4239	363	3442	375	3448	339	3275	325
B	17.4	4355	376	4698	360	4346	380	3448	352	3541	385	3396	318
C	15.4	3760	373	3457	340	3646	346	3140	383	2873	384	2894	382
D	15.4	3427	357	3590	331	3522	380	2739	341	2675	359	2843	356
E	13.4	3367	434	3375	328	3468	397	2703	402	2703	428	2804	304
F	13.4	3133	415	3099	359	3093	377	2456	423	2621	329	2510	396
G	13.4	.954[d]	.395	.933	.439	.927	.436	.820	.447	.889	.407	.826	.439
H	12.7	.880	.410	.875	.443	.886	.414	.832	.430	.793	.423	.850	.439
I	12.7	.902	.380	.861	.438	.846	.449	.807	.441	.786	.426	.772	.421
J	12.7	.944	.392	.941	.428	.874	.473	.813	.467	.830	.404	.837	.400
K	12.7	.961	.441	.949	.440	.942	.448	.829	.503	.865	.445	.883	.436
L	9.4	.829	.454	.762	.441	.753	.411	.746	.433	.722	.424	.703	.447

Table A.1 (Cont'd.).

TLD ID	THICKNESS (mg/cm²)	60 mR Exposure						40 mR Exposure					
		1st[a]	2nd[b]	1st	2nd	1st	2nd	1st	2nd	1st	2nd	1st	2nd
A	16.7	2735[c]	442	2555	327	2394	350	1825	365	1826	331	1824	370
B	17.4	2744	361	2686	364	2700	338	1981	356	1804	327	1979	320
C	15.4	2441	366	2209	396	2192	354	1603	334	1594	352	1573	378
D	15.4	2335	306	2112	423	2079	398	1623	333	1598	291	1585	313
E	13.4	2147	317	2015	355	2098	353	1530	340	1521	286	1506	398
F	13.4	2060	292	1975	393	1849	455	1497	468	1417	353	1417	342
G	13.4	.802[d]	.423	.717	.438	.792	.432	.659	.430	.663	.459	.643	.432
H	12.7	.728	.423	.692	.445	.718	.465	.585	.449	.702	.444	.642	.438
I	12.7	.757	.462	.709	.432	.684	.427	.610	.494	.627	.439	.614	.496
J	12.7	.728	.469	.693	.503	.690	.440	.634	.452	.631	.431	.612	.434
K	12.7	.765	.445	.761	.417	.715	.417	.639	.439	.660	.420	.628	.420
L	9.4	.700	4.32	.590	.428	.623	.454	.720	.517	.595	.417	.561	.446

Table A.1 (Cont'd.).

TLD ID	THICKNESS (mg/cm²)	20 mR Exposure						10 mR Exposure					
		1st[a]	2nd[b]	1st	2nd	1st	2nd	1st	2nd	1st	2nd	1st	2nd
A	16.7	1171[c]	352	1122	391	1164	436	774	317	920	356	777	411
B	17.4	1221	339	1208	305	1115	361	806	404	810	364	800	426
C	15.4	987	361	1121	406	961	326	691	306	701	418	732	375
D	15.4	1044	381	1051	317	972	345	682	395	794	417	1020	319
E	13.4	1088	349	1006	382	1039	367	762	435	710	331	794	394
F	13.4	1013	372	953	353	1072	307	716	455	692	415	771	364
G	13.4	.531[d]	.422	.541	.437	.587	.472	.522	.474	.517	.447	.527	.461
H	12.7	.529	.411	.557	.403	.547	.332	.526	.438	.510	.400	.493	.414
I	12.7	.545	.422	.522	.421	.601	.466	.481	.406	.500	.443	.482	.421
J	12.7	.478	.430	.524	.413	.545	.440	.471	.461	.523	.422	.612	.446
K	12.7	.584	.399	.547	.454	.536	.470	.517	.453	.498	.462	.516	.469
L	9.4	.497	.430	.505	.403	.521	.405	.483	.437	.586	.442	.491	.413

Table A.1 (Cont'd.).

TLD ID	THICKNESS (mg/cm²)	5 mR Exposure					
		1st[a]	2nd[b]	1st	2nd	1st	2nd
A	16.7	592[c]	354	696	431	585	316
B	17.4	705	369	555	411	576	334
C	15.4	561	408	560	352	563	391
D	15.4	754	293	709	385	820	353
E	13.4	522	292	592	402	608	345
F	13.4	613	347	633	398	629	387
G	13.4	.492[d]	.472	.495	.454	.483	.441
H	12.7	.507	.413	.489	.442	.484	.429
I	12.7	.506	.442	.460	.469	.455	.435
J	12.7	.439	.415	.480	.446	.500	.452
K	12.7	.487	.398	.471	.423	.522	.427
L	9.4	.461	.428	.516	.447	.490	.410

[a] 1st response data from 2-cycle readout in photon counting and current integrating systems.

[b] 2nd response data from 2-cycle readout in photon counting and current integrating systems.

[c] TLD's A-F were cycled through photon counting system, thus, the readout is in number of photons.

[d] TLD's G-L were cycled through current integrating system, thus, the readout is in nC.

Table A.2. Beta particle response data for thin LiF TLDs.

		100 mrad Absorbed Dose						80 mrad Absorbed Dose					
TLD ID	THICKNESS (mg/cm^2)	1st[a]	2nd[b]	1st	2nd	1st	2nd	1st	2nd	1st	2nd	1st	2nd
A	16.7	3996[c]	346	4296	503	3844	373	3465	386	3267	381	3415	417
B	17.4	4247	283	4284	352	4182	285	3760	331	3511	404	3522	306
C	15.4	3519	390	3634	361	3510	367	3025	371	2795	263	2833	408
D	15.4	3412	316	3814	432	3468	393	3190	314	2903	314	3143	450
E	13.4	3302	315	3412	369	3183	377	2869	416	3162	353	2728	354
F	13.4	2895	401	3123	344	2900	367	2707	381	2546	333	2404	298
G	13.4	.992[d]	.583	1111	.495	1.001	.500	.932	.462	.908	.471	.895	.486
H	12.7	.991	.560	.991	.485	.976	.510	.916	.474	.876	.474	.888	.468
I	12.7	1.036	.583	.971	.465	.916	.461	.852	.476	.857	.468	.854	.534
J	12.7	1.050	.523	1.067	.497	1.058	.480	1.014	.462	.946	.506	.902	.455
K	12.7	1.072	.557	1.091	.546	.937	.505	.972	.484	.903	.474	.895	.498
L	9.4	.875	.527	.802	.505	.849	.524	.784	.515	.746	.470	.846	.465

Table A.2 (Cont'd).

TLD ID	THICKNESS (mg/cm²)	60 mrad Absorbed Dose						40 mrad Absorbed Dose					
		1st[a]	2nd[b]	1st	2nd	1st	2nd	1st	2nd	1st	2nd	1st	2nd
A	16.7	2502[c]	381	2657	357	2670	423	1874	327	1948	353	1869	345
B	17.4	2630	360	2825	321	2875	404	1866	375	1966	371	1915	350
C	15.4	2199	432	2239	336	2243	371	1649	487	1559	317	1705	416
D	15.4	2273	301	2324	352	2251	364	1746	391	1777	353	1718	380
E	13.4	2139	334	2196	397	2253	382	1666	446	1566	347	1667	439
F	13.4	1972	410	1948	376	1979	344	1444	473	1518	370	1448	346
G	13.4	.838[d]	.450	.811	.474	.804	.479	.764	.525	.792	.509	.731	.499
H	12.7	.794	.486	.779	.474	.824	.496	.769	.505	.717	.499	.681	.511
I	12.7	.745	.483	.749	.488	.771	.482	.673	.506	.692	.575	.691	.490
J	12.7	.815	.502	.833	.489	.822	.549	.764	.528	.751	.519	.719	.497
K	12.7	.788	.561	.816	.476	.837	.450	.757	.501	.760	.530	.776	.506
L	9.4	.706	.504	.692	.590	.673	.478	.680	.524	.708	.473	.661	.506

Table A.2 (Cont'd).

TLD ID	THICKNESS (mg/cm²)	20 mrad Absorbed Dose					
		1st[a]	2nd[b]	1st	2nd	1st	2nd
A	16.7	1198[c]	354	1052	363	1192	365
B	17.4	1259	343	1136	436	1287	310
C	15.4	1115	394	1052	434	1057	427
D	15.4	1135	393	1155	390	1114	314
E	13.4	1010	447	1077	358	1051	361
F	13.4	901	390	1048	356	999	307
G	13.4	.641[d]	.493	.657	.498	.645	.422
H	12.7	.641	.523	.649	.478	.652	.479
I	12.7	.619	.491	.664	.601	.660	.536
J	12.7	.654	.491	.641	.474	.680	.544
K	12.7	.677	.563	.651	.532	.651	.499
L	9.4	.613	.550	.634	.549	.571	.486

[a] 1st response data from 2-cycle resdout in photon counting and current integrating systems.

[b] 2nd response data from 2-cycle readout in photon counting and current integrating systems.

[c] TLD's A-F were cycled through photon counting system, thus, the readout is in number of photons.

[d] TLD's G-L were cycled through current integrating system, thus, the resdout is in nC.

APPENDIX B: ANNEALING STUDY

Gamma ray response experimental data from large doses followed by high temperature anneals.

Table B.1. Gamma ray response experimental data from 1000 R ^{60}Co exposures followed by various high temperature anneals for 10 minutes[a] taken by the KSU photon counting system.

TLD ID	350°C 1st[b]	350°C 2nd[c]	325°C 1st	325°C 2nd	300°C 1st	300°C 2nd	275°C 1st	275°C 2nd
0	556[d]	407	590	455	2682	1335	180987	2656
1	1148	480	1143	558	2868	1883	123227	3695
2	638	432	695	391	1494	1562	363315	3732
3	736	520	796	423	1735	1562	28414	5059
4	847	462	1215	739	8609	3507	499896	4230
5	613	411	2206	970	4766	3726	60324	4477
6	1149	434	1119	540	4312	1245	32239	2016
7	540	417	862	597	2963	1566	17732	2130
8	537	373	1661	824	14796	1969	60783	2203
9	666	417	909	817	5003	1958	20836	2284

[a] A previous study on a commercial Harshaw reader concluded a 10 min anneal at 325°C would be sufficient to remove the trapped energy from the thin LiF TLD.

[b] 1st response data from the 2-cycle KSU photon counting system.

[c] 2nd response data from the 2-cycle KSU photon counting system.

[d] No. of photons emitted.

APPENDIX C: ABSORBED DOSE PERCENTILE DISTANCES

Absorbed dose percentile distance graphs for various personnel badge cover, TLD, and backing materials. Data are also included for muscle tissue for comparison. These values were calculated using Berger's scaling procedure and numerical values for water as the reference.[a] Average energies were used for the following beta particle spectra: ^{147}Pm, ^{133}Xe, ^{204}Tl, ^{47}Ca, ^{132}I, ^{86}Rb, ^{15}O, ^{49}Sc, ^{90}Y, ^{76}As, and ^{28}Al, respectively. Average and maximum endpoint energies of these spectra are shown in Table C.1.

[a]Martin J. Berger, "Distribution of absorbed dose around point sources of electrons and beta particles in water and other media," NM/MIRD Pamphlet No. 7 (1971).

Table C.1. Average and endpoint energies for beta spectra used to predict absorbed dose percentile distances.

Beta Particle Emitter	Beta Particle Spectra E_{av} (MeV)[a]	Beta Particle Spectra E_{max} (MeV)[b]
^{147}Pm	.0621	.224
^{133}Xe	.1005	.346
^{204}Tl	.2433	.766
^{47}Ca	.3444	1.98 (18%)
^{132}I	.5063	2.12 (20%)
^{86}Rb	.6670	1.76
^{15}O	.7378	1.74
^{49}Sc	.8266	2.01
^{90}Y	.9367	2.27
^{76}As	1.0712	2.98
^{28}Al	1.2397	2.87

[a] p. 12 reference no. 16.

[b] Radiological Health Handbook, revised edition, January 1970.

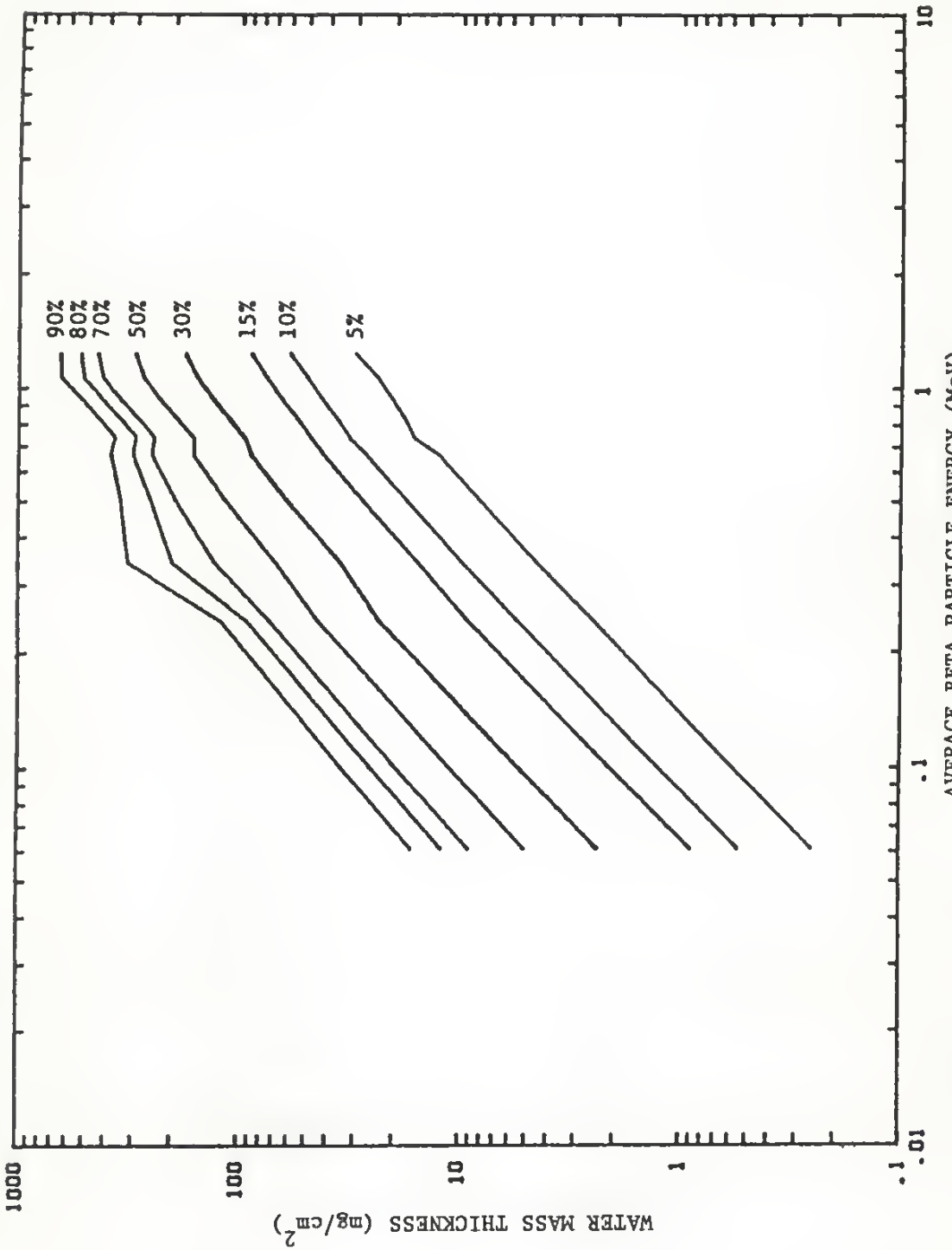

Fig. C.1. Absorbed dose percentile distances in water.

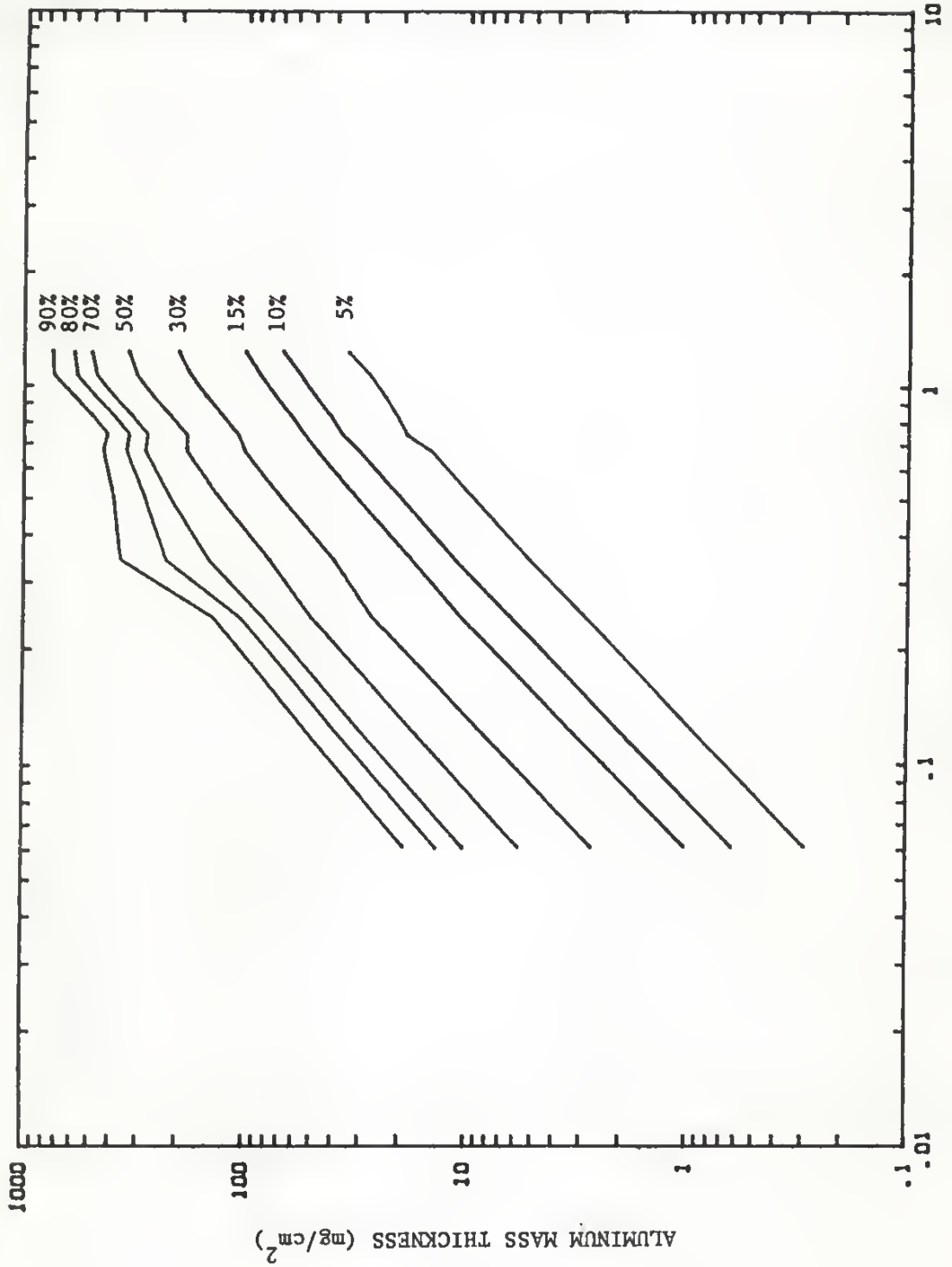

Fig. C.2. Absorbed dose percentile distances in aluminum.

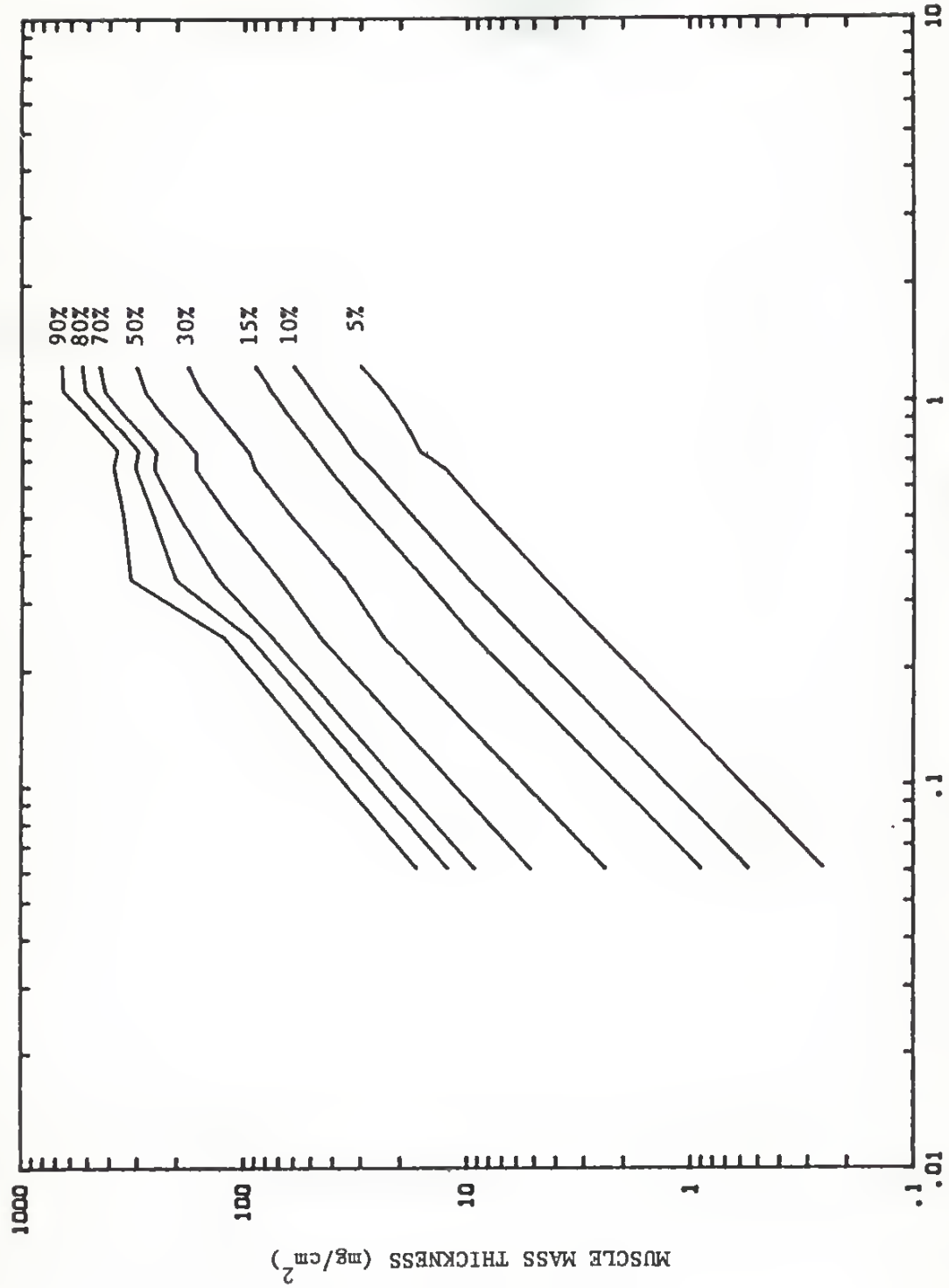

Fig. C.3. Absorbed dose percentile distances in muscle tissue (10.2% H, 12.3% C, 72.9% O, 0.08% Na, 0.02% Mg, 0.2% P, 0.5% S, 0.3% K by weight).

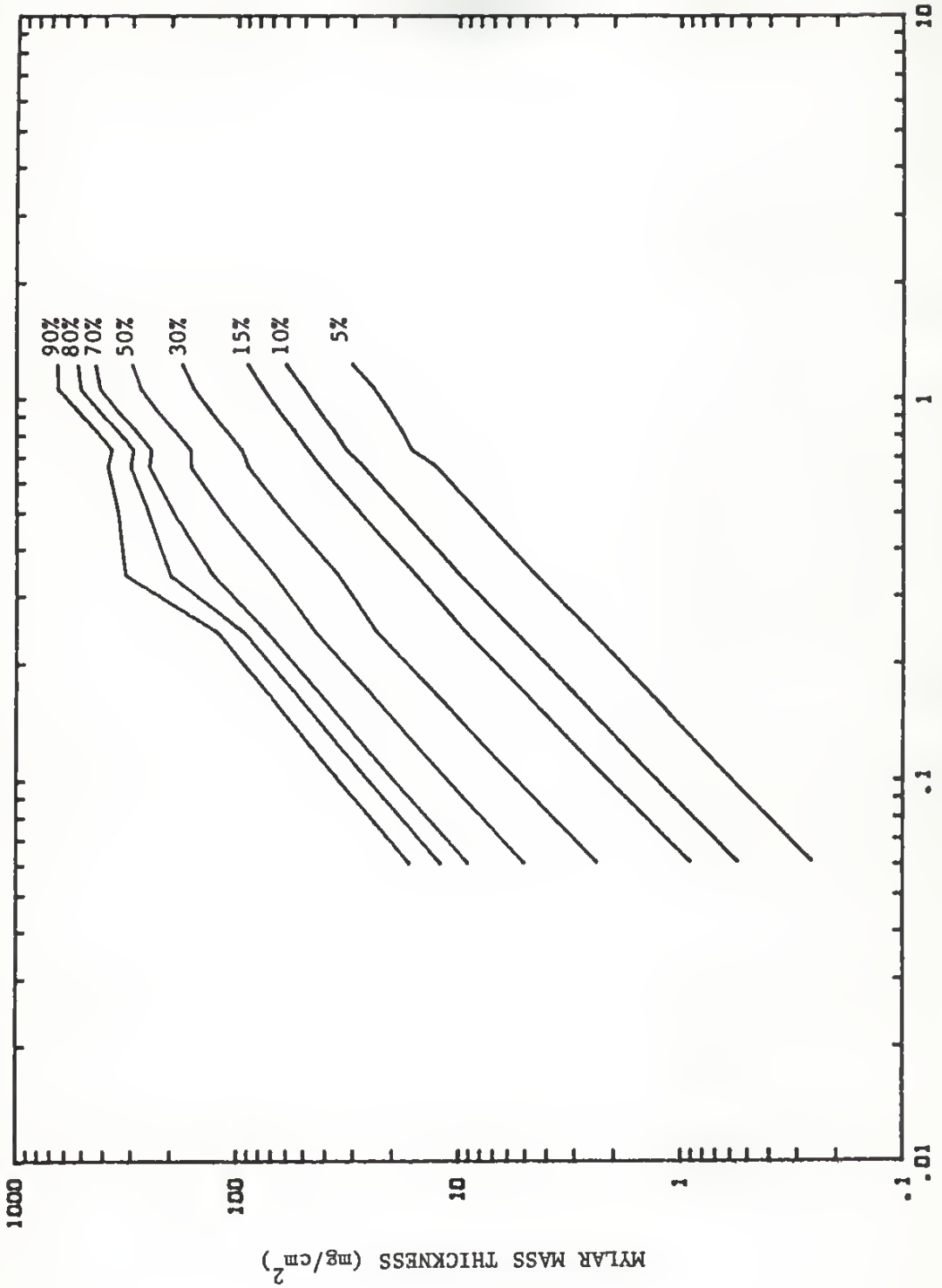

Fig. C.4. Absorbed dose percentile distances in mylar.

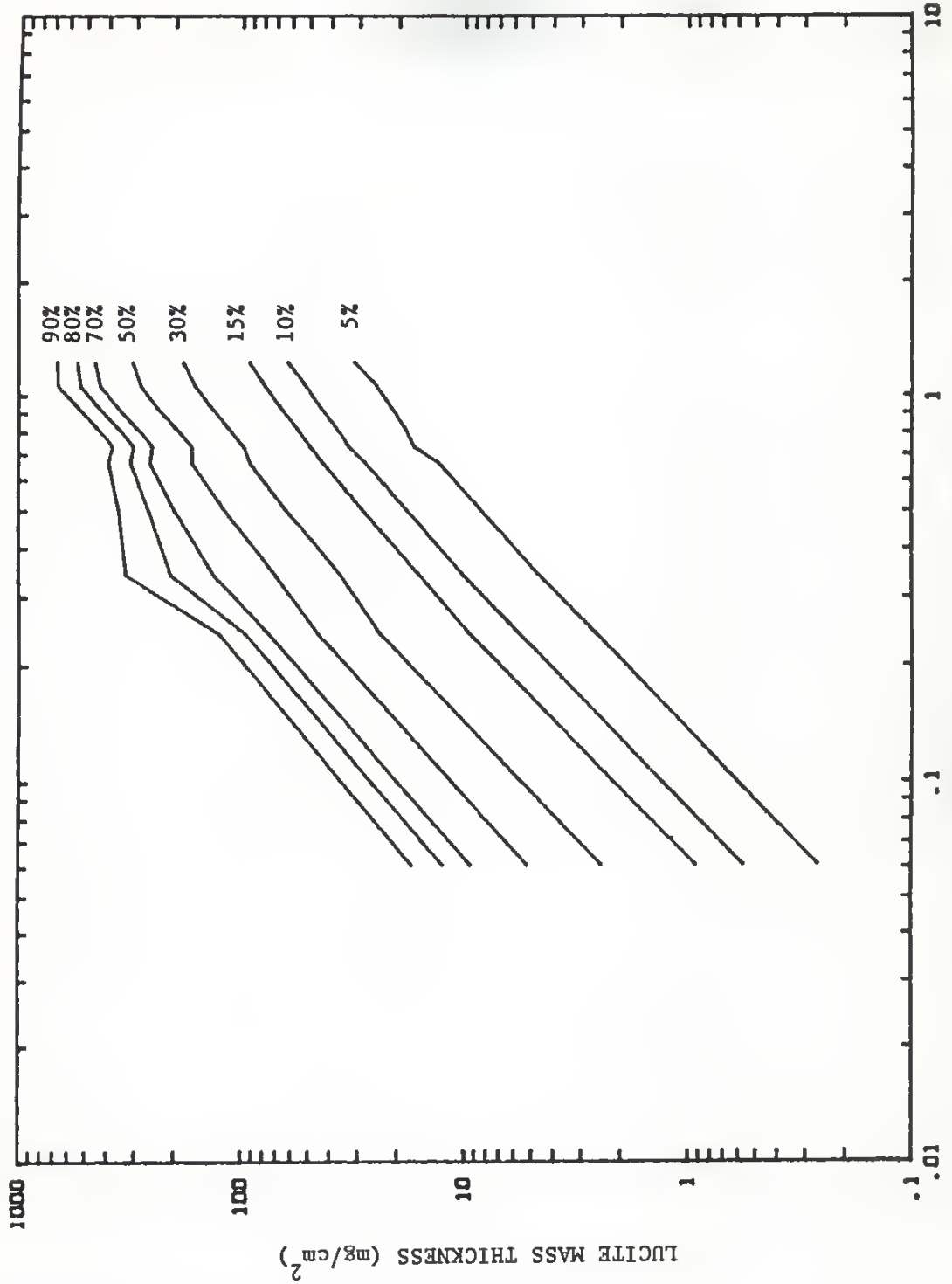

Fig. C.5. Absorbed dose percentile distances in lucite.

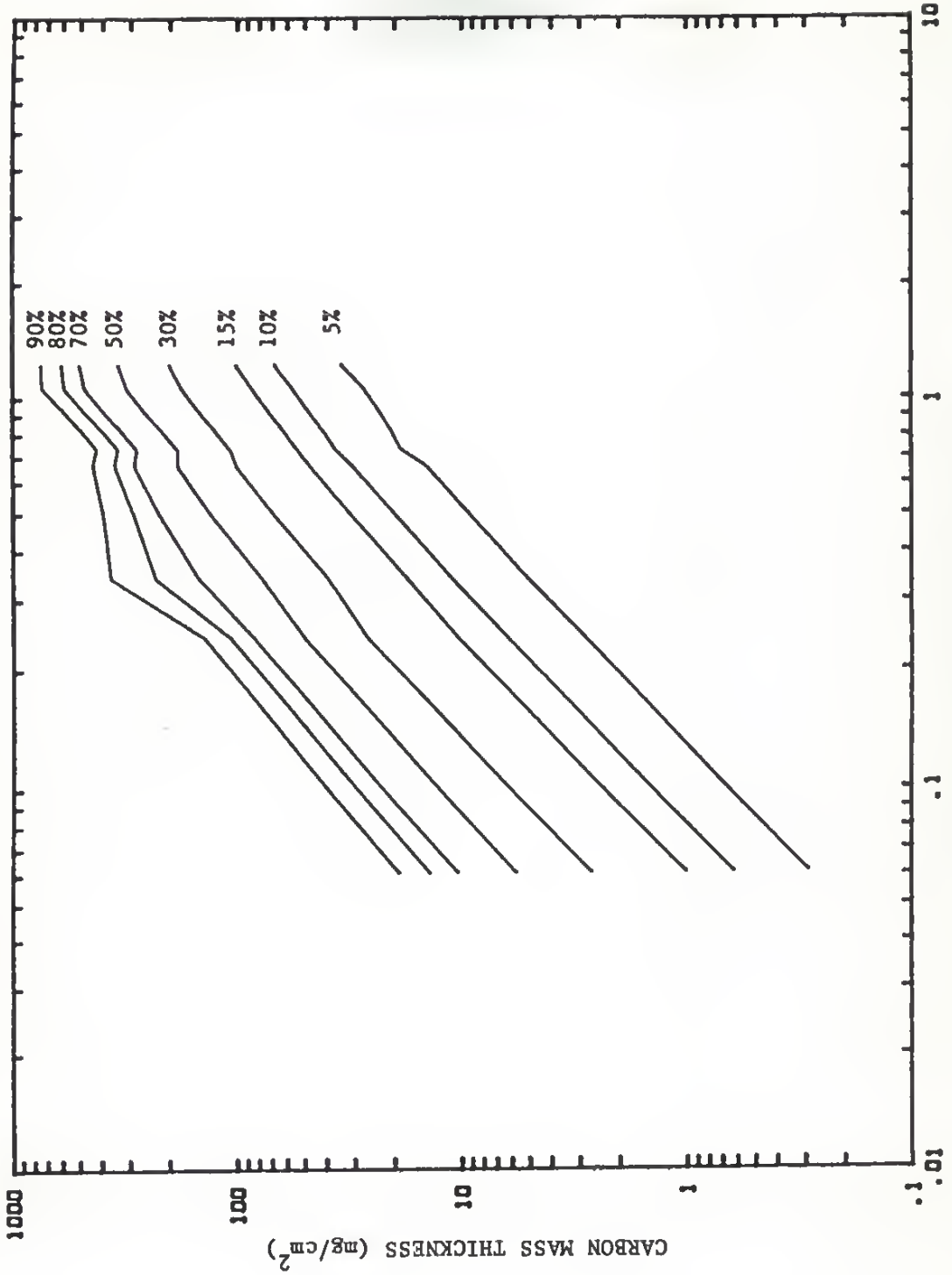

Fig. C.6. Absorbed dose percentile distances in carbon.

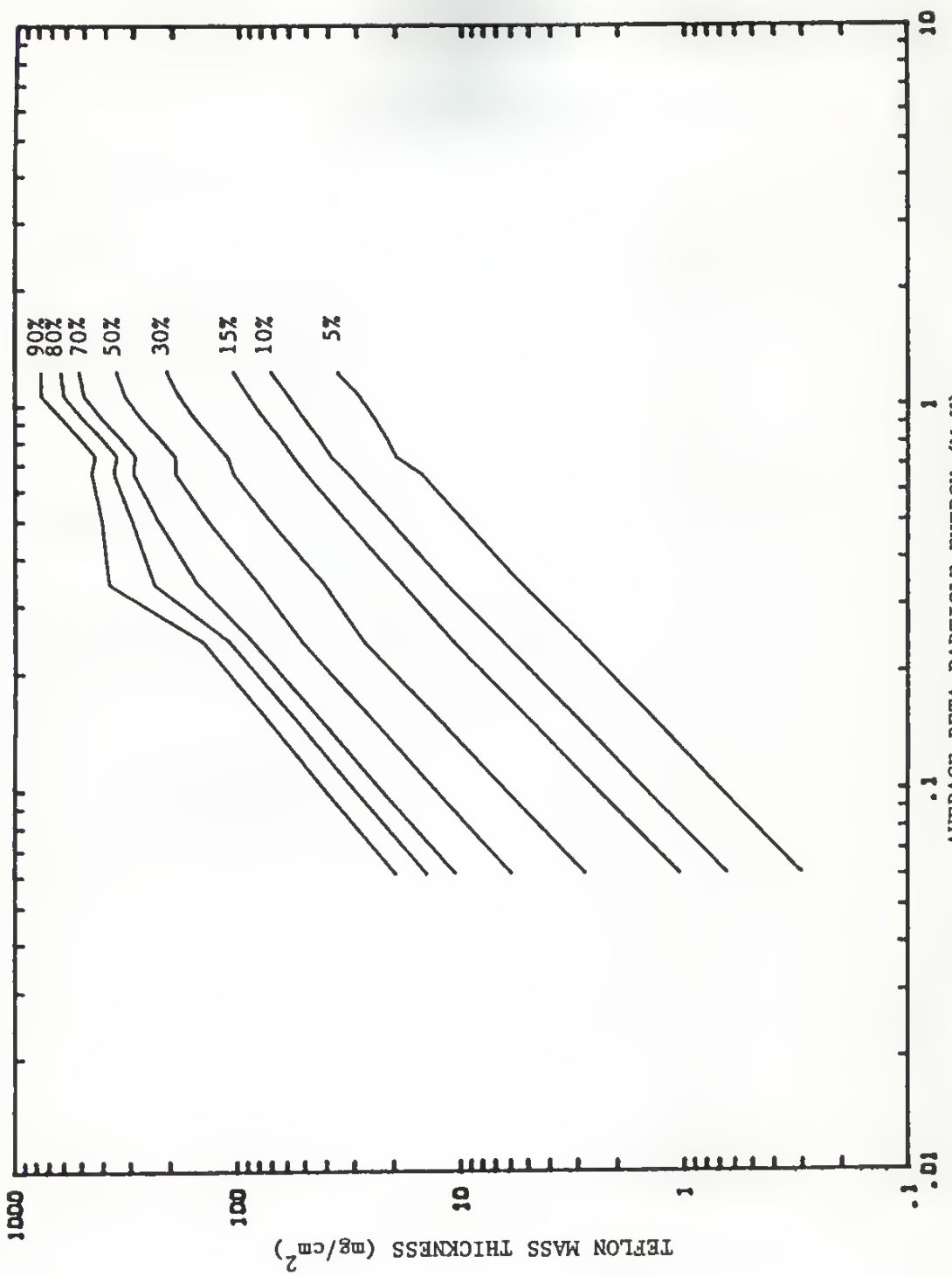

Fig. C.7. Absorbed dose percentile distances in teflon.

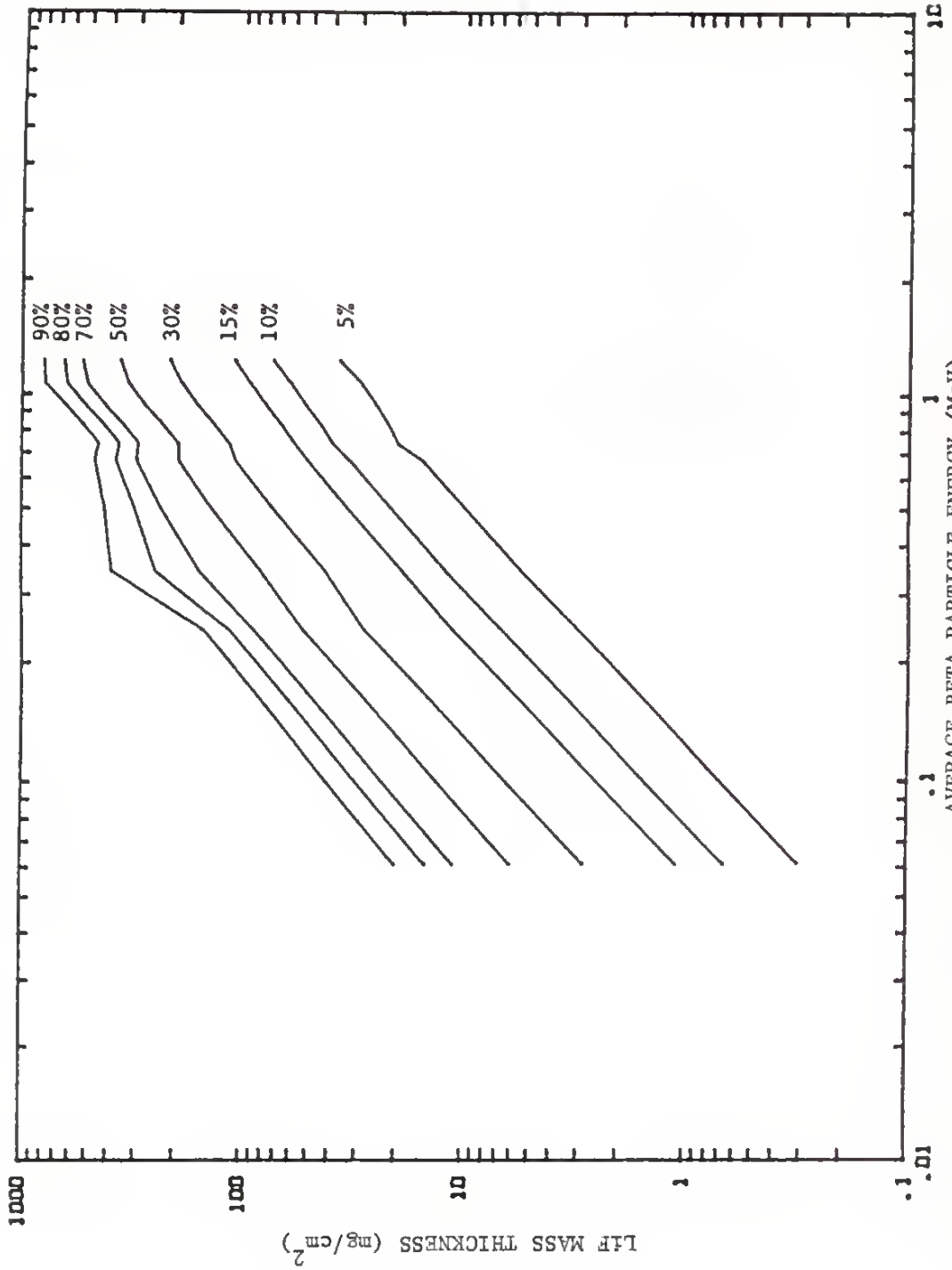

Fig. C.8. Absorbed dose percentile distances in lithium flouride.

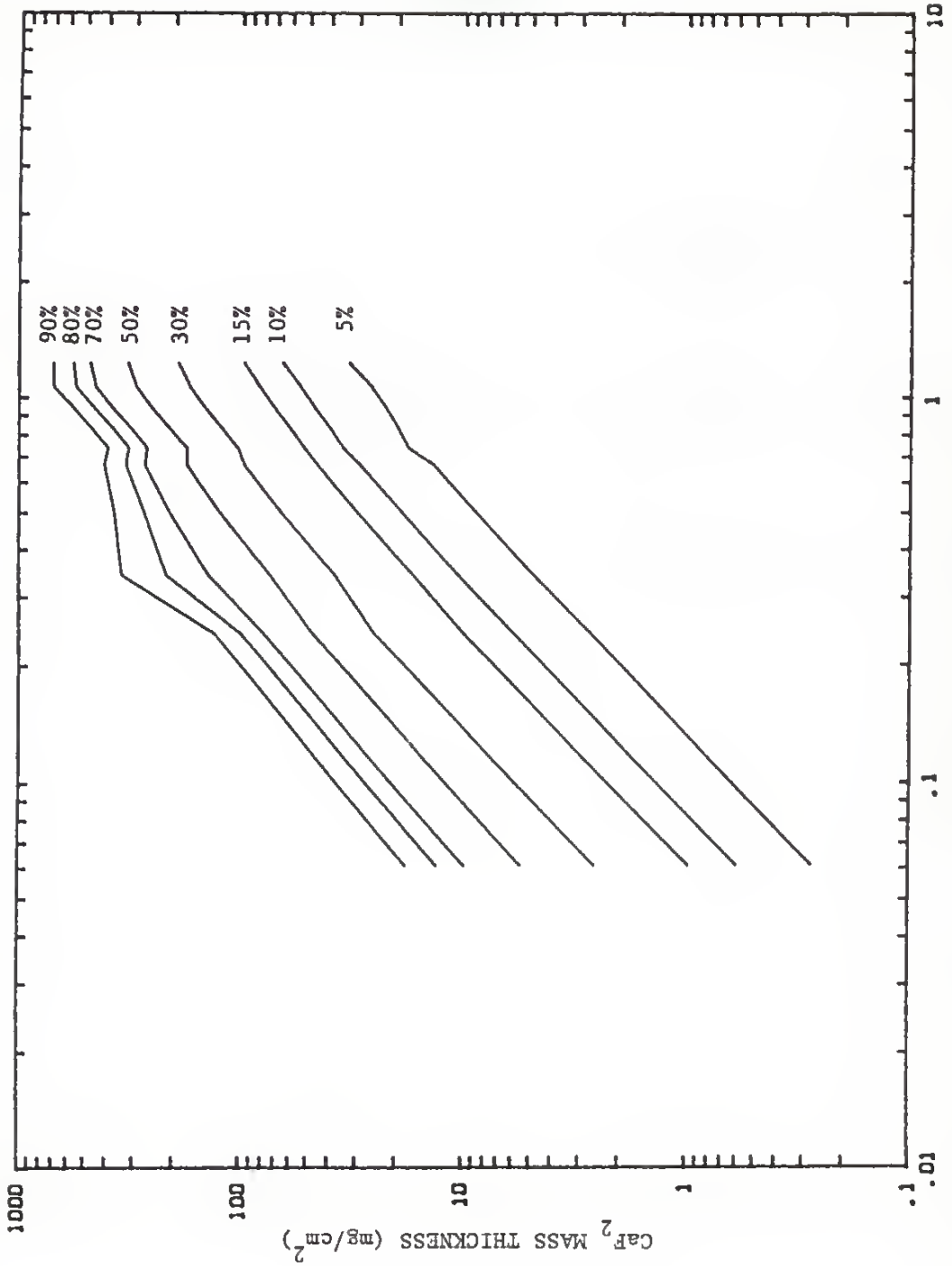

Fig. C.9. Absorbed dose percentile distances in calcium flouride.

APPENDIX D: DERIVATION OF ELECTRON RANGE-ENERGY RELATIONSHIPS

Electron energy can be expressed as a function of electron range, and since the incident range can be calculated as a function of the emergent particle energy and absorber mass thickness, the following relationship can be obtained:[a]

$$\phi_e(E_e) = \phi_i\{E_i[R_e(E_e)+r]\} \frac{dR_i(E_e)/dE_e}{dR_i(E_i)/dE_i} \quad , \tag{D.1}$$

where E = kinetic energy of the electron,

$\phi(E)$ = flux density of beta particles,

$R(E)$ = range of beta particle,

i = subscript for incident particles,

e = subscript for emerging particles,

and r = absorber mass thickness.

The electron range-energy relationship developed by Katz and Penfold for aluminum was chosen to estimate $\phi_e(E_e)$:[b]

$$R(E) = R_o E^n \quad , \tag{D.2}$$

where $R(E)$ = beta particle range in g/cm^2,

$R_o = 0.412$,

E = kinetic energy in MeV,

and $n = 1.265 - 0.0954 \ln E$ for $0.01 \leq E < 2.5$ MeV.

The following is the derivation of the emerging energy and spectra equations for beta particles.

Evaluating equation (D.2), the range equation becomes:

$$R_e(E_e) = 0.412\ E_e^{(1.265-0.0954\ \ln\ E_e)} \quad . \tag{D.3}$$

Now, the natural logarithm is taken of both sides, and from the 3rd law of logarithms equations (D.3) becomes:

$$\ln[R_e(E_e)] - \ln(0.412) = (1.265-0.0954 \ln E_e) \ln E_e . \qquad (D.4)$$

Since this equation is of order 2, the inverse of the 2nd order term is multiplied through and a constant is added to both sides to complete the square. Thus, equation (D.4) becomes:

$$[(\ln E_e) - 6.63]^2 = 43.9569 - [9.2949 - 10.4822 \ln R_e(E_e)]. \qquad (D.5)$$

Finally, solving for $(\ln E_e)$ and then taking the exponential of each side,

$$E_e = \exp \{6.63 - 3.2376 [3.3067 - \ln R_e(E_e)]^{\frac{1}{2}}\} . \qquad (D.6)$$

From the 23rd edition CRC standard mathematical tables, $\frac{d}{dx}(u^v) = vu^{v-1} \frac{du}{dx} + (\ln u)u^v \frac{dv}{dx}$. Thus, applying this to equation (D.2),

$$\frac{dR_e(E_e)}{dE_e} = R_o n_e E_e^{n_e-1} + R_o(\ln E_e) E_e^{n_e} \left(\frac{dn_e}{dE_e}\right) , \qquad (D.7)$$

$$= R_o n_e E_e^{n_e-1} + R_o(\ln E_e)E_e^{n_e}(-0.0954/E_e) , \qquad (D.8)$$

$$= R_o E_e^{n_e-1} [n_e - 0.0954 \ln E_e] . \qquad (D.9)$$

From inspection we see that equation (D.9) will be the same for incident particles. Thus,

$$\frac{dR_e(E_e)/dE_e}{dR_i(E_i)/dE_i} = \frac{E_e^{n_e-1}[n_e-0.0954 \ln E_e]}{E_i^{n_i-1}[n_i-0.0954 \ln E_i]} . \qquad (D.10)$$

REFERENCES

[a]A.B. Chilton, J.K. Shultis, and R.E. Faw, Principles of Radiation Shielding (Prentice-Hall, Englewood Cliffs, New Jersey, 1983) pp. 67 - 74.

[b]L. Katz and A.S. Penfold, Rev. of Mod. Phys., 24, 28 (1952).

APPENDIX E: EFFECT OF ABSORPTION ON CALCULATED KURIE PLOTS

Kurie plots were calculated for original beta spectra and attenuated spectra based on an electron range-energy relationship developed by Katz and Penfold.[a] Figures E.1 - E.3 represent Kurie plots of ^{147}Pm, ^{204}Tl, and ^{90}Y spectra for various mass absorber thicknesses.

[a] L. Katz and A. S. Penfold, Rev. of Mod. Phys., 24, 28 (1952).

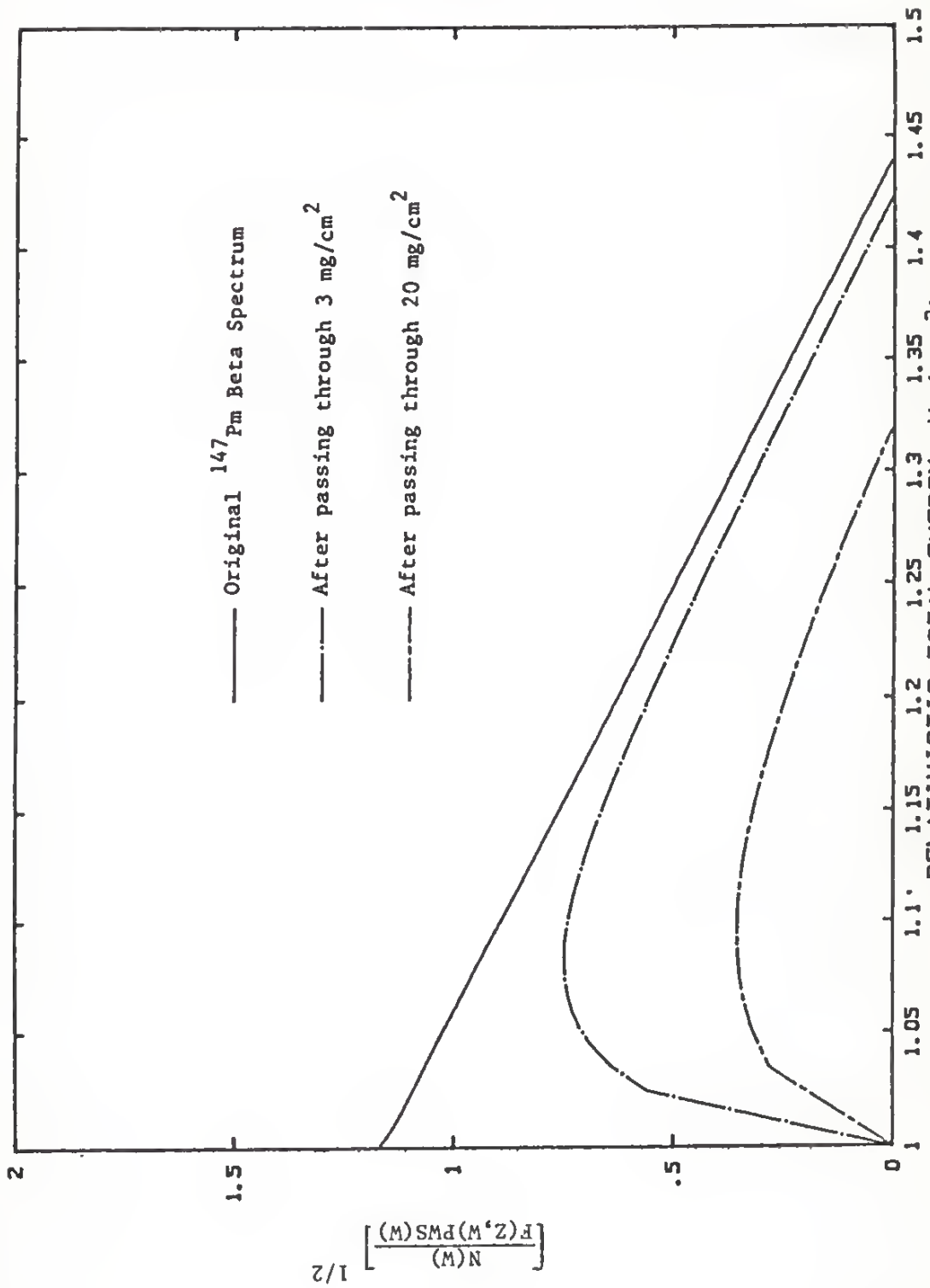

Fig. E.1. Calculated Kurie plot for the ^{147}Pm beta particle energy distribution as a function of increasing absorber thickness.

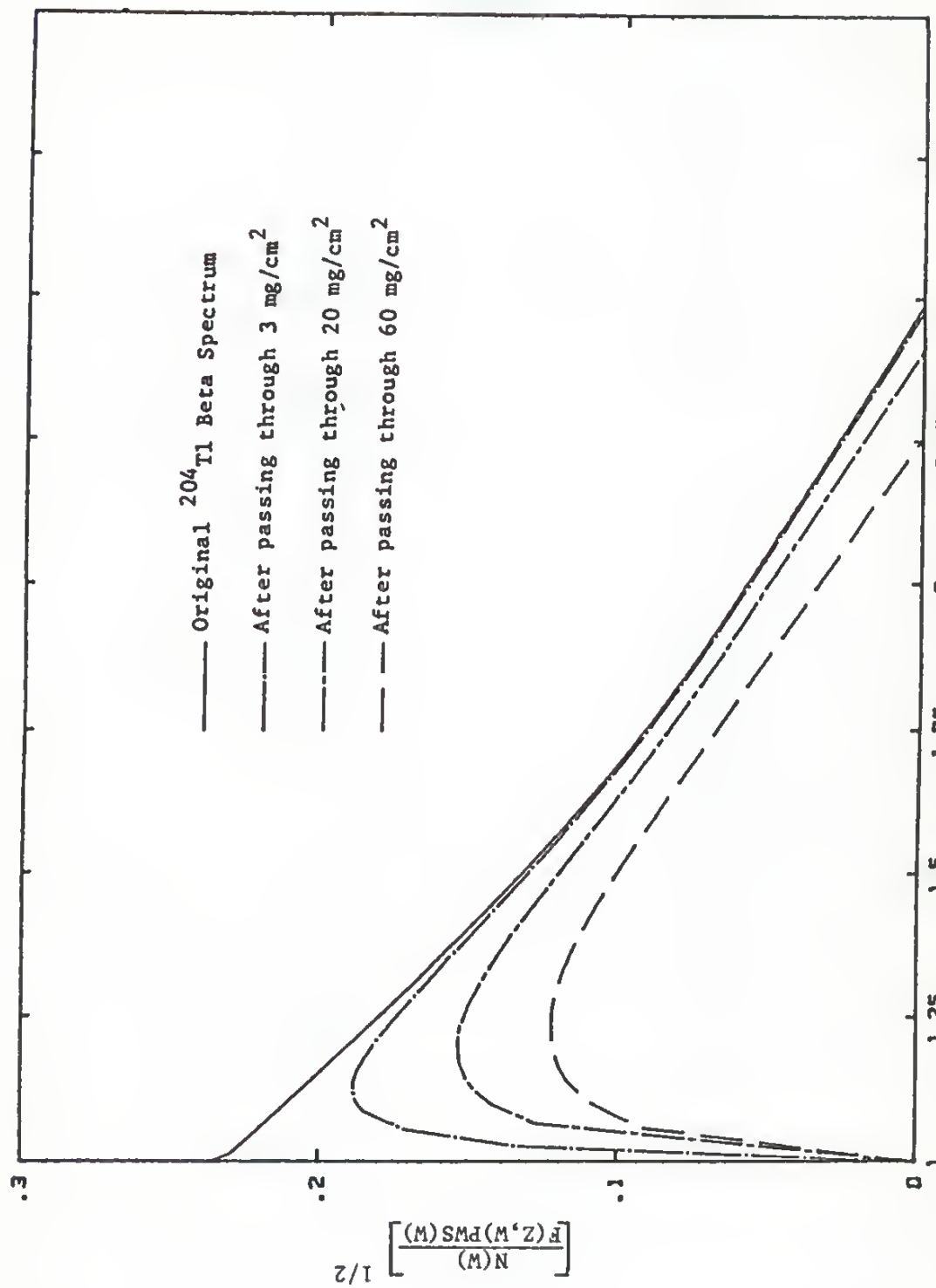

Fig. E.2. Calculated Kurie plot for the ^{90}Y beta particle energy distribution as a function of increasing absorber thickness.

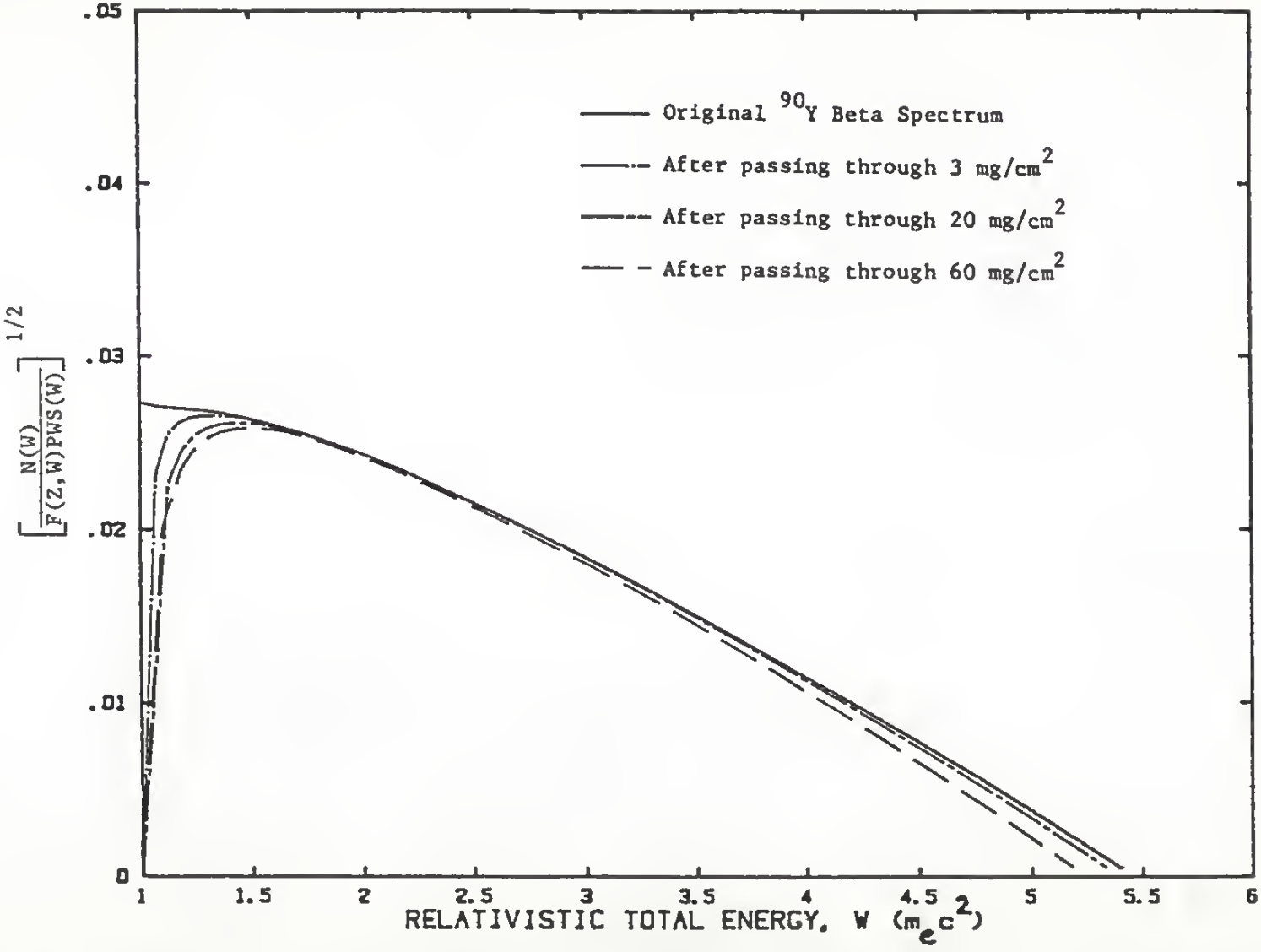

Fig. E.3. Calculated Kurie plot for the ^{90}Y beta particle energy distribution as a function of increasing absorbtion thickness.

APPENDIX F: THE SPECTRUM-CHANGE COMPUTER CODE

The following computer listing reveala the computer program used to calculate changes in ^{147}Pm spectra due to absorber thicknesses based on a range-energy relationship. Remark statementa (!) discuss the program's step-by-step procedure.

Important variables in the program are:

T_i, T_e ≡ incident and emergent beta particle kinetic energy,

Speci, Spece ≡ incident and emergent spectral height,

Rat ≡ Ratio of range differentials,

R ≡ range of beta particles,

W ≡ relativistic total energy,

and Kur ≡ left side of Eq. (2.9).

```
1000  ' ##################################################
1100  ' # THIS PROGRAM CALCULATES THE CHANGE IN BETA SPECTRUM  #
1200  ' # AS IT PASSES THROUGH AN ABSORBER WITH A CERTAIN MASS #
1300  ' # THICKNESS.  THIS PROGRAM ALSO EVALUATES THE AVERAGE  #
1400  ' # ENERGY OF THE BETA SPECTRUM USING A SIMPLE NUMERICAL #
1500  ' # INTEGRATION AND EVALUATES THE ENDPOINT ENERGY OF THE #
1600  ' # SPECTRUM USING A KURIE PLOT AND A SIMPLIFIED FERMI   #
1700  ' # FUNCTION.  THIS PROGRAM EVALUATES ALL THESE FOR THE  #
1800  ' # 147-Pm SPECTRA.                                     #
1900  ' ##################################################
2000  '
2100  '
2200  '
2300  '
2400  DATA .0006,11.263,.0023,11.094,.0045,10.87,.0079,10.61
2500  DATA .0112,10.4,.0135,10.26,.0158,10.11,.0180,9.968
2600  DATA .0203,9.822,.0225,9.675,.0243,9.528,.027,9.393
2700  DATA .0293,9.232,.0315,9.084,.0339,8.935,.036,8.787
2800  DATA .0393,8.638,.0406,8.499,.0428,8.339,.0451,8.17
2900  DATA .0473,8.041,.0496,7.892,.0518,7.742,.0541,7.593
3000  DATA .0563,7.444,.0586,7.295,.0608,7.147,.0631,6.959
3100  DATA .0653,6.851,.0676,6.703,.0698,6.555,.0721,6.409
3200  DATA .0743,6.262,.0766,6.116,.0789,5.971,.0811,5.926
3300  DATA .0834,5.892,.0856,5.538,.0879,5.395,.0901,5.253
3400  DATA .0924,5.112,.0946,4.971,.0969,4.932,.0991,4.673
3500  DATA .1014,4.556,.1036,4.4139,.1059,4.283,.1081,4.149
3600  DATA .1104,4.015,.1126,3.883,.1149,3.752,.1171,3.625
3700  DATA .1194,3.494,.1216,3.368,.1239,3.242,.1262,3.118
3800  DATA .1284,2.996,.1307,2.875,.1329,2.756,.1352,2.639
3900  DATA .1374,2.523,.1397,2.409,.1419,2.297,.1442,2.187
4000  DATA .1464,2.079,.1487,1.973,.1509,1.869,.1532,1.767
4100  DATA .1554,1.669,.1577,1.57,.1599,1.475,.1622,1.383
4200  DATA .1644,1.293,.1667,1.205,.1689,1.119,.1712,1.037
4300  DATA .1735,.9572,.1757,.88..1779,.8056,.1802,.7341
4400  DATA .1825,.6655,.1847,.5979..1869,.5373,.1892,.4778
4500  DATA .1915,.4214,.1937,.3683,.1960,.3185,.1982..2721
4600  DATA .2005,.2290,.2027,.1895,.2049,.1534,.2072,.1211
4700  DATA .2095,.0923,.2118,.0674,.2140,.0462,.2163,.0289
4800  DATA .2185,.0157,.2208,.0064,.2230,.0012,.2241,.0001
4900  '     ##########################################################
5000  '     THESE DATA ARE FROM A PRIVATE COMMUNICATION FROM CROSS
5100  '     AND ARE FOR Pm-147.
5200  '     ##########################################################
5300  N=100        ' NUMBER OF DATA POINTS IN SPECTRA
5400  DIM R(100),Ti(100),Pat(100),Speci(100),Te(100),Spece(100),W(100),Kur(100)
5500  FOR I=1 TO 100
5600  READ Ti(I),Speci(I)
5700  NEXT I
5800  CALL Kurie(Ti(0),Speci(0),W(0),Kur(0),I-1)
5900  INPUT "DO YOU WANT INITIAL KURIE PLOT (1=YES,2=NO)",Qa
6000  IF Qa=2 THEN 6600
6100  CALL Gdata(W(0),Kur(0),I-1)
6110  Sum=0
6120  Esum=0
```

```
6200  !     ##################################################
6300  !       THE PROCEEDING SECTION EVALUATES THE AVERAGE ENERGY
6400  !       AND THE DATA FOR THE KURIE PLOT FOR THE ENDPOINT.
6500  !     ##################################################
6800  FOR I=1 TO 100
6900  Sum=Sum+Ti(I)*Speci(I)
7000  Esum=Esum+Speci(I)
7100  NEXT I
7200  Eavg=Sum/Esum
7300  PRINT "THE INITIAL AVERAGE BETA ENERGY IS (MeV)";Eavg
7400  Emax=(W(100)-1)*.511
7500  PRINT "AND THE ENDPOINT ENERGY IS (MeV)";Emax
7600  INPUT "DO YOU WANT BDAT FILE FOR INITIAL RANGE PLOT (1=YES,2=NO)",Q
7700  IF Q=2 THEN 7900
7800  CALL Bdata(Ti(*),Speci(*),I-1)
7900  INPUT "MASS THICKNESS OF COVER (mg/cm^2)",Ra
8000  Ra=Ra/1000
8100  !     ##################################################
8200  !       NOW WE WILL CALCULATE THE RANGE OF EMERGENT BETAS
8300  !     ##################################################
8400  FOR I=1 TO 100
8500  IF Ti(I)<.01 THEN 10200
8600  Ni=1.265-.0954*LOG(Ti(I))
8700  R(I)=.412*Ti(I)^Ni-Ra
8800  IF R(I)<=0 THEN 10200
8900  !     ##################################################
9000  !       NOW WE CALCULATE THE EMERGENT ENERGY OF EACH BETA.
9100  !     ##################################################
9200  Te(I)=EXP(6.63-3.2376*(3.3067-LOG(R(I)))^.5)
9300  !     ##################################################
9400  !       NOW WE CALCULATE THE RATIO OF RANGE DIFFERENTIALS.
9500  !     ##################################################
9600  Ne=1.265-.0954*LOG(Te(I))
9700  Numer=Te(I)^(Ne-1)*(Ne-.0954*LOG(Te(I)))
9800  Denom=Ti(I)^(Ni-1)*(Ni-.0954*LOG(Ti(I)))
9900  Rat(I)=Numer/Denom
10000 Spece(I)=Rat(I)*Speci(I)
10100 GOTO 7900
10200 Te(I)=0
10300 Spece(I)=0
10400 NEXT I
10500 Sum=0
10600 Esum=0
10700 FOR I=1 TO 100
10800 Sum=Sum+Te(I)*Spece(I)
10900 Esum=Esum+Spece(I)
11000 NEXT I
11100 Emavg=Sum/Esum
11200 PRINT "THE AVERAGE BETA ENERGY IS NOW (MeV)";Emavg
11300 INPUT "DO YOU WANT BDAT FILE FOR ATTENUATED RANGE PLOT (1=YES,2=NO)",Qq
11400 IF Qq=2 THEN 11600
11500 CALL Bdata(Te(*),Spece(*),I-1)
11600 FOR I=1 TO 100
11700 Ti(I)=Te(I)
```

```
11800 Speci(I)=Spece(I)
11900 NEXT I
12000 CALL Kurie(Ti(*),Speci(*),N(*),Kur(*),I-1)
12100 Emax=(W(100)-1)*.511
12200 PRINT "THE NEW ENDPOINT ENERGY IS ";NeV)";Emax
12300 INPUT "DO YOU WANT BDAT FILE FOR ATTENUATED KURIE PLOT (1=YES,2=NO)",Bw
12400 IF Bw=2 THEN 12600
12500 CALL Bdata(W(*),Kur(*),I-1)
12600 INPUT "ANY MORE THICKNESSES? (1="ES) (2=NO)",K
12700 IF K=1 THEN 7900
12800 END
12900 !     ***************************************************
13000 !       A SUBROUTINE TO CREATE BDATA FILES FOR MASS
13100 !       STORAGE ON A DISK.  THIS ALLOWS THE USER TO
13200 !       RECALL THE FILE AT A LATER DATE TO BE PLOTTED
13300 !       ON THE PH PLOTTER FOUND IN WARD HALL.
13400 !     ***************************************************
13500 SUB Bdata(X(*),Y(*),N)
13600 ALLOCATE G(1:N,1:2)
13700 FOR I=1 TO N
13800 G(I,1)=X(I)
13900 G(I,2)=Y(I)
14000 NEXT I
14100 INPUT "WHAT IS YOUR BDAT FILE NAME?",N$
14200 MASS STORAGE IS ":HP82901,700,0"
14300 CREATE BDAT N$,2*N,15
14400 ASSIGN @Path TO N$
14500 OUTPUT @Path USING "N5DE";G(*)
14600 ASSIGN @Path TO *
14700 SUBEND
14800 !     ***************************************************
14900 !       A SUBROUTINE TO CALCULATE KURIE PLOT COORDINATES
15000 !       IN ORDER THAT THE ENDPOINT ENERGY OF A BETA
15100 !       SPECTRUN MAY BE FOUND.  A SIMPLIFIED FERNI
15200 !       FUNCTION APPROXIMATION WAS USED.
15300 !     ***************************************************
15400 SUB Kurie(Ti(*),Speci(*),W(*),Kur(*),N)
15500 FOR I=1 TO 100
15600 W(I)=Ti(I)/.511+1
15700 P=(W(I)^2-1)^.5
15800 IF Ti(I)<.6132 THEN Alpha=2.3115
15900 IF Ti(I)>=.6132 THEN Alpha=2.3101
16000 IF Ti(I)<.6132 THEN Beta=-.1998
16100 IF Ti(I)>=.6132 THEN Beta=-.1962
16200 IF P=0 THEN GOTO 16600
16300 F=W(I)/P*EXP(Alpha*Beta*(W(I)/.511-1)^.5)
16400 Kur(I)=(Speci(I)/F/P/W(I))^.5
16500 GOTO 16700
16600 Kur(I)=0
16700 !   PRINT W(I),Kur(I)
16800 NEXT I
16900 SUBEND
```

APPENDIX G: RESULTS OF KSU PERSONNEL DOSIMETER EVALUATIONS

The individual badge results for evaluations of the KSU personnel dosimeter are shown in Table G.1.

Table G.1. Individual badge results for evaluations of the KSU personnel dosimeter for various beta particle and gamma ray irradiations.

PERSONNEL BADGE NO.	GAMMA RAY EXPOSURE GIVEN (mR)	BETA PARTICLE DOSE GIVEN (mrad)	MEASURED GAMMA RAY EXPOSURE (mR)	MEASURED BETA PARTICLE DOSE (mrad)
	50	54	51.7	53.3
	250	54	270.0	60.2
11	50	272	42.6	254.3
	300	33	316.4	36.1
	30	325	16.9	312.3
	50	54	61.7	38.9
	250	54	252.7	64.2
12	50	272	40.2	251.8
	300	33	325.4	30.0
	30	325	22.9	314.2
	50	54	51.7	46.7
	250	54	252.2	48.1
13	50	272	40.8	287.8
	300	33	292.2	33.0
	30	325	24.8	286.0
	50	54	51.6	53.3
	250	54	257.9	49.1
14	50	272	46.0	260.5
	300	33	321.1	33.4
	30	325	16.2	322.9
	50	54	57.3	49.6
	250	54	47.6	263.2
15	50	272	62.5	247.5
	300	33	298.9	34.4
	30	325	24.7	309.1

DESIGN OF A BETA-GAMMA PERSONNEL BADGE USING THIN LiF THERMOLUMINESCENT DOSIMETERS

by

James Darren Gale

B.S., Kansas State Univeraity, 1983

AN ABSTRACT OF
A MASTER'S THESIS

Submitted in partial fulfillment of the
requirements for the degree

MASTER OF SCIENCE

Department of Nuclear Engineering
KANSAS STATE UNIVERSITY
Manhattan, Kanaaa

1984

ABSTRACT

Applied personnel dosimetry has been in a constant state of reform aince the accident at the Three Mile Island nuclear power facility. It was right after this accident that inadequacies in personnel dosimetry were realized. The goal of this project was to design and characterize a personnel badge which would meet the requirementa for skin dosimetry.

Theoretical calculations ahowed how beta particle spectra are affected by personnel badge cover and radiation aensitive element thicknesses. These data showed that a cover material thickness for a beta dose element should be chosen that ia as thin aa can reasonably be used considering the environment and handling of the badge. Data also showed that the thickneas of the radiation sensitive element (TLD) used for beta dosimetry should be made to match the 5-10 mg/cm^2 thickness which the ICRP recommends that the skin dose be reported.

Tests conducted on thin LiF TLDs developed at Kansas State indicated that the minimum detectable doaes for these elements were 3.1 mR for gamma ray expoaures and 4.2 mrad for beta particle doses, and 13.2 mR for gamma exposure and 18.1 mrad for beta particle doaes for the KSU photon counting system and current integrating snalyzers, respectively. Additional tests also showed the relative insensitivity of the LiF TLDs to environmental effects. Tests also indicated that the thin TLD can withstand high temperature anneals in case an accidental over-exposure should occur.

A two-element lucite personnel badge was developed and tested for use in mixed beta, gamma fields. Data indicated that the badge, can predict mixed beta, gamma field doses at several dose ratio levels and have good material propertiea to withatand routine use without being damaged.